

# **Forecasting Techniques for Seedable Storms over the Western Hajar Mountains in the Sultanate of Oman**

**Hamid Ahmed Sulaiman Al-Brashdi**

**21126519**

**Master of Science (Meteorology)**

**2007**

**Department of Geography, Geoinformatics and Meteorology  
UNIVERSITY OF PRETORIA**

## **DECLARATION**

I declare that the thesis that I hereby submit for the degree in Master of Science (Meteorology) at the University of Pretoria has not previously been submitted by me for degree purposes at any other university.

## ABSTRACT

### **Forecasting Techniques for Seedable Storms over the Western Hajar Mountains in the Sultanate of Oman Hamid Ahmed Sulaiman Al-Brashdi**

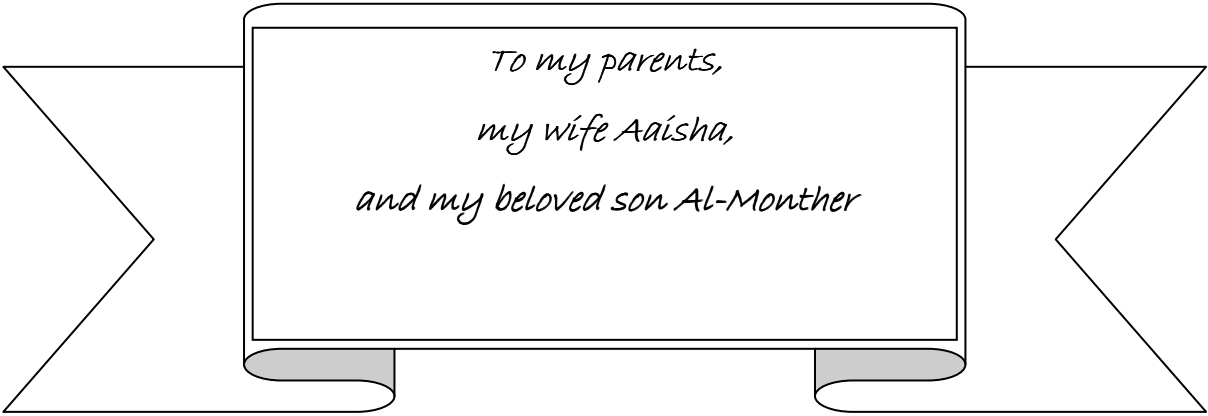
Supervisor: Ms. Liesl Dyson  
Faculty: Natural and Agricultural Sciences  
Department: Geography, Geoinformatics and Meteorology  
University: Pretoria  
Degree: Master in Science (Meteorology)

Oman faces a water resources crisis as the demand of fresh water increases day by day. Most of the renewable water resources in the country are directly or indirectly dependent on the rainfall. The Western Hajar Mountains extend to the borders with the UAE. This area is a very important source of ground water for both countries. A collaborative program to investigate the feasibility of rainfall enhancement over the Omani mountains by means of hygroscopic cloud seeding was implemented in the UAE during the summer of 2003 and 2004. Due to the complicated logistics and astronomical cost involved in the cloud seeding experiment, it is crucial that timely and accurate forecasts are made for these mesoscale storms. However, convective clouds of the Al Hajar Mountains are notoriously difficult to predict as they result from mesoscale circulation.

This study developed forecasting techniques for seedable storms over the Western Hajar Mountains in the Sultanate of Oman. A period of 10 days (5<sup>th</sup>-14<sup>th</sup> of July 2004) was investigated in order to describe the differences in the atmospheric parameters between days when convection occurred and days which remained dry. The main ingredient for convective development is the influx of surface moisture from southeast over the Arabian Sea. This moisture often results from the circulation around the surface low over the central part of the Arabian Peninsula but may occasionally be caused by the sea breeze circulation. The northeasterly sea breeze moves in from the Gulf of Oman to the mountains where it converges with the southeasterly moist flow and this may result in the occurrence of convective clouds. Localized wind convergence zones near the mountains are good indicators of the onset of convection. The Oman Convection Index (OCI) was developed to replace the K-index (KI) and was found to provide a good indication of convective development over the mountains. A forecasting decision tree table for predicting convective storms over the Al Hajar Mountains is proposed where circulation criteria are stipulated as well as critical values for meteorological variables. The ingredients includes the location of the heat low over the centre of Arabian Peninsula, latent instability of the atmosphere, and critical values of mixing ratio and the OCI.

This research results have shown that careful investigation and manipulation of the available data allow for increased accuracy in the forecast of convection. The OCI was developed to describe the conditions favorable for summer convection over the mountains of Oman specifically. The results show that the OCI fairs considerably better than the KI in identifying days when significant convection is likely to occur. However, the OCI is only one element of the forecasting techniques table. For truly significant convection to occur there are at least four other circulation criteria which should be satisfied. The forecasting decision tree table provides a systematic approach to the forecasting of convection of the mountains and therefore, for the first time in Oman, objective verification is possible and opens the door for improving these and other forecasting techniques. The techniques developed here may therefore contribute to future cloud seeding projects in the mountains of Oman.

## Dedication



*To my parents,  
my wife Aaisha,  
and my beloved son Al-Monther*

## **Acknowledgments**

First and foremost, my deep gratitude goes to Ms. Liesl Dyson from the University of Pretoria for her insightful guidance and supervision of this research.

Secondly, I would like to thank H.E. Sheikh Mohammed Al-Harthy, the Minister of Civil Service for his continuous support for my study at the University of Pretoria. I also wish to thank the Department of Meteorology in the Sultanate of Oman, the UAE Department of Atmospheric Sciences, Mr. Roelof Burger from the University of Witwatersrand, and Mrs. Tara Jensen from NCAR for making the research data available to me.

Thanks are also due to my parents and family members for their support and valuable advice during my study. A special word of thanks goes to my dearest sister Ms. Badria Al-Brashdi for her help in language revision, Ms. Ghaitha Al-Brashdi for her help in the organization of figures and my brother Mr. Mahmood Al-Brashdi for his help in the printing of this dissertation.

Finally, thanks are forwarded to Mr. Graig Powell for his help in satellite data analysis and Mr. Khalid Al-Habsi for his continuous support.

## Table of Contents

<b>Chapter 1</b>	<b>Introduction .....</b>	<b>1</b>
1.1	Geography and climate of Oman.....	1
1.2	The rainfall climatology over Oman.....	3
1.3	Synoptic weather systems over Oman.....	4
1.3.1	Low pressure systems/upper troughs during winter over Oman	4
1.3.2	Monsoon (Khareef) over Salalah and adjoining areas	5
1.3.3	Tropical storms and cyclones	5
1.3.4	Convective rain during summer over the Al Hajar Mountains	6
1.4	Aims .....	7
<b>Chapter 2</b>	<b>Data and Methodology.....</b>	<b>9</b>
2.1	Types of data.....	9
2.1.1	Surface observations	9
2.1.2	Upper air soundings	12
2.1.3	Radar	13
2.1.4	The mesoscale model (MM5)	13
2.1.5	National Center for Environmental Prediction (NCEP) data	14
2.2	Methodology.....	14
<b>Chapter 3</b>	<b>Cloud Seeding Experiment and Convective Development .....</b>	<b>17</b>
3.1	Introduction.....	17
3.2	Cloud seeding in Oman.....	18
3.2.1	Hygroscopic cloud seeding	18
3.2.2	Characteristics of the regional clouds and their amenability to the hygroscopic seeding	21
3.3	Observed convection .....	21
3.3.1	The 6 <sup>th</sup> of July	22
3.3.2	The 7 <sup>th</sup> of July	25
3.3.3	The 8 <sup>th</sup> of July	28
3.3.4	The 9 <sup>th</sup> of July	29
3.3.5	The 10 <sup>th</sup> of July	32
3.3.6	The 11 <sup>th</sup> of July	36

3.3.7	The 12 <sup>th</sup> of July	41
3.3.8	The 13 <sup>th</sup> and 14 <sup>th</sup> of July	45
<b>3.4</b>	<b>Seeding cases during the study period</b>	<b>45</b>
<b>3.5</b>	<b>General discussion</b>	<b>47</b>
<b>Chapter 4</b>	<b>Data Analysis and Results</b>	<b>48</b>
<b>4.1</b>	<b>Introduction</b>	<b>48</b>
<b>4.2</b>	<b>Synoptic conditions</b>	<b>48</b>
4.2.1	NCEP data	48
4.2.2	The mesoscale model (MM5)	55
<b>4.3</b>	<b>The Impact of the synoptic conditions on the mesoscale development</b>	<b>59</b>
4.3.1	Coastal stations	59
4.3.2	Inland stations	62
4.3.3	Sea breeze	69
<b>4.4</b>	<b>Upper air and sounding parameters</b>	<b>75</b>
4.4.1	Upper air	75
4.4.2	Sounding parameters	80
<b>4.5</b>	<b>General discussion</b>	<b>83</b>
<b>Chapter 5</b>	<b>The Oman Convection Index (OCI)</b>	<b>85</b>
<b>5.1</b>	<b>Introduction</b>	<b>85</b>
<b>5.2</b>	<b>The KI</b>	<b>85</b>
5.2.1	Physical analysis of KI	85
5.2.2	Statistical analysis of KI	88
<b>5.3</b>	<b>The Oman Convection Index (OCI)</b>	<b>90</b>
5.3.1	Physical analysis of OCI	90
5.3.2	Statistical analysis of OCI	93
<b>5.4</b>	<b>KI and OCI during this study period</b>	<b>95</b>
<b>5.5</b>	<b>General discussion</b>	<b>96</b>
<b>Chapter 6</b>	<b>Forecasting Techniques</b>	<b>97</b>

<b>6.1</b>	<b>Introduction.....</b>	<b>97</b>
<b>6.2</b>	<b>Techniques formulation and application.....</b>	<b>97</b>
6.2.1	Table of convection forecasting techniques (TCFT)	98
6.2.2	Applications of the TCFT	99
<b>Chapter 7</b>	<b>Conclusion and Recommendations .....</b>	<b>101</b>
<b>7.1</b>	<b>General summary.....</b>	<b>101</b>
<b>7.2</b>	<b>Summary of results .....</b>	<b>101</b>
<b>7.3</b>	<b>Conclusions .....</b>	<b>102</b>
<b>7.4</b>	<b>Recommendations.....</b>	<b>102</b>
	<b>References.....</b>	<b>104</b>



## List of Figures

Figure 1-1:	A regional map showing the position of Oman in the Arabian Peninsula. The map indicating the four governorates and the five administrative regions of Oman (red). (Adapted from: Network Overseas, 2007).....	1
Figure 1-2:	The topography of Oman. (Adapted from: Wikimedia, 2007). .....	2
Figure 1-3:	The convection mostly covered the entire Al Hajar Mountains on the 10 <sup>th</sup> of July 2004. (Adapted from: MODIS, 2007).....	7
Figure 2-1:	The network of meteorological station over Oman belongs to DGCAM. (Adapted from: DGCAM, 2006). .....	10
Figure 2-2:	Some of the DAS weather stations network 2003. (Adapted from: Annual Climate Report 2003, DAS). .....	11
Figure 3-1:	The Seeding Study Area (SSA) with Al Ain radar coverage denoted by range rings. The radius of the radar coverage areas is about 150 Km, with Al Ain near the centre of the site. (Adapted from: DWRS, 2003). .....	20
Figure 3-2:	Radar reflectivity (dBz) on the 6 <sup>th</sup> of July 2004 at 1012 UTC. The wind vectors are surface observations at 1000 UTC.....	23
Figure 3-3:	Radar reflectivity (dBz) on the 6 <sup>th</sup> of July 2004 at 1112 UTC.....	23
Figure 3-4:	Radar reflectivity (dBz) on the 6 <sup>th</sup> of July 2004 at 1332 UTC. The wind vectors are surface observations at 1330 UTC. ....	24
Figure 3-5:	Radar reflectivity (dBz) on the 6 <sup>th</sup> of July 2004 at 1407 UTC.....	24
Figure 3-6:	Radar reflectivity (dBz) on the 7 <sup>th</sup> of July 2004 at 1117 UTC. The wind vectors, temperature and dew point values are surface observations at 1115 UTC while the pink shaded area indicates the estimated convergence zone.....	25
Figure 3-7:	Radar reflectivity (dBz) on the 7 <sup>th</sup> of July 2004 at 1202 UTC.....	26
Figure 3-8:	Radar reflectivity (dBz) on the 7 <sup>th</sup> of July 2004 at 1317 UTC.....	26
Figure 3-9:	Radar reflectivity (dBz) on the 7 <sup>th</sup> of July 2004 at 1357 UTC.....	27
Figure 3-10:	Radar reflectivity (dBz) on the 8 <sup>th</sup> of July 2004 at 1027 UTC.....	28
Figure 3-11:	Radar reflectivity (dBz) on the 8 <sup>th</sup> of July 2004 at 1152 UTC. The wind vectors, temperature and dew point values are surface observations at 1145 UTC while the pink shaded area indicates the estimated convergence zone.....	29
Figure 3-12:	Radar reflectivity (dBz) on the 9 <sup>th</sup> of July 2004 at 0832 UTC.....	30
Figure 3-13:	Radar reflectivity (dBz) on the 9 <sup>th</sup> of July 2004 at 957 UTC. The wind vectors, temperature and dew point values are surface observations at 1000 UTC while the pink shaded area indicates the estimated convergence zone.....	30
Figure 3-14:	Radar reflectivity (dBz) on the 9 <sup>th</sup> of July 2004 at 1107 UTC.....	31
Figure 3-15:	Radar reflectivity (dBz) on the 9 <sup>th</sup> of July 2004 at 1237 UTC.....	31
Figure 3-16:	Radar reflectivity (dBz) on the 10 <sup>th</sup> of July 2004 at 0838 UTC.....	32

Figure 3-17:	Radar reflectivity (dBz) on the 10 <sup>th</sup> of July 2004 at 0918 UTC.....	33
Figure 3-18:	Radar reflectivity (dBz) on the 10 <sup>th</sup> of July 2004 at 1003 UTC.....	33
Figure 3-19:	Radar reflectivity (dBz) on the 10 <sup>th</sup> of July 2004 at 1033 UTC.....	34
Figure 3-20:	Radar reflectivity (dBz) on the 10 <sup>th</sup> of July 2004 at 1218 UTC. The wind vectors, temperature and dew point values are surface observations at 1215 UTC while the pink shaded area indicates the estimated convergence zone.....	34
Figure 3-21:	Radar reflectivity (dBz) on the 10 <sup>th</sup> of July 2004 at 1333 UTC. The wind vectors, temperature and dew point values are surface observations at 1330 UTC. ....	35
Figure 3-22:	Radar reflectivity (dBz) on the 11 <sup>th</sup> of July 2004 at 0803 UTC.....	36
Figure 3-23:	Radar reflectivity (dBz) on the 11 <sup>th</sup> of July 2004 at 0903 UTC.....	37
Figure 3-24:	Radar reflectivity (dBz) on the 11 <sup>th</sup> of July 2004 at 0923 UTC.....	37
Figure 3-25:	Radar reflectivity (dBz) on the 11 <sup>th</sup> of July 2004 1003 UTC.....	38
Figure 3-26:	Radar reflectivity (dBz) on the 11 <sup>th</sup> of July 2004 1108 UTC.....	38
Figure 3-27:	Radar reflectivity (dBz) on the 11 <sup>th</sup> of July 2004 at 1328 UTC.....	39
Figure 3-28:	Radar reflectivity (dBz) on the 11 <sup>th</sup> of July 2004 at 0833 UTC. The wind vectors, temperature and dew point values are surface observations at three minutes before the volume scan time. ....	40
Figure 3-29:	Radar reflectivity (dBz) on the 11 <sup>th</sup> of July 2004 at 0933 UTC. The wind vectors, temperature and dew point values are surface observations at three minutes before the volume scan time while the pink shaded area indicates the estimated convergence zone. ....	40
Figure 3-30:	Radar reflectivity (dBz) on the 12 <sup>th</sup> of July 2004 at 0853 UTC.....	41
Figure 3-31:	Radar reflectivity (dBz) on the 12 <sup>th</sup> of July 2004 at 0923 UTC.....	42
Figure 3-32:	Radar reflectivity (dBz) on the 12 <sup>th</sup> of July 2004 at 0958 UTC.....	42
Figure 3-33:	Radar reflectivity (dBz) on the 12 <sup>th</sup> of July 2004 at 1103 UTC.....	43
Figure 3-34:	Radar reflectivity (dBz) on the 12 <sup>th</sup> of July 2004 at 1123 UTC.....	44
Figure 3-35:	Radar reflectivity (dBz) on the 12 <sup>th</sup> of July 2004 at 1303 UTC.....	44
Figure 3-36:	Aqua True color image at 0900 UTC on 13 <sup>th</sup> (A) & at 0940 UTC on 14 <sup>th</sup> (B) of July 2004.....	45
Figure 3-37:	Randomized seeding experiment locations of 23 seeding cases (blue solid squairs) during the period (6 <sup>th</sup> -13 <sup>th</sup> )of July 2004. (Data from DAS and NCAR). ....	46
Figure 4-1:	The geopotential heights (gpm) at 1000 hPa from the 5 <sup>th</sup> to the 14 <sup>th</sup> of July. (Adapted from: NCEP, 2007). ....	50
Figure 4-2:	The geopotential heights (gpm) at 850 hPa for the 5 <sup>th</sup> (A) & the 6 <sup>th</sup> of July 2004. (Adapted from: NCEP, 2007). ....	51
Figure 4-3:	The geopotential heights (gpm) at 850 hPa for the 7 <sup>th</sup> (A), 8 <sup>th</sup> (B), 9 <sup>th</sup> (C) & the 10 <sup>th</sup> (D) of July 2004. (Adapted from: NCEP, 2007).....	52
Figure 4-4:	The geopotential heights (gpm) at 850 hPa for the 11 <sup>th</sup> (A), 12 <sup>th</sup> (B), 13 <sup>th</sup> (C) & the 14 <sup>th</sup> (D) of July 2004. (Adapted from: NCEP, 2007).....	53

Figure 4-5: The geopotential heights (gpm) at 500 hPa for the 5<sup>th</sup> (A), 7<sup>th</sup> (B), 10<sup>th</sup> (C), 11<sup>th</sup> (D), 12<sup>th</sup> (E) and 13<sup>th</sup> (F) of July. (Adapted from: NCEP, 2007). ..... 55

Figure 4-6: The MM5 prognosis of mean sea level pressure (hPa) on the 5<sup>th</sup> (A), 7<sup>th</sup> (B), 10<sup>th</sup> (C) and 14<sup>th</sup> (D) July 2004 at 0600 UTC (solid lines) and temperatures in °C (red lines). Contour intervals of the isobars are 3 hPa..... 57

Figure 4-7: The MM5 prognosis of 850 hPa geopotential heights (blue lines), winds (kt) and air temperatures (°C) on the 5<sup>th</sup> (A), 7<sup>th</sup> (B), 10<sup>th</sup> (C) & the 14<sup>th</sup> (D) of July 2004 at 0600 UTC. .... 58

Figure 4-8: The MM5 prognosis of the surface water vapor mixing ratio in g/kg (color contours) and the wind (kt) on the 10<sup>th</sup> (A) and 14<sup>th</sup> (B) of July 2004 at 0600 UTC..... 59

Figure 4-9: Regional maps showing the eastern coastal stations (A) and the western coastal stations (B) marked by red circles/ellipsoids. The three inland analyzed stations are marked by yellow circles/ellipsoids (B). ..... 60

Figure 4-10: The hourly temperature (blue) and dew point temperature (pink) in °C on the 5<sup>th</sup> of July 2004 at Seeb from 0100 UTC to 1400 UTC. The wind direction in degrees and time (UTC) is given below. .... 61

Figure 4-11: The hourly temperature (blue) and dew point temperature (pink) in °C on the 11<sup>th</sup> of July 2004 at Seeb from 0100 UTC to 1400 UTC. The wind direction in degrees and time (UTC) is given below. .... 61

Figure 4-12: The temperature (blue) and dew point (pink) in °C on the 5<sup>th</sup> (A), 7<sup>th</sup> (B) and 11<sup>th</sup> (C) at Al Foah from 0600 UTC to 1400 UTC. The wind direction in degrees and time (UTC) is given below. .... 63

Figure 4-13: The temperature (blue) and dew point (pink) in °C on the 5<sup>th</sup> (A), 7<sup>th</sup> (B) and 13<sup>th</sup> (C) at Jabal Hafeet from 0600 UTC to 1400 UTC. The wind direction in degrees and time (UTC) is given below. .... 65

Figure 4-14: The temperature (blue) and dew point (pink) in °C on the 5<sup>th</sup> of July 2004 at Hatta from 0600 UTC to 1400 UTC. The wind direction in degrees and time (UTC) is given below..... 66

Figure 4-15: The temperature (blue) and dew point (pink) in °C on the 6<sup>th</sup> of July 2004 at Hatta from 0600 UTC to 1400 UTC. The wind direction in degrees and time (UTC) is given below..... 67

Figure 4-16: The temperature (blue) and dew point (pink) in °C on the 10<sup>th</sup> of July 2004 at Hatta from 0600 UTC to 1400 UTC. The wind direction in degrees and time (UTC) is given below. .... 67

Figure 4-17: The temperature (blue) and dew point (pink) in °C on the 12<sup>th</sup> of July 2004 at Hatta from 0600 UTC ..... 68

Figure 4-18: Significant increase of dew point temperature over some stations during the day according to the northwesterly sea breeze on the 5<sup>th</sup> of July 2004. .... 70

Figure 4-19: Significant increase of dew point temperature over some stations during the day according to the northwesterly sea breeze on the 6<sup>th</sup> of July 2004. .... 71

Figure 4-20: The effect of the sea breeze (if any) on the dew point temperature during the study period at three selected stations. .... 72

Figure 4-21:	The observed time (UTC) of the dry airmass movement over the stations (from the northwest to the southeast) marked under the stations name.....	74
Figure 4-22:	Skew T diagrams at 0000 UTC on the 5 <sup>th</sup> of July 2004 (A) for Seeb & (B) for Abu Dhabi. (Adapted from: University of Wyoming, 2006).....	76
Figure 4-23:	Abu Dhabi sounding (Skew T diagram) at 1200 UTC on the 5 <sup>th</sup> of July 2004. (Adapted from: University of Wyoming, 2006).....	76
Figure 4-24:	Skew T diagrams at 0000 UTC on the 7 <sup>th</sup> of July 2004 (A) for Seeb & (B) for Abu Dhabi. (Adapted from: University of Wyoming, 2006) .....	77
Figure 4-25:	Skew T diagrams at 1200 UTC on the 7 <sup>th</sup> of July 2004 (A) for Seeb & (B) for Abu Dhabi. (Adapted from: University of Wyoming, 2006). .....	78
Figure 4-26:	Skew T diagrams at 0000 UTC on the 10 <sup>th</sup> of July 2004 (A) for Seeb & (B) for Abu Dhabi. (Adapted from: University of Wyoming, 2006).....	78
Figure 4-27:	Skew T diagrams at 1200 UTC on the 10 <sup>th</sup> of July 2004 (A) for Seeb & (B) for Abu Dhabi. (Adapted from: University of Wyoming, 2006).....	79
Figure 5-1:	The Skew T diagram at Seeb at 0000 UTC on 7 <sup>th</sup> of July 2004. (Adapted from: University of Wyoming, 2006).....	86
Figure 5-2:	The 850 hPa dew point temperature at 0000 UTC at Seeb from the 5 <sup>th</sup> to 14 <sup>th</sup> of July 2004.....	87
Figure 5-3:	The 700 hPa dew point depression at 0000 UTC at Seeb from the 5 <sup>th</sup> to 14 <sup>th</sup> of July 2004. ....	88
Figure 5-4:	Different LCL height (black line) of Seeb 0000 UTC soundings at 5 <sup>th</sup> (A) and 10 <sup>th</sup> (B) of July 2004. (Adapted from: RAOB, 2007).....	91
Figure 5-5:	The dew point depression using the average values in the lowest 50 hPa (blue) and surface values (red).....	92
Figure 5-6:	The dew point depression using the average values in the lowest 50 hPa (blue) and of the 700 hPa .....	93
Figure 5-7:	The 5 categorical statistics of KI of 22 (blue) and OCI of 36 (red). .....	95
Figure 5-8:	The OCI (blue) and the KI (red) during the study period (5 <sup>th</sup> -14 <sup>th</sup> of July 2004). The dashed lines are representing the considered threshold values of OCI (blue) and the KI (red). The marked NA, A and VA means Non Active, Active and Very Active respectively.....	96
Figure 6-1:	The 1000 and 850 hPa geopotential heights on the 11 <sup>th</sup> of July 2004. The deep low pressure over the Arabian Peninsula is clearly indicated at 1000 hPa (A) and at 850 hPa (B). .....	98

## List of Tables

Table 1-1:	Long term monthly average and the annual mean rainfall (mm) of Oman meteorological stations.	3
Table 2-1:	The geographic details of some of the Oman meteorological stations used in this study.....	11
Table 2-2:	The geographic details of some of the DAS weather stations used in this study.....	12
Table 2-3:	The contingency table.....	15
Table 3-1:	Flights summary of the 23 randomized seeding cases during the period (6 <sup>th</sup> -13 <sup>th</sup> )of July 2004. ...	46
Table 4-1:	The long term average, minimum and maximum values of the KI, Mean mixed layer mixing ratio (MXR) and Precipitable Water (PW) for the Seeb soundings at 0000 UTC.....	80
Table 4-2:	Sounding parameters of KI, Mean mixed layer mixing ratio (MXR), Precipitable water (PW) and the lifting condensation level (LCL) of Seeb sounding at 0000 UTC for the days 5 <sup>th</sup> -14 <sup>th</sup> of July 2004. The conditional instability for each day is also included along with the values of convective inhibition (CIN) and the convective available potential energy (CAPE).....	81
Table 5-1:	The long term average, maximum and minimum of the KI and its three terms.....	88
Table 5-2:	Average KI values for Non Active, Active and Very Active days for the June and July of .....	89
Table 5-3:	The contingency table of 83 days of different KI values with threshold value of 22.....	89
Table 5-4:	The long term average, maximum and minimum values of the OCI and its second and third terms. ....	93
Table 5-5:	Average OCI values for Non Active, Active and Very Active days for the June and July of 2005 and 2006.....	94
Table 5-6:	The contingency table of 83 days of different OCI values with threshold value of 36.....	94
Table 6-1:	Table of the convection forecasting techniques (TCFT) for predicting the convective storms over the Al Hajar Mountains. ....	98
Table 6-2:	The categories of the days' convection forecast according to the overall score of the TCFT.....	99
Table 6-3:	The TCFT application for the whole study period days (5 <sup>th</sup> -14 <sup>th</sup> of July 2004). ....	100

## Abbreviations

ADP	:	Active Day Period (0600-1430 UTC)
AGL	:	Above Ground Level
AMS	:	American Meteorological Society
MSL	:	Above Mean Sea Level
DAS	:	Department of Atmospheric Studies (UAE)
DGCAM	:	Directorate of Civil Aviation and Meteorology (Oman)
DWRS	:	Department of Water Resources (UAE)
hPa	:	Hectopascal (100 Pascals or 1 millibar)
HRPT	:	High Resolution Picture Transmission
ITCZ	:	Inter-Tropical Convergence Zone
KI	:	K-index (George's index)
KSA	:	Kingdom of Saudi Arabia
kt	:	knot (the unit of speed in the nautical system)
MRMEWR:		Ministry of Regional Municipalities, Environment and Water Resources
MSG	:	Meteosat Second Generation
MXR	:	Mean Mixed Layer Mixing Ratio
NCAR	:	National Center for Atmospheric Research (USA)
NCEP	:	National Center for Environmental Prediction (USA)
OCI	:	Oman Convection Index
RSA	:	Republic of South Africa
SSA	:	Seeding Study Area
UAE	:	United Arab Emirates
UCAR	:	University Corporation for Atmospheric Research (USA)
UKMO	:	United Kingdom Meteorological Office
UTC	:	Coordinated Universal Time
WVMR	:	Water Vapor Mixing Ratio

## Chapter 1 Introduction

### 1.1 Geography and climate of Oman

The Sultanate of Oman lies on the extreme southeastern edge of the Arabian Peninsula and is located between latitudes 16° 40' and 26° 20' North and longitudes 51° 50' and 59° 40" East. The Republic of Yemen is its southwestern neighbor, the Kingdom of Saudi Arabia (KSA) lies to the west, while the United Arab Emirates (UAE) lies to the northwest (Fig. 1-1). It extends along the extreme east of the Arabian Gulf, the west of the Gulf of Oman and Arabian Sea, with a coastline of about 3165 km (National Survey Authority, 2007) with several islands from the Strait of Hormuz in the north to the border of Yemen in the south. The total land area is approximately 309,500 km<sup>2</sup> and it is the third largest country in the Arabian Peninsula. The Sultanate is divided into four governorates (Muhafadhat) - Muscat, Dhofar, Musandam and Al Buraimy and five administrative regions: A'Dakhliyah; A'Dhahira; Al Batinah; Al Wusta and A'Sharqiya (Fig. 1-1). Each of these is subdivided into smaller districts called wilayats, which are governed by the Wali, the person responsible for the area and who reports to the Ministry of Interior.

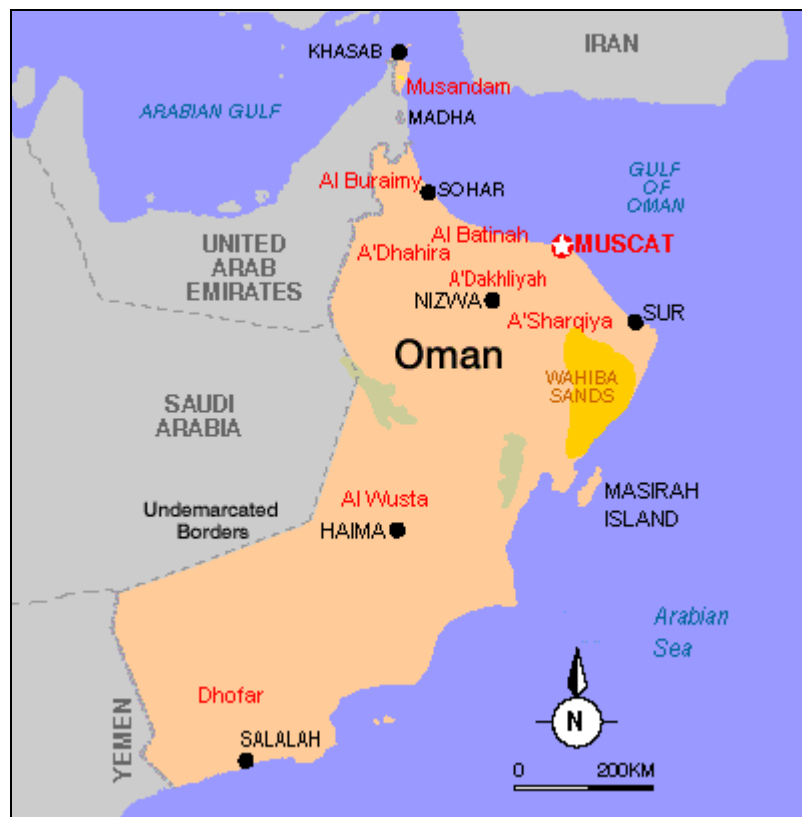


**Figure 1-1:** A regional map showing the position of Oman in the Arabian Peninsula. The map indicating the four governorates and the five administrative regions of Oman (red). (Adapted from: Network Overseas, 2007).



The topography of the Sultanate has a wide variation between the coastal areas (plains), mountain ranges, wadis (valleys) and deserts (Fig. 1-2). The Al Hajar (the Rocky) Mountains are a huge range of rocky mountains in an arc extending about 700 km southwards from the extreme north of the Sultanate (Musandam), curving eastwards towards the coast bordering the Arabian sea south of Sur (Ras Al Hadd). The highest peak, at about 3,075 m, is Jabal Shams (mountain of the sun) which lies in Al Jabal Al Akhdar (the Green Mountain) at the heart of the Al Hajar range. Around 82% of Oman consists of desert. Most conurbations arise on the coast. Like most of the Arabian Peninsula, Oman is characterized by an arid and semi-arid climate. The long coastline of Oman together with the high mountains causes significant rainfall over some elevated areas.

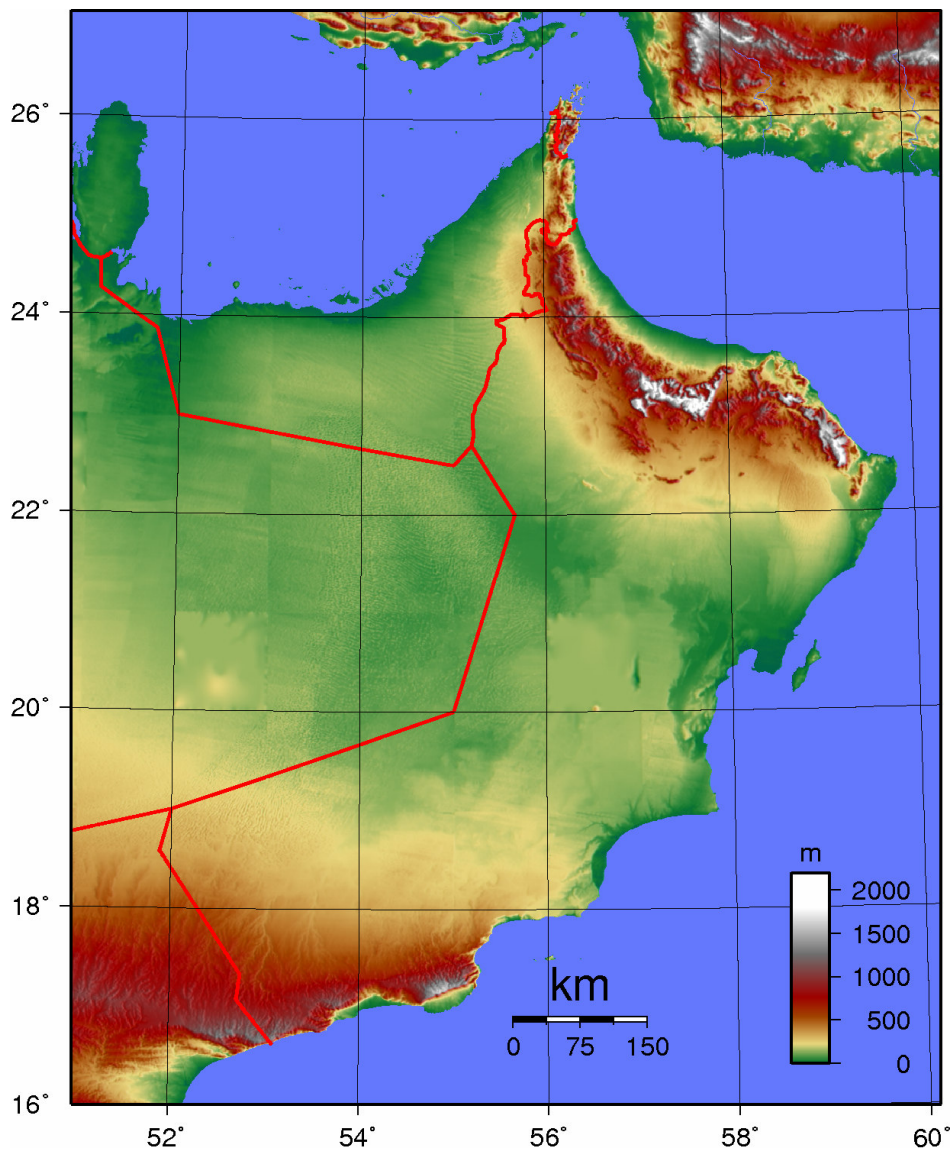


**Figure 1-2: The topography of Oman. (Adapted from: Wikimedia, 2007).**

Oman experiences two broad seasons (DGCAM, 1996). The summer extends from May to September and the winter from November to February. The change over season occurs during the months March, April and October.



## 1.2 The rainfall climatology over Oman

The variety of the topography along with the vast extent of the country provide different types of precipitation and make it vary both spatially and temporally. In general, there are four synoptic scale weather systems causing rainfall over Oman. The first one is the passage of the troughs originating in the North Atlantic and the Mediterranean Sea during the winter season. The second is the local development of thunderstorms over the Al Hajar Mountains over northern Oman during the summer. Thirdly, there is the monsoon (locally known as Khareef) from June to September over Salalah and its adjoining mountains. Finally, tropical cyclones/storms and easterly waves. Tropical cyclones/storms move in from the Arabian Sea during May/June and/or October/November (Bruitjes & Yates, 2003). Easterly disturbances move in from the Arabian Sea and Gulf of Oman and the oscillation of the Inter-Tropical Convergence Zone (ITCZ) between land and sea during the summer may also bring wet weather to the country. The rainfall data over the Sultanate are available with varying record lengths collected from the DGCAM meteorological stations network. Table 1-1 represent the long term monthly average and the annual mean rainfall of some of these stations.

Table 1-1: Long term monthly average and the annual mean rainfall (mm) of Oman meteorological stations.

STATION	JANUARY	FEBRUARY	MARCH	APRIL	MAY	JUNE	JULY	AUGUST	SEPTEMBER	OCTOBER	NOVEMBER	DECEMBER	ANNUAL MEAN	PERIOD TO 2002
KHASAB	50.0	46.7	41.0	9.3	0.8	0.0	0.7	2.5	0.0	1.1	7.0	42.8	192.0	1947
DIBA	0.0	0.2	8.1	0.0	0.0	0.9	0.0	0.0	0.0	0.3	10.7	0.8	21.2	2000
BURAIMI	7.6	22.5	16.9	6.0	2.2	1.0	11.7	2.9	3.0	0.3	0.0	9.6	77.3	1977
SOHAR	14.6	35.4	19.5	6.4	1.1	0.0	2.0	0.3	0.3	6.2	4.6	17.2	108.5	1980
SAIQ	20.3	40.3	51.9	34.2	27.3	15.5	49.2	55.3	26.3	1.2	6.6	10.0	349.1	1979
SEEB	13.0	17.6	15.5	9.9	2.5	0.5	2.7	1.4	0.0	0.7	4.7	11.1	79.5	1975
NIZWA	8.6	9.6	23.8	5.0	6.7	1.2	12.7	8.2	0.8	4.6	0.9	4.6	85.5	1989
FAHUD	0.6	5.2	4.8	4.8	0.0	0.0	0.9	2.1	0.3	0.3	0.0	0.5	17.8	1985
BAHLA	11.7	6.7	4.4	11.6	11.7	7.2	8.1	13.4	5.8	6.8	1.8	0.3	71.6	1998
IBRA	0.8	9.0	5.2	3.5	1.2	2.6	10.6	8.5	3.8	1.0	6.0	0.0	50.2	1998
SUR	13.5	21.8	15.4	8.9	1.5	4.0	2.7	2.4	0.0	1.7	7.1	9.3	87.1	1977
MASIRAH	5.0	7.9	10.6	10.1	1.0	12.6	4.2	2.2	0.1	1.3	2.6	5.4	62.9	1956
QARN ALAM	0.0	0.0	0.0	3.1	0.0	0.0	0.0	0.0	0.0	0.0	0.7	0.0	3.8	2000
THUMRAIT	0.3	3.6	8.2	10.1	1.0	5.7	0.1	2.8	0.0	0.9	0.0	0.4	33.1	1980
QAIROON	0.5	1.7	11.1	5.2	16.3	26.7	86.5	61.1	13.9	0.3	0.8	6.8	214.3	1984
HAIRITI														
SALALAH	1.2	3.2	5.0	10.2	10.6	7.9	25.8	26.1	3.6	5.8	4.5	3.8	107.7	1943

Source: DGCAM, 2002

Considering the long-term monthly average rainfall (Table 1-1), the northern stations (Khasab & Diba) and the coastal stations in the Gulf of Oman (Sohar, Seeb & Sur) received their highest rainfall during November to March. For example, the highest long term average monthly rainfall for Khasab is 50 mm in January, for Sohar it is 35.4 mm in February and for Seeb is 17.6 mm in February. It is clear that they receive maximum precipitation in winter as they are the first stations influenced by the passage of the winter troughs. The Al Hajar Mountains and adjoining areas (Saiq & Bahla) record their maximum rainfall during the summer due to the local thunderstorms. The highest long term average monthly rainfall for Saiq is 55.3 mm in August, for Bahla it is 13.4 mm in August. The southern stations affected by the summer monsoon like Salalah (26.1 mm in August) and Qairoon Hairiti (86.5 mm in July) show their precipitation maximum during the summer.

In general, the annual mean rainfall reaches a maximum over Al Hajar Mountains (about 350 mm at Saiq) and the minimum rainfall occurs over the desert (about 4 mm in Qarn Alam).

### **1.3 Synoptic weather systems over Oman**

#### **1.3.1 Low pressure systems/upper troughs during winter over Oman**

During the northern hemisphere winter a strong zonal flow exists over North Africa and the Mediterranean as a result of upper troughs or westerly depressions. Perturbations in this zonal flow lead to a succession of sinusoidal troughs and ridges steadily advancing from west to east, and the appearance of a low-pressure system at the surface is evidence of a trough in the upper troposphere (DGCAM, 1996).

Usually, low-pressure systems/troughs can be detected on upper-air charts at the 500 hPa level and occasionally deepening up to the 200 hPa level. They are usually more frequent during the months of December to February. When these troughs continue to occur during March, convective development often results over the northern mountains of Oman. On average four to five troughs occur per month during the winter period, although there is a marked variation from year to year (DGCAM, 1996).

Widespread dynamical induced rain may occur when a sharp trough exists over Oman extending to as far south as Yemen. At this time, a considerable amount of moisture is advected over the southeastern coast from the Arabian Sea and significant uplift occurs through forced ascent over the Al Hajar Mountains. Deep convection and thunderstorms with occasional heavy showers and sometimes accompanied by hail may develop if the atmosphere becomes potentially unstable. On some occasions, the low-pressure systems/troughs remain stationary over the country causing clouds and rain for several days.

However, it has to be stressed that the conditions described above are the exception rather than the rule and on many occasions the passage of an upper trough is identified only by patchy cloud conditions and a

surface wind shift accompanied by increasing surface pressure (DGCAM, 1996). On these occasions, widespread dust may occur due to the strong to gale force northerly winds which accompany a significant pressure rise over the region. The steep pressure –gradient-induced geostrophic wind causes the lifting of dust particles. (De Villiers & Van Heerden, 2007). The interior of Oman is mostly affected by this dust-raising northerly wind, known as 'Shamal' and this condition may continue for several days.

### **1.3.2 Monsoon (Khareef) over Salalah and adjoining areas**

The Salalah plane is a coastal area of about 50 km long and 12 km wide at the centre. The plane is bordered by mountains (known as the Dhofar Mountains) to the north with the highest peak at approximately 2000 m.

The Khareef, starts at Salalah and the adjoining mountain area (southern coast of Oman) from the last week of June and ends around mid September. As a result of the pressure gradient that exists between high pressure over the Arabian Sea and heat low pressure over the Empty Quarter, strong south to southwesterly winds affect the coastal waters of Dhofar & Al Wusta region during the summer months (DGCAM, 1996). The strong monsoon currents along the southeastern coast cause upwelling over the Arabian Sea lowering the sea surface temperature. This leads to the formation of ragged stratus accompanied by poor visibility in a solid bank of fog over the sea. Layers of persistent stratocumulus may be found above this stratus. The surface winds strengths over the Arabian Sea are between 30 to 40 kt, but over the Salalah plane, they are gentle southeasterly winds of 5 to 15 kt, veering southwest in the afternoon with a slight increase in velocity. Over the Dhofar Mountains the winds are always southerly during the monsoon with speeds of around 20 kt. There is not much difference between day and night temperatures during the Khareef and the air remains close to saturation. The average maximum temperature is 27 °C and the average minimum temperature is 23 °C. The average maximum humidity is 97% and the minimum 85%. The average dew point is at approximately 23 °C. Drizzle and/or light rain are the most frequent form of precipitation received over the Salalah plane and adjoining areas. Rainfall totals rarely exceeds 5 mm in a 24 hours period (DGCAM, 1996).

### **1.3.3 Tropical storms and cyclones**

There are two cyclone seasons namely the pre-monsoonal period (May-June) and the post-monsoonal period (October-November) respectively where tropical storms and cyclones may form over the Arabian Sea and the Indian Ocean (DGCAM, 1996). Most storms originate over the southeastern Arabian Sea in the vicinity of the Laccadive Islands, but some late season storms start over the southern Bay of Bengal and move westwards across southern India re-generating as they cross over the warm waters of the Arabian Sea (DGCAM, 1996). About one in three of these storms/cyclones approach the Arabian Peninsula, and statistics show that

storms/cyclones cross the Omani coast about once every three years. Only half of these storms are characterized as cyclones where the winds strength reaches 64-71 kt (DGCAM, 1996).

The latest tropical cyclone to have an impact on Oman was Gonu in June 2007. This storm was classified as a category five cyclone which weakened slightly to category four as it moved past the east coast of Oman on the 5<sup>th</sup> - 6<sup>th</sup> of June. Widespread devastation resulted in the northeastern parts of Oman and Muscat, the capital, had heavy rainfall, flash flooding, gale force winds and high waves. Jabal Asfar, in the mountains surrounding Muscat, recorded about 1000 mm of accumulated rainfall in 24-hrs on the 6<sup>th</sup> of June. Forty nine lives were lost and the estimated damage is set at approximately US\$ 4 billion (DGCAM, 2007). Prior to this, the last storm occurred in May 2002 and was named 01A. It crossed the coast south of Salalah in the morning of Friday the 10<sup>th</sup> of May 2002 and caused torrential rainfall over Muhafadhat Dhofar resulting in floods in Salalah city and 9 deaths resulted. Salalah reported 59 mm of rainfall on this day. The storm also caused significant rainfall to A'Dhahira, A'Dakhilia and Al Batinah Regions while Al Sahrqiya Region and Muhafadhat Muscat received light rain (DGCAM, 2002).

#### **1.3.4 Convective rain during summer over the Al Hajar Mountains**

During the summer season, convective development occurs over the Al Hajar Mountains. However, summer is characterized by mainly clear skies and high temperatures. The average summer maximum temperatures are in excess of 40 °C and this is associated with very high levels of humidity especially over the coastal areas. Even minimum temperatures (> 30 °C) are among the hottest in the world (DGCAM, 1996). The mean regional synoptic feature during the summer is a succession of thermal lows over the Empty Quarter of Oman and Saudi Arabia, Pakistan and northwestern India. These thermal lows contribute to the dynamics of the southwesterly circulation over the Indian Ocean and Arabian Sea, and are very closely associated with the development of the Indian monsoon system (DGCAM, 1996).

It is assumed that summer rainfall over the Oman Mountains is dominated by convection (Bruitjes & Yates, 2003). During the summer season, the ITCZ moves towards the southeast coast of the country. It may oscillate between land and sea causing some instability with convective clouds and showers. The ITCZ reaches its most northern most position over A'Dakhliya Region and the Al Hajar Mountains during July and August, where a low-level, relatively moist southeasterly flow from the Arabian Sea meets a dry northerly flow from the Arabian Gulf (DGCAM, 1996). The strong insulation over the Al Hajar Mountains may allow convection to break through the temperature inversion and convective clouds start to develop over the mountain peaks (DGCAM, 1996). Figure 1-3 is a good example of convection development over the Al Hajar Mountains. The convective clouds mostly covered the entire Al Hajar Mountains on the 10<sup>th</sup> of July 2004. Showers and thunderstorms are a regular occurrence over a relatively limited area of northern Oman. Moisture can also be advected via the northeasterly to easterly sea breeze from Gulf of Oman on hot sunny day. These storms normally occur and last

for a short period, generally taking place during the afternoon and clearing overnight. However, this short duration may be costly when the storms are accompanied with a sudden gust front, hail and flash floods especially over mountains and their adjoining areas.



**Figure 1-3:** The convection mostly covered the entire Al Hajar Mountains on the 10<sup>th</sup> of July 2004. (Adapted from: MODIS, 2007).

#### **1.4 Aims**

The aim of this research is to improve the forecasting of convective storms over the Al Hajar Mountains of the Sultanate of Oman but with special emphasis on those storms suitable for hygroscopic seeding. The research has the following objectives

- To determine how available real time data aid the forecasting of convection?
- To test the accuracy of the K-index (KI) in forecasting convection and to adjust it for local conditions.
- To develop objective techniques to improve the forecasting of convection over the Al Hajar mountains.
- To determine if the new techniques and the adjusted index can help to identify those storms suitable for hygroscopic seeding.

In order to achieve these objectives the following steps are applicable:

Chapter 2 discusses the different types of data used in this research.

In chapter 3, a brief introduction about the cloud seeding strategy is provided with emphasis on hygroscopic seeding. The UAE seeding project over the Seeding Study Area (SSA) is discussed as well as the

properties of the storms which developed over the Western Hajar Mountains. Radar and satellite images are used to describe the convection.

Chapter 4 discusses the data analysis and the results obtained. The period of 5<sup>th</sup> to 14<sup>th</sup> of July 2004 is discussed by utilizing surface observation data, upper air data from Seeb and Abu Dhabi and NWP data.

In Chapter 5, the KI is analyzed physically and statistically and it is shown how misleading it can be when forecasting convection over mountains. The KI is a convective index which considers the atmospheric lapse rate as well as the moisture content of the atmosphere through which the parcel will travel. A new index called 'Oman Convection Index (OCI)' is developed consequently from the KI to provide better prediction of convection. The OCI is similar to the KI in many respects but considers the moisture content very close to the surface of the earth to be more important. The OCI is also physically and statistically analyzed and tested on different cases.

Techniques for forecasting the seedable storms over the Western Hajar Mountains of Oman are then highlighted in chapter 6. The techniques were the result of the analysis in chapters 3, 4 and 5. The techniques show promising results.

Finally, a general conclusion and recommendations are listed in chapter 7 including the summary of results and findings.

## Chapter 2

## Data and Methodology

### 2.1 *Types of data*

The meteorological data used in this research were collected from Oman and the UAE with the upper air sounding data adapted from the University of Wyoming. Numerical Weather Prediction (NWP) data were obtained from the National Center for Environmental Prediction (NCEP) websites and MM5 model prognosis from the University Corporation for Atmospheric Research (UCAR). This data includes surface observations, upper air soundings, radar, numerical weather prediction (MM5) and reanalyzed synoptic charts. Satellite images of the MODIS and the Meteosat Second Generation (MSG) are also used to identify and analyze convection over the Al Hajar Mountains.

#### 2.1.1 *Surface observations*

For every case study discussed in chapter 4, the surface observations were collected from the available meteorological weather stations around the SSA. Hourly information was obtained from the Meteorological Terminal Aviation Report (METAR) format from manned and automatic weather stations that belong to DGCAM. Fifteen-minute data were also gathered from the UAE as reported by the automatic weather station network of the Department of Atmospheric Studies (DAS).

Essential observed parameters were studied in order to find guidelines to improve the forecasting of seedable storms. Those parameters are wind direction (in degrees true North) and speed (kt), temperature (°C), dew point temperature (°C), weather and cloud types observed at the station (when available) and the atmospheric pressure at the station (hPa).

##### 2.1.1.1 *Oman stations*

There were only three Omani stations inside the SSA (circles in Fig. 2-1). The coastal station Sohar (OOSH) is the eastern most station and is situated at Sohar City on the coast of the Gulf of Oman. Ibri (OOIB) lies close to the northern Al Hajar mountain range at Ibri City and at Al Buraimy City there is an automatic station (OOBR) close to the center of the SSA. Other stations were helpful to study like Seeb (OOMS) at Seeb International Airport and Saiq (OOSQ) at the top of the green Mountain on the Eastern Hajar Mountains. In Table 2-1 the geographic information about the Oman stations are provided.

From the table, the highest altitude station is Saiq located on the Eastern Hajar Mountains and the lowest is Sohar on the coast of the Gulf of Oman inside the SSA. Buraimi and Ibri stations are closer to the Western Hajar Mountains but both stations are lower than 300 m above mean sea level (MSL). Seeb station is a coastal station located to the southeast of the SSA at 8.4 m.



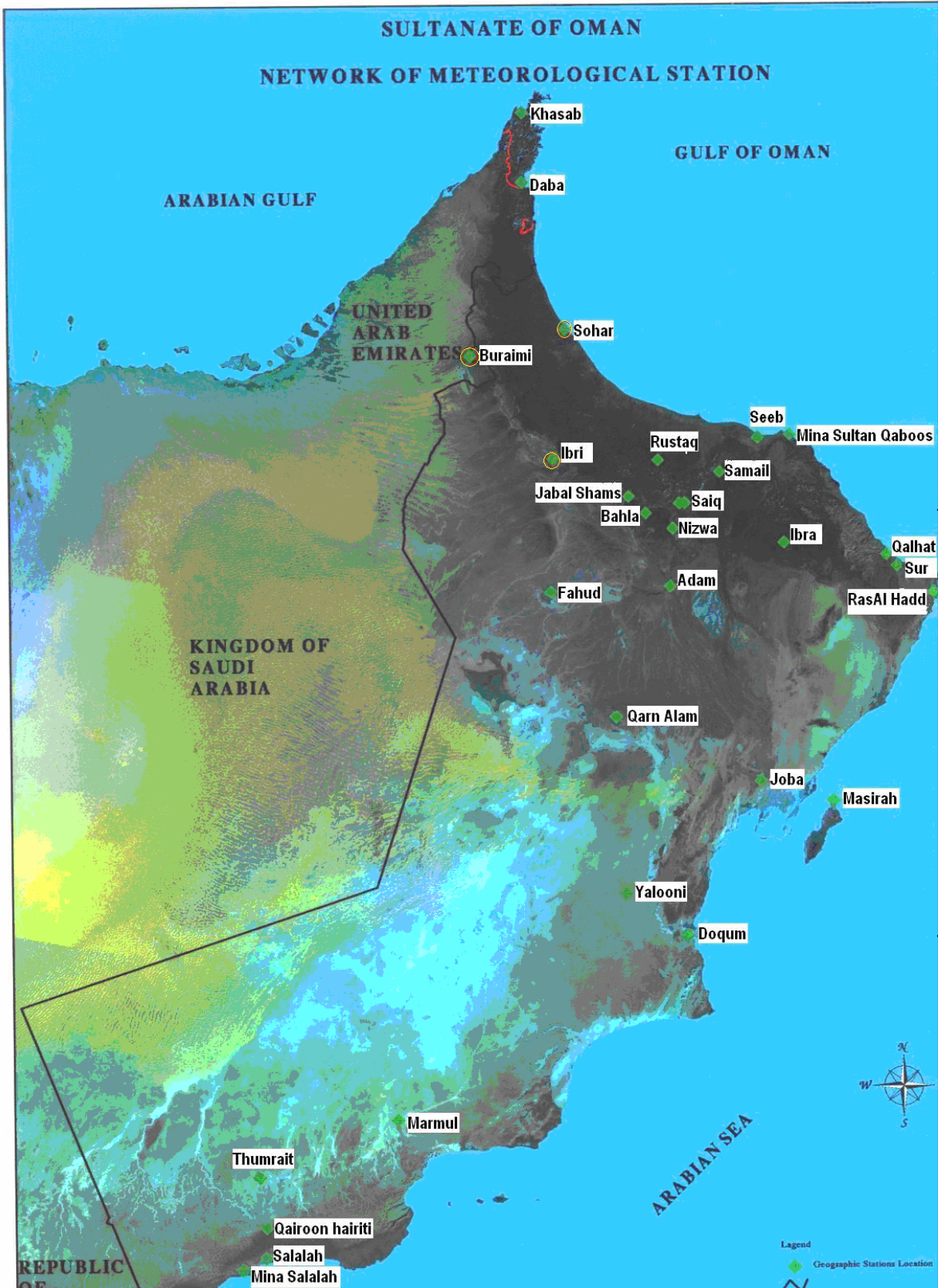


Figure 2-1: The network of meteorological station over Oman belongs to DGCAM (Adapted from: DGCAM, 2006).



**Table 2-1: The geographic details of some of the Oman meteorological stations used in this study.**

Station	Longitude (E)	Latitude (N)	Altitude (m)
Seeb	23° 35' 00"	58° 17' 00"	0008
Buraimi	24° 14' 29"	55° 47' 14"	0299
Saiq	23° 04' 29"	57° 38' 36"	1755
Ibri	56° 31' 00"	23° 25' 00"	0244
Sohar	24° 28' 10"	56° 38' 27"	0004
Source: DGCAM, 2002			

### 2.1.1.2 The UAE stations

DAS has a comprehensive network of automatic land stations over the UAE (Fig. 2-2). Data from most of these stations were used in this research. Table 2-2 provides the geographical location and the altitude of the stations used in this study. Of the 23 stations, Jabal Hafeet is the highest at about 1059 m. Other stations are located in mountain passes like Masafi (525 m) and Hatta (325 m). Many stations with different elevations are positioned around the mountains like Al Shiweb (306 m), Al Foah (335 m), Khatam Al Shaklah (433 m), and Al Saa (424 m). Abu Dhabi, Ghantuat and Al Samha stations are the lowest three stations (less than 40 m) located to the west of the mountains along the coast of the Arabian Gulf.

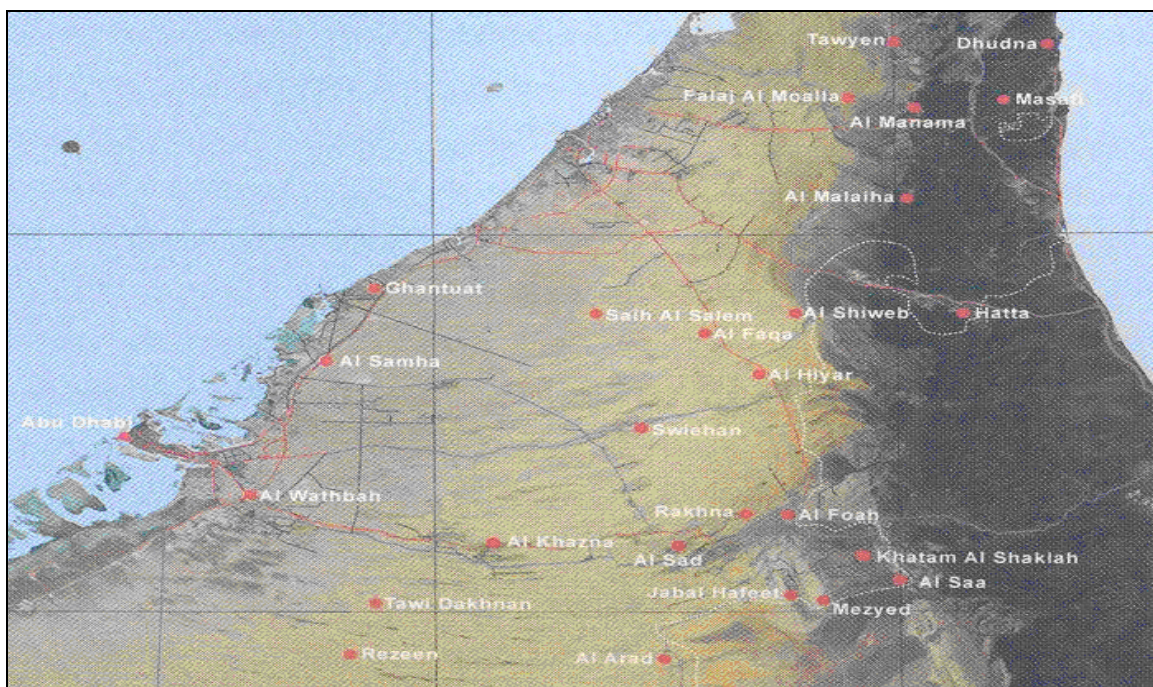


**Figure 2-2: Some of the DAS weather stations network 2003. (Adapted from: Annual Climate Report 2003, DAS).**

**Table 2-2: The geographic details of some of the DAS weather stations used in this study.**

Station	Longitude (E)	Latitude (N)	Altitude (m)
Abu Dhabi	54° 19' 44"	24° 28' 34"	007
Al Arad	55° 31' 27"	23° 50' 41"	212
Al Faqa	55° 37' 17"	24° 43' 08"	235
Al Foah	55° 48' 22"	24° 20' 02"	335
Al Hiyar	55° 46' 59"	24° 35' 55"	325
Al Khazna	55° 06' 02"	24° 09' 31"	170
Al Malaiha	55° 53' 17"	25° 07' 50"	150
Al Saa	56° 00' 38"	24° 05' 56"	424
Al Sad	55° 30' 44"	24° 12' 35"	199
Al Samha	54° 47' 18"	24° 42' 03"	035
Al Shiweb	55° 47' 53"	24° 46' 34"	306
Al Wathbah	54° 41' 57"	24° 10' 47"	063
Falaj Al Moalla	55° 51' 58"	25° 20' 16"	120
Ghantuat	54° 50' 34"	24° 53' 13"	029
Hatta	56° 08' 15"	24° 48' 40"	325
Jabal Hafeet	55° 46' 31"	24° 03' 24"	1059
Khatam Al Shaklah	55° 57' 07"	24° 12' 40"	433
Manama	56° 00' 31"	25° 19' 23"	200
Masafi	56° 09' 42"	25° 21' 32"	525
Mezyed	55° 50' 52"	24° 01' 43"	345
Rakhna	55° 42' 24"	24° 20' 38"	288
Saih Al Salem	55° 18' 43"	24° 49' 39"	105
Swiehan	55° 19' 53"	24° 27' 58"	170
Source: Annual Climate Report 2003, DAS.			

### **2.1.2 Upper air soundings**

The upper air data were obtained from Seeb in Oman and Abu Dhabi in the UAE. Although they are outside of the SSA, they are the only upper air sounding stations in the vicinity. Seeb (Muscat, OOMS) is located at Seeb International Airport and belongs to DGCAM. It is about 50 km east of Al Hajar Mountains, but more than 150 km from the nearest mountains in the SSA. One balloon is launched per day at 0000 UTC. In contrast, Abu Dhabi does two ascents per day at 000 UTC and 1200 UTC. Abu Dhabi soundings are done at about 120 km west of the nearest mountains in the SSA. Most of these data were collected from Department of Meteorology in

Oman and from the University of Wyoming upper air web site (University of Wyoming, 2006). The data are displayed in Skew T-log p (Skew T) diagrams in chapters 4 and 5.

### **2.1.3 Radar**

The radar images were captured from the main radar of the seeding project at Al Ain City by using the TITAN (Dixon and Wiener, 1993) software system. Al Ain Doppler radar was erected at the centre of the SSA with 5 cm wavelength operating in an automated volume-scan mode with the National Center for Atmospheric Research (NCAR) HiQ radar processor outfit. The scan parameters, initially planned for this radar (Jensen, 2004) are:

- PRF = 620 Hz (maximum range, 204 km).
- Pulse length = 0.8 us (120 m).
- Gate spacing = 240 m (850 range gates).
- Number of samples = 28.
- PPI scan rate at  $20^{\circ} \text{ s}^{-1}$  and set to complete a full  $360^{\circ}$  PPI before stepping up to next elevation.
- Elevation angles (deg): 0.5, 1.5, 2.5, 3.5, 4.5, 6.0, 8.0, 11.0, 15.0, 22.0 and 32.0.
- Resulting volume scan time, about 4:30 min.
- Volume repeat time set for 5 min.
- Latitude =  $24^{\circ} 26' 56''$ , Longitude =  $55^{\circ} 61' 97''$ , Altitude =  $\sim 280 \text{ m}$ .

For the study of the seeding experiments and its quantification, the experimental unit is the summertime convective clouds. Based on the results from Dixon *et al.* (1993), the reflectivity of threshold of 30 dBz was set in order to identify a seedable storm (UCAR, 2006).

### **2.1.4 The mesoscale model (MM5)**

The UAE MM5 was the NWP model used by forecasters during the cloud seeding project at DAS in Abu Dhabi. It has a regional, limited area non-hydrostatic, terrain following sigma coordinate. It provided a daily real-time forecast of weather conditions and the Clark-Hall model was used as a tool to describe the precipitation formation mechanisms.

The initial and boundary atmospheric conditions, including the  $1^{\circ}$  sea surface temperature (SST) data, were supplied by the 0000 UTC or 1200 UTC AVN global model.

MM5 has three nested domains. The first domain has a horizontal resolution of 30 km; the second has a one of 10 km and the third has 3.3 km. Each of the nested grids has 32 vertical levels and are two-way interactive during the simulations (Jensen & Ziady, 2006).

A 36-hour forecast was created once a day with the initialization time at 1200 UTC. The model prognoses were available in 3 hourly intervals. In this study, the forecast from the first domain (30 km) was utilized in order to capture the synoptic scale influences on the area. All the charts discussed in chapter 3 are the 18-hour forecast valid for 0600 UTC. This time was chosen to depict the model prognosis of the synoptic circulation before the onset of the thermal convection (UCAR, 2006).

### ***2.1.5 National Center for Environmental Prediction (NCEP) data***

The NCEP re-analysis data were used to produce general information on the synoptic scale over the whole region. In order to investigate the time of thermal convection, the 0600 UTC analysis of the NCEP data were used in all of the 10 cases in this research.

The NCEP data used here have a horizontal resolution of 2.5 degrees and have 17 pressure levels in the vertical. The surface pressure analysis over the area did not show any difference between the days of the period and hence not used in this study. Ultimately, only three pressure levels are used here. They are the 1000 hPa, 850 hPa (closest layer to the mountain heights) and 500 hPa geopotential heights.

This research focuses on mesoscale features and local convection. The NCEP data set is therefore inadequate to identify these features. However, a general view of the synoptic circulations is helpful to understand the mesoscale features which develop.

## ***2.2 Methodology***

Most of the clouds considered for seeding during the cloud seeding experiment developed over the Western Hajar Mountains. The most days with continuous convective storms were from the 6<sup>th</sup> to the 13<sup>th</sup> of July 2004. This ten day period was chosen partly because of the large number of seeding cases (23) which was preformed over the Al Hajar Mountains and the surrounding areas.

The radar and satellite pictures were used to identify the developed convective storms over the SSA during the study period. The synoptic conditions were analyzed for each day by studying the geopotential heights at different levels (1000, 850 and 500 hPa reanalyzed charts from NCEP). Then, the MM5 data was used to verify its capability of predicting the synoptic conditions by comparing the forecast with the actual conditions. After this the local conditions of the area were studied by analyzing the surface observations collected from the

weather stations. That was done in order to understand the impact of circulation on the local conditions over the area. The upper air data of Seeb and Abu Dhabi soundings were analyzed to find the main upper air characteristics on convective days. Some sounding parameters related to the instability and moisture were investigated and compared.

The KI is widely used by the Omani forecasters to predict the locally convective clouds over the Al Hajar Mountains. This index was analyzed physically and statistically to explain its limitations and misleading in forecasting convection over the mountains. The KI consists of three terms, lapse rate term, the dew point temperature at 850 hPa and the dew point depression at 700 hPa. Each term was discussed separately in section 5.2.1. A data set was created in order to test the ability of the KI to forecast convection over the Al Hajar Mountains. The statistical methods of *joint distribution* described by Ebert (2007) were used to verify the KI. Two way contingency tables (Table 2-3) were utilized and categorical statistical scores were calculated for a KI chosen threshold value.

**Table 2-3: The contingency table.**

		Observed		
		yes	No	Total
Forecast	yes	<i>hits</i>	<i>false alarms</i>	<i>forecast yes</i>
	no	<i>misses</i>	<i>correct negatives</i>	<i>forecast no</i>
	Total	<i>Observed yes</i>	<i>Observed no</i>	<i>total</i>

The four combinations of forecasts (yes or no) and observations (yes or no), known as *joint distribution* (Ebert, 2007), are:

- hit – convection forecast to develop, and did develop.
- miss – convection forecast not to develop, but did develop.
- false alarm – convection forecast to develop, but did not develop.
- correct negative – convection forecast not to develop, and did not develop.

The *marginal distribution*, the total numbers of observed and forecast developments and non-developments are shown in the shaded areas on the contingency table.

In this study, only five categorical statistics are used to describe the forecast performance, they are:

- Accuracy (fraction correct) which provides an overall correct forecast fraction, range from 0 to 1 with perfect score 1, and calculated by

$$Accuracy = \frac{hits + correct\ negatives}{total}$$

- Bias score (frequency bias) which gives an idea of how the forecast frequency of “yes” convection compare to the observed frequency of “yes” convection, range from 0 to infinity with perfect score 1, and calculated by

$$BIAS = \frac{hits + false\ alarms}{hits + misses}$$

- Probability of detection (hit rate) which provides the fraction of the observed “yes” convection was correctly forecast, range from 0 to 1 with perfect score 1, and calculated by

$$POD = \frac{hits}{hits + misses}$$

- False alarm ratio which gives the fraction of the predicted “yes” convection actually did not occur, range from 0 to 1 with perfect score 0, and calculated by

$$FAR = \frac{false\ alarms}{hits + false\ alarms}$$

- Probability of false detection (false alarm rate) which provides the fraction of the observed “no” convection were incorrectly forecast as “yes”, ranged from 0 to 1 with perfect score 0, and calculated by

$$POFD = \frac{false\ alarms}{correct\ negatives + false\ alarms}$$

Oman Convection Index (OCI) was developed consequently and also verified by the same methods.

Finally, a table of convection forecasting techniques (TCFT) was introduced for forecasting the seedable storms over the Western Hajar Mountains of Oman. The elements of this table considered all the results and findings obtained in this study.



## Chapter 3 Cloud Seeding Experiment and Convective Development

### 3.1 Introduction

In this chapter, an overview about the water resources in Oman and the feasibility of the cloud seeding solution is highlighted. The seeding project in the UAE and its experiments over the Al Hajar mountains in Oman airspace is briefly discussed. The hygroscopic seeding technique is discussed and the forecasting challenges detailed. Characteristics of the regional clouds and their amenability to the hygroscopic seeding according to the NCAR study at the UAE are then very briefly listed.

In this study, all the days of the period from the 5<sup>th</sup> to the 14<sup>th</sup> of July 2004 are considered as case studies in order to illustrate atmospheric conditions on the days when convective clouds developed over the Al Hajar Mountains and for the days when they did not. During this period, there was considerable change in the weather over the SSA. According to the researcher's experience during the seeding project in the UAE in 2004, the eight days from the 6<sup>th</sup> to the 13<sup>th</sup> of July were the longest period of continuous convection over the SSA during the entire summer of 2004. Many cloud seeding experiments were conducted on convective clouds mainly over the Al Hajar Mountains and the surrounding areas during this time.

This chapter provide a brief introduction on the observed convection during the study period (5<sup>th</sup>-14<sup>th</sup> of July 2004) as depicted by the radar images from Al Ain radar (Fig. 3-1) and some satellite images. For the purpose of this research, the following definitions apply:

- Non Active days: Refer to the days when no convective clouds were observed over the SSA.
- Active days: Refer to the days when convective clouds were observed over the SSA but only in isolated cells.
- Very Active days: Those are the days when numerous convective clouds developed over the SSA in multi-cellular convective systems.

The Very Active days were from the 10<sup>th</sup>-13<sup>th</sup> while the Non Active days were on the 5<sup>th</sup> and the 14<sup>th</sup>. The Non Active days are included in order to understand the difference in the atmospheric conditions between the Active and the Non Active days. The remaining days in this period are classified as Active days (6<sup>th</sup>-9<sup>th</sup>). Finally, a short discussion about the seeding cases during the study period is provided.

### **3.2 Cloud seeding in Oman**

Oman faces a water resources shortage. The persistent need for water is due to changes in climate, land use, a growing population, pollution, the economy and agriculture. The demand of water increases day by day. Most of the water resources used in the country, directly or indirectly, depends on the rainfall (Bruitjes & Yates, 2003). Oman has a unique traditional system of irrigation called "Falajs". Falajs are narrow, long channels mostly drilled under the mountains allowing the groundwater to flow under the ground towards the villages. Falajs and groundwater wells are mostly recharged by the run-off from mountains. Only minor direct recharge of water occurs over Al Batinah alluvial aquifers via rain falling directly on the plain and infiltrating this groundwater system. The coastal aquifers are hydraulically connected to the aquifers originating in the mountains. The intrusion of the underground seawater to the coastal and inland groundwater has become a serious problem as a result of the huge extraction of groundwater (Bruitjes & Yates, 2003). The Northern Omani Al Hajar Mountains lie close to the border with the UAE. This area is a very important source of ground water for both countries. Beyond the desalination of sea water and other projects like water recycling, a way of enhancing the rainfall over these mountains deserves thorough consideration. Weather modification may be applied and tried seriously in the country and should be viewed as a part of an integrated water resources management strategy (WMO, 2001).

After three years of extensive studies, it was found that no significant hydrological events took place in the UAE between 2001 and 2002. In fact, the Omani mountains were the only source of summer rainfall during this period. It, therefore, shows that summer convection over the Omani mountains does provide sufficient opportunities for rainfall enhancement and the clouds could be amendable to cloud seeding (Bruitjes & Yates, 2003; DWRS, 2002).

#### **3.2.1 Hygroscopic cloud seeding**

Weather modification research has been undertaken in many countries of the world during the past few decades. Two cloud seeding techniques namely glaciogenic, cold-cloud seeding by seeding material such as dry ice and silver iodide and the hygroscopic seeding or warm-cloud seeding with hygroscopic flares have been investigated. The glaciogenic seeding results were published by Krauss *et al.* (1987) and Mather *et al.* (1996). However, the most dramatic results were shown by the locally warm-cloud seeding experiments (Mather *et al.*, 1997).

An earlier cloud process intervention was made as a new approach to cloud seeding. When this new approach was suggested, Mather (1991) was doing routine microphysical measurements and he noticed that the coalescence was enhanced in a convective storm that ingested the emissions from a major paper mill. Clear differences between storms that grew in the vicinity of the paper mill and those not affected by this pollution source were indicated by radar studies. In response to this, the National Precipitation Research Programme in



South Africa developed a hygroscopic flare that could be used to deliver artificially generated cloud condensation nuclei (CCN) with a mean size of 0.5 micron to the base of developing storms.

These artificial CCN were intended to indirectly hasten rainfall through accelerating coalescence and droplet growth. Numerous experiments were designed in South Africa to test the developed flares impact on cloud processes. A five year randomized experiment that investigated the impacts of hygroscopic seeding on rainfall and subsequent experiments have evaluated the feasibility of operational seeding and its impact on rainfall from advanced analysis of radar data (Mather & Terblanche, 1993; Mather *et al.*, 1997; Terblanche *et al.*, 2000). All the experiments conducted so far have shown in a compatible manner that the radar determined rain mass of seeded storms is significantly more than of the control storms. Producing water by earlier condensation implies greater loading of the updrafts by larger particles with a related increase in the downdrafts. It is this invigorated storm outflow that probably undercuts more of the surrounding warm air to trigger new more vigorous cloud growth on the flanks of the treated storm; thus extending the life of the storm (Mather *et al.*, 1997). The South African studies have also been analyzed by independent international experts who confirmed the findings (Biggs, 1997; Silverman, 2000). In addition, the South African randomized hygroscopic seeding experiment and its results were also duplicated in Mexico under the guidance of NCAR scientists. The South African developed hygroscopic flare seeding technology has been labeled as one of the most significant advancements in weather modification (Orville, 1995).

It was found that not every convective storm can be amended for the hygroscopic seeding in order to enhance its rainfall. A randomized seeding experiment with flares, that produce very small hygroscopic particles in the updraft regions of continental, mixed-phase convective clouds, has produced evidence of a modified, more effective droplet spectrum near cloud base that enhances the formation of large drops early in the lifetime of the cloud (AMS, 1998). In general, isolated, convective cells (cauliflower-like growing cloud bubbles aloft) with a solid and low cloud base (lower than 4570 m) and a considerable updraft (at least  $1-2 \text{ m s}^{-1}$ ) can be treated via hygroscopic seeding to increase their rainfall (DWRS, 2004). The updraft or the thermal strengths are classified as nil ( $0 \text{ m s}^{-1}$ ), weak ( $\leq 1.5 \text{ m s}^{-1}$ ), moderate ( $>1.5 \leq 3 \text{ m s}^{-1}$ ) or strong ( $>3 \text{ m s}^{-1}$ ) (UKMO, 1997). A crucial part of the cloud seeding experiment is to be able to predict convective cloud with these characteristics. Generally most of the summer convective clouds over the Al Hajar Mountains have characteristics amenable to the hygroscopic clouds seeding (DWRS, 2002).

A collaborative program between the Department of Water Resources Studies (DWRS) (now known as Department of Atmospheric Studies (DAS)) in the UAE, the University of the Witwatersrand in RSA, the South African Weather Service in RSA and the NCAR in USA was implemented during the summer of 2003. This program aimed to investigate the feasibility of rainfall enhancement over the Omani mountains by means of hygroscopic cloud seeding. The SSA was chosen to be the area inside a circle of about 150 km radius centered at Al Ain city. The SSA covers a large part of the northern Omani mountains or the Western Hajar Mountains as

well as most of the central and northern parts of the UAE. A weather radar was erected at Al Ain airport and data available from the radar covers the SSA (Fig. 3-1). The radar studies show that the vast majority of convective storms occurred over the Oman mountains (DWRS, 2002). The radar data provides a unique opportunity to investigate the characteristics of thunderstorms over the area.

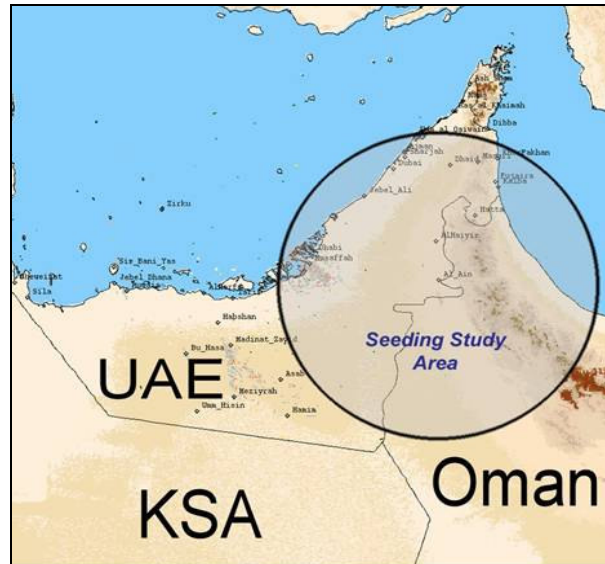


**Figure 3-1:** The Seeding Study Area (SSA) with Al Ain radar coverage denoted by range rings. The radius of the radar coverage areas is about 150 Km, with Al Ain near the centre of the site. (Adapted from: DWRS, 2003).

One crucial fact that must be noted here is that the type of mesoscale convective weather system suitable for seeding is very difficult to forecast since the life time of the storms is very short and many of them last in the order of 20 to 30 minutes (Jensen *et al.*, 2003). This makes it very difficult to observe these storms by conventional means, *i.e.* the weather and cloud observations from weather stations. Even the 15 minute images, available on the recently launched of Meteosat 8, will sometimes not be able to capture the development of the storms adequately. Due to the complicated logistics and astronomical cost involved in the cloud seeding experiment, it is crucial that timely and accurate forecasts are made of these mesoscale storms. Moreover, an accurate forecast of these weather systems is essential to the success of the cloud seeding experiment (DWRS, 2002).

Bruintjes & Yates (2003), from NCAR, has submitted a report to the Sultanate government assessing the potential of cloud seeding to enhance rainfall in the Sultanate of Oman. Their initial findings suggested to the Ministry of Regional Municipalities, Environment and Water Resources (MRMEWR) that research should be focused on determining the suitability of hygroscopic cloud seeding over Oman. They also recommended close collaboration with the Department of Meteorology in Oman. There is no clear decision yet if this research will be funded soon by Oman. However, if the project goes ahead, the whole Al Hajar Mountains will be part of the

seeding project and special instruments, like radars and other essential project infrastructures, shall be made available in the country. Although the government hasn't made a decision, the research in the UAE continued in the summer 2004 and this research contributed to developing forecasting techniques for the storms over the Omani mountains.

### ***3.2.2 Characteristics of the regional clouds and their amenability to the hygroscopic seeding***

In its study (DWRS, 2002) of the rainfall enhancement and air chemistry during 2001-2002 over the UAE, NCAR identified the main observed characteristics of the clouds over this area including the clouds developing over the Western Hajar Mountains of Oman. Hundreds of flights were made during these two years field seasons to take some measurements of the microphysical characteristics and precipitation processes in the clouds in this region. This was done in order to find how amenable the clouds were to seeding with hygroscopic flares. The results show that the summer clouds were found suitable for seeding because mostly all clouds were convective in nature.

The regional clouds were classified into two categories namely convective and stratiform. This was further subdivided into eight cloud types. They are boundary layer cumulus (low cloud base with small vertical development), towering cumulus (low to mid-level cloud base with large vertical development), cumulonimbus (a cloud exhibiting thunder or lightning), altocumulus (mid-level cloud bases with small vertical extent), stratus (low cloud base and stratiform), stratocumulus (stratus exhibiting convective elements), altostratus (high cloud base and stratiform), and altostratus or altocumulus (altostratus exhibiting convective elements) (DWRS, 2002).

The dominant clouds during the summer were boundary layer cumulus and deeper cumulus with relatively high bases (3000-4000 m AGL). The main forcing mechanisms of these clouds are the orographic lifting by the Al Hajar Mountains and convergence of mesoscale boundaries (DWRS, 2002). The convective growth of these clouds was regularly stunted by the thermal inversion at mid-levels but that did not stop the strong convection from developing.

### ***3.3 Observed convection***

This research will focus on the atmospheric conditions from the 5<sup>th</sup> to the 14<sup>th</sup> of July 2004. These days were all part of the cloud seeding experiment detailed above and due to the significant convection over the Al Hajar Mountains many cloud seeding cases were concluded during this period. A brief introduction is provided here on the convection as observed by the radar located at Al Ain (Fig. 3-1). Some comments made by the cloud seeding team members are also included.

Convective storms were observed over Al Hajar Mountains from the 6<sup>th</sup> (Fig. 3-2) with a gradual increase in their intensity and quantity until the 13<sup>th</sup> of July. The radar images confirmed that the best days of active storms were from the 10<sup>th</sup>-12<sup>th</sup> of July. Although there were no radar images for the 13<sup>th</sup> satellite data were utilized to confirm the presence of convective clouds of this day (Fig. 3-36A). The atmosphere on the 5<sup>th</sup> and the 14<sup>th</sup> of July was dry over the SSA. However, on the 14<sup>th</sup> some clouds developed over the Eastern Hajar Mountains outside the boundaries of the SSA to the south (Fig. 3-36B).

Most of the storms over this area are relatively short-lived. However, occasional long-lived multi-cellular systems exist and produce a large fraction of the total precipitation from summer storms (Breed *et al.*, 2005). From the 6<sup>th</sup> to the 8<sup>th</sup> of July, the storms developed late (after 1000 UTC) and to the west of the mountain peaks over surface wind convergence zones. They were isolated, not intense and short-lived when compared with the storms which developed on the following days. On the 9<sup>th</sup> of July, the storms formed earlier (around 0800 UTC) starting over the mountains peaks and later moved to the west (Fig. 3-13). On the 10<sup>th</sup>-13<sup>th</sup> of July, the storms became very intense, long-lived and active multi-cellular systems.

### **3.3.1 The 6<sup>th</sup> of July**

The radar showed the first echo of a storm (storm A) over the mountains east of Al Hiyar station (Fig. 3-2) at 1012 UTC with reflectivity of less than 20 dBz.

The wind observations around the convection area 12 minutes before indicated the convergence zone created by the wind circulations are also shown in the same Figure. The sea breeze from the Gulf of Oman travelled all the way from the east and propagated through the mountains to converge with drier westerly wind. The area of wind convergence is represented by an elliptical shape (Fig. 3-2). After one hour, the storm intensified to almost 40 dBz (Fig. 3-3).

Another cell developed at 1127 UTC just south of the previous one. After 10 minutes, the reflectivity of this cell was 40 dBz. Later on the day (1330 UTC), another favorable area for wind convergence was southeast of Al Saa (Fig. 3-4) where another cell developed. This cell (storm B) moved to the west with a reflectivity of about 40 dBz at 1407 UTC (Fig. 3-5).

Although it was not a Very Active day, it was the first day of the convection over the mountains during the study period. Storm A (Fig. 3-3) was used in the cloud seeding experiment by the research team. The seeding team noticed moderate convection with light rain during their operation through this storm. The research flight also reported a cloud base at 3660 m and the updraft was moderate.

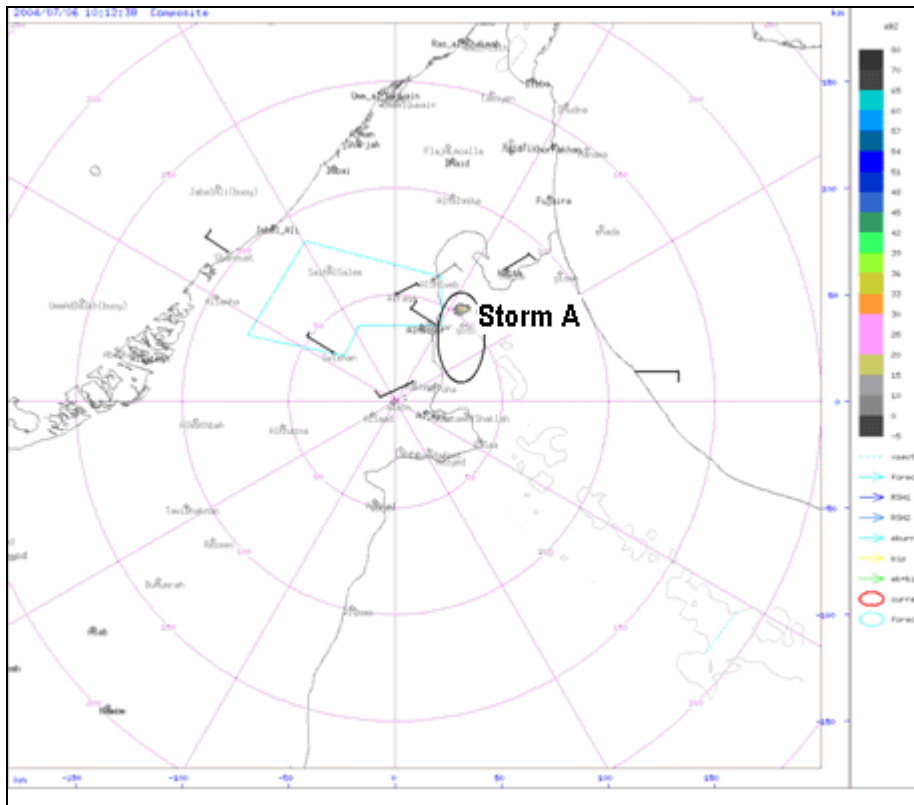


Figure 3-2: Radar reflectivity (dBz) on the 6<sup>th</sup> of July 2004 at 1012 UTC. The wind vectors are surface observations at 1000 UTC.

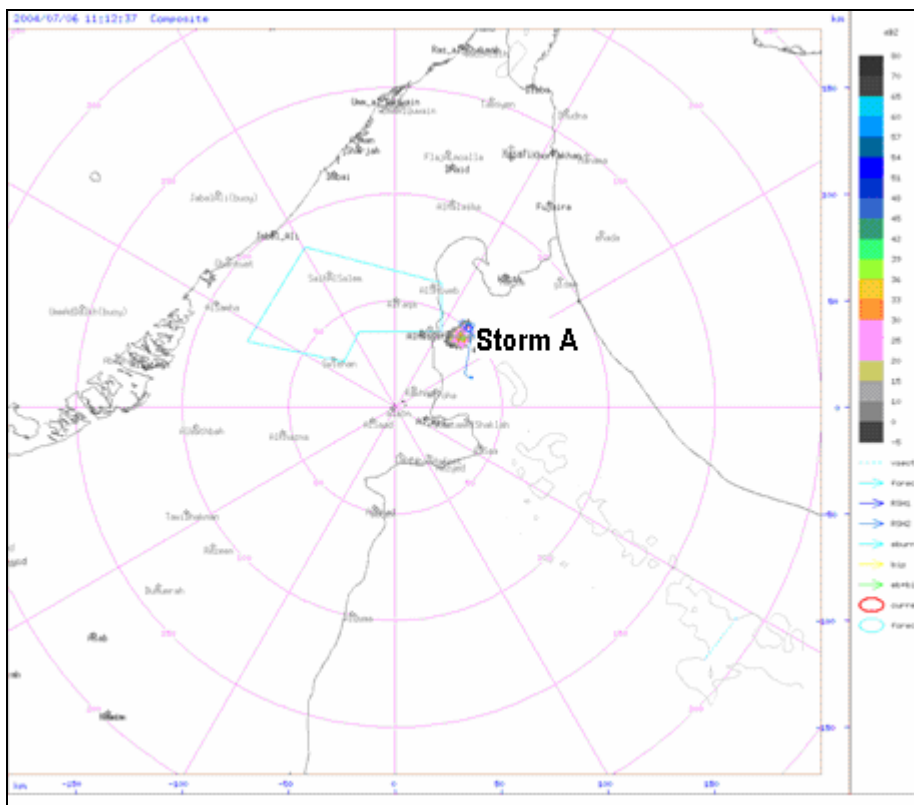


Figure 3-3: Radar reflectivity (dBz) on the 6<sup>th</sup> of July 2004 at 1112 UTC.

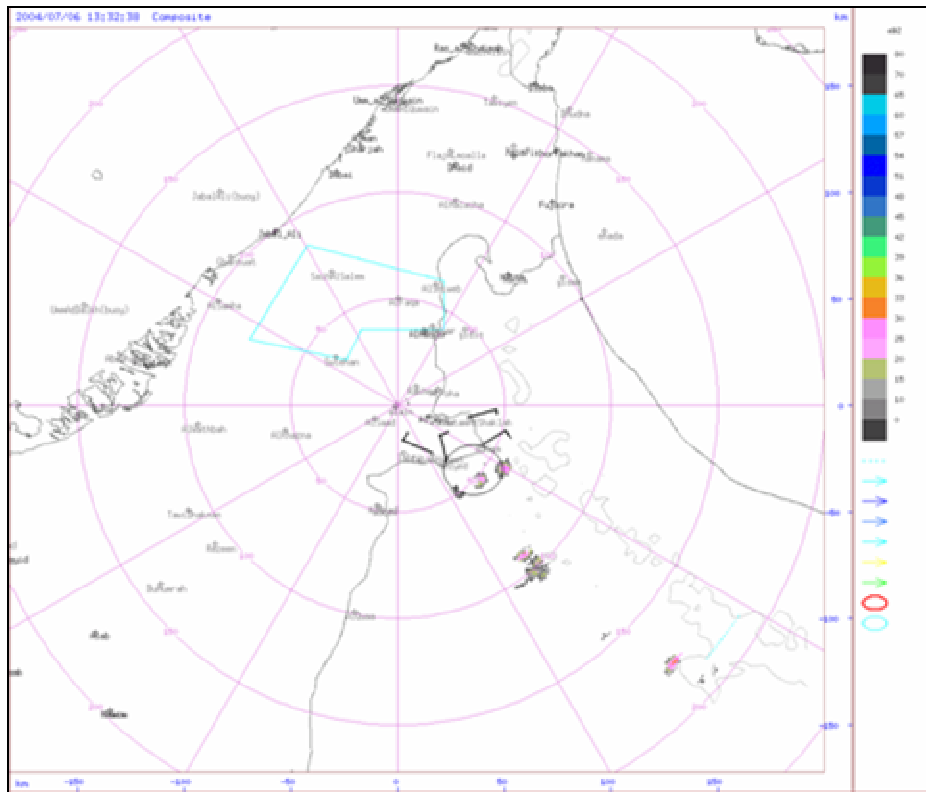


Figure 3-4: Radar reflectivity (dBz) on the 6<sup>th</sup> of July 2004 at 1332 UTC. The wind vectors are surface observations at 1330 UTC.

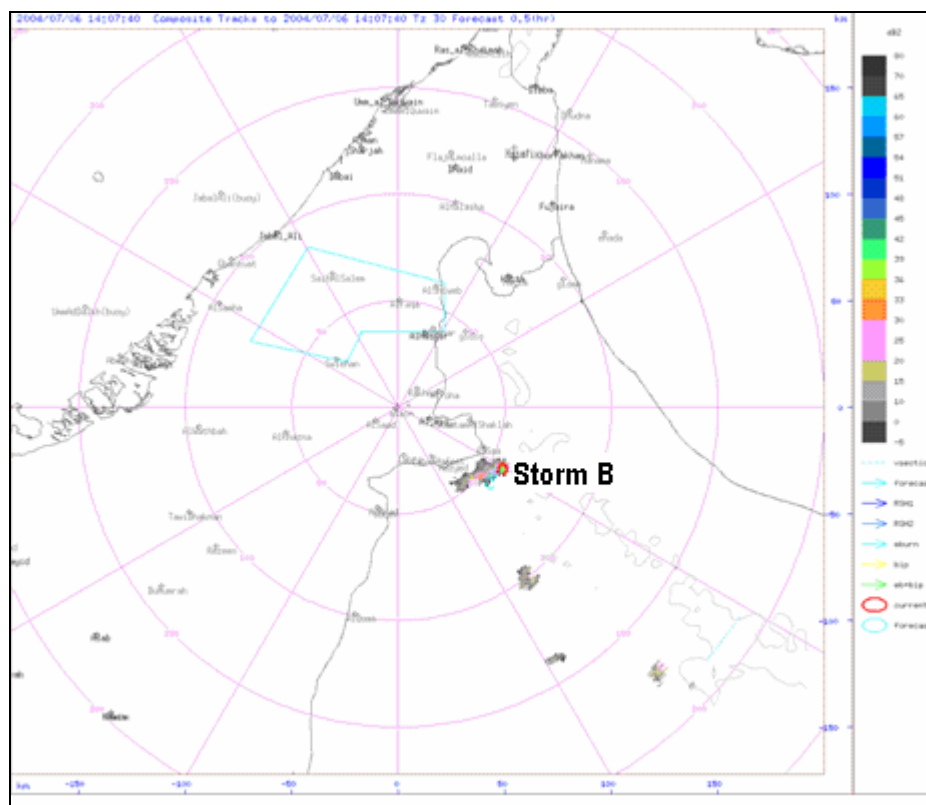
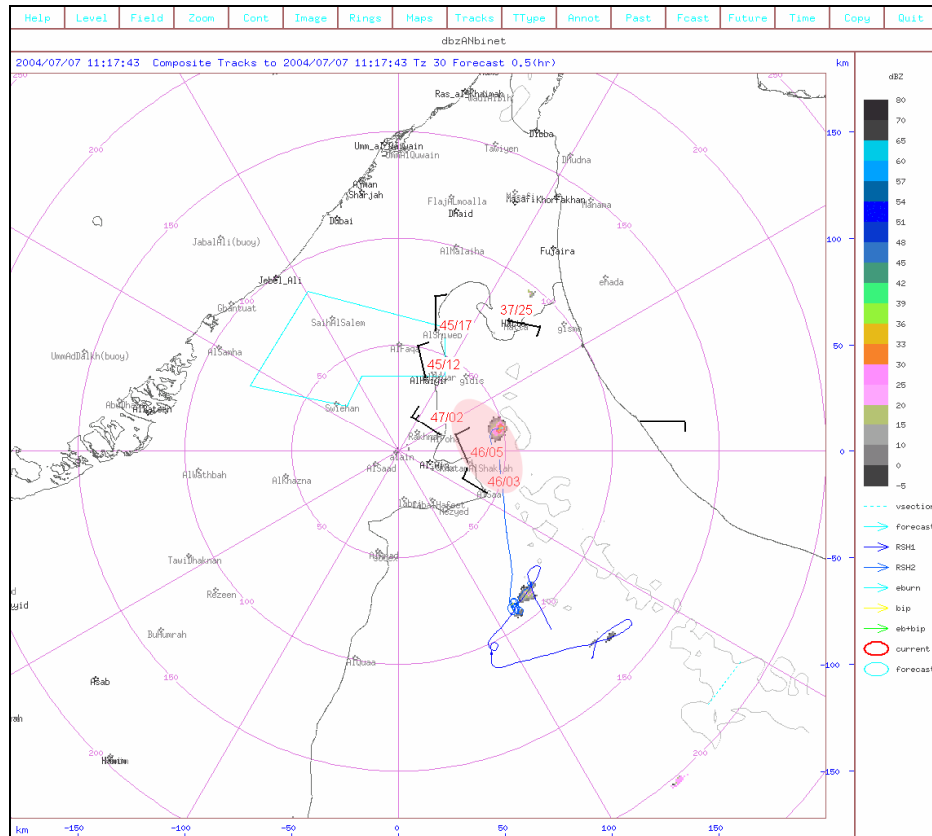


Figure 3-5: Radar reflectivity (dBz) on the 6<sup>th</sup> of July 2004 at 1407 UTC.

### 3.3.2 The 7<sup>th</sup> of July

The first echo was observed at 1007 UTC about 100 km southeast of Al Ain with a reflectivity of 30 dBz. An hour later at about 1117 UTC, another storm started to develop just 50 km east of Al Ain (Fig. 3-6).

The surface wind, temperature and dew point temperature observations at 1115 UTC were also included in this Figure. The surrounding surface temperatures were above 45 °C. These hot conditions enhance convective development.



**Figure 3-6: Radar reflectivity (dBz) on the 7<sup>th</sup> of July 2004 at 1117 UTC. The wind vectors, temperature and dew point values are surface observations at 1115 UTC while the pink shaded area indicates the estimated convergence zone.**

The wind circulation in Figure 3-6: suggests a favourable wind convergence zone (marked by a pink shadow area) where most of the convective clouds developed later as can be seen in Figure 3-7:.

At 1247 UTC, there was another storm that developed at about 70 km southeast of Al Ain which lasted for an hour. At 1317 UTC, the maximum reflectivity of this storm was about 40 dBz (Fig. 3-8).



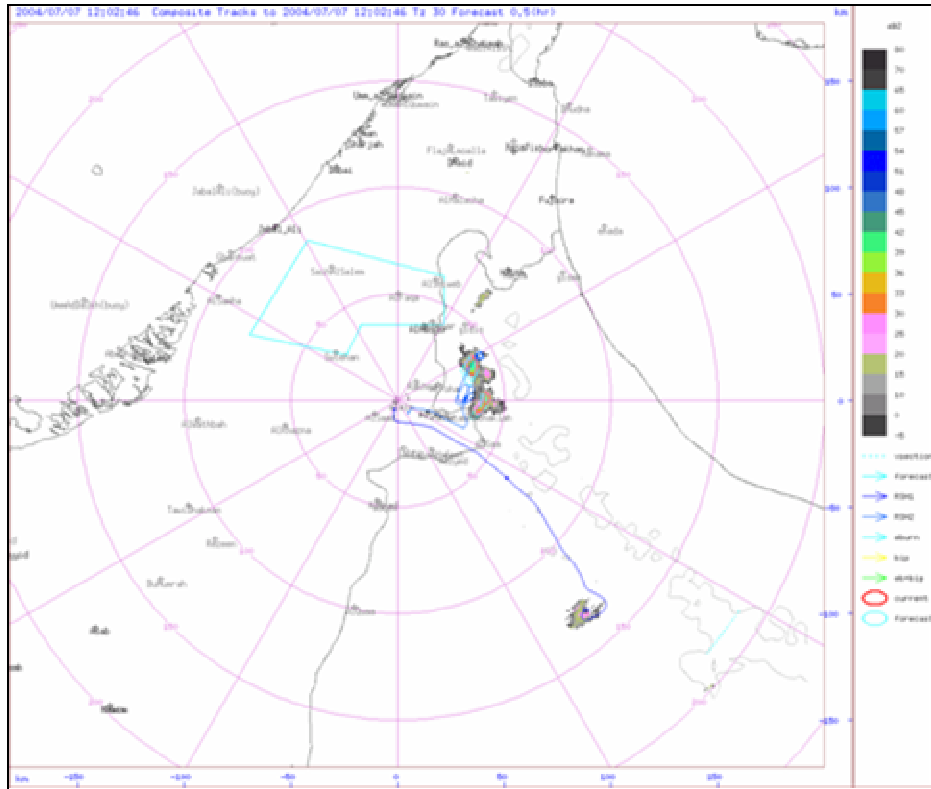


Figure 3-7: Radar reflectivity (dBz) on the 7<sup>th</sup> of July 2004 at 1202 UTC.

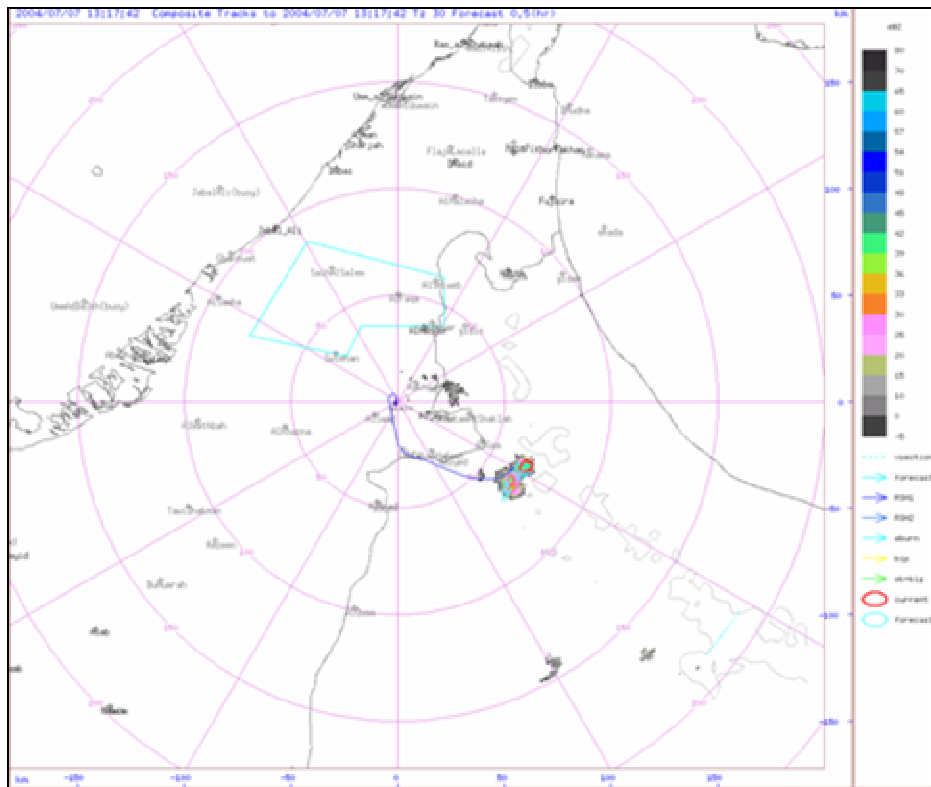
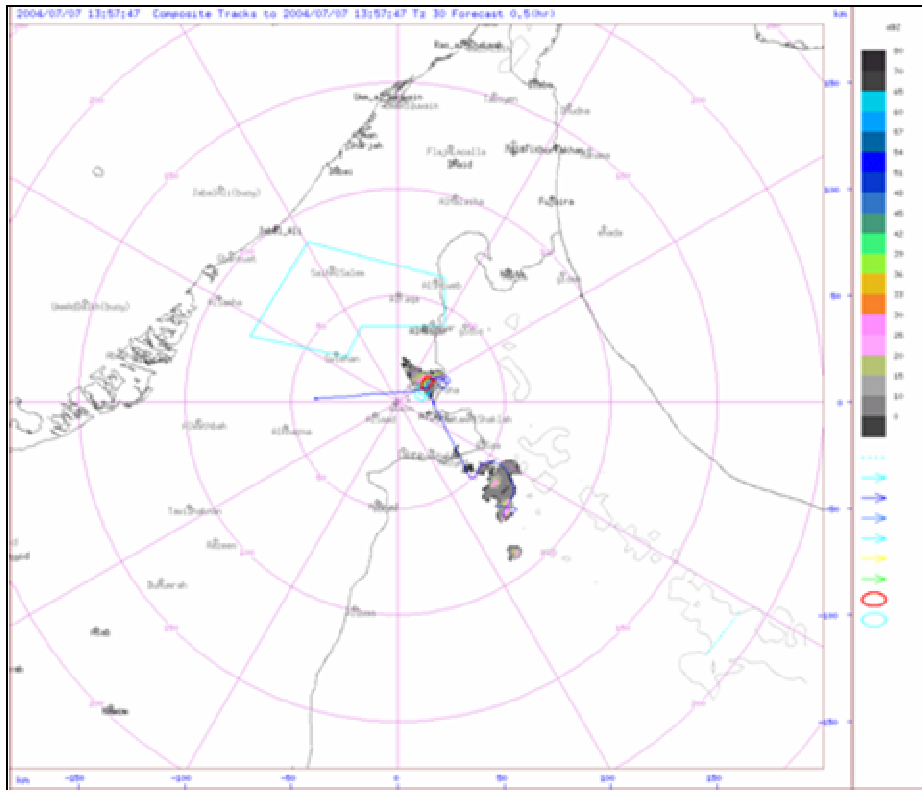


Figure 3-8: Radar reflectivity (dBz) on the 7<sup>th</sup> of July 2004 at 1317 UTC.



The convergence zone (Fig. 3-6) east of Al Ain remained the preferred area for convection until about 1400 UTC (Fig. 3-9).



**Figure 3-9: Radar reflectivity (dBZ) on the 7<sup>th</sup> of July 2004 at 1357 UTC.**

On this day storms moved to the south or southwest and the steering winds at 500 hPa were northeasterly. In this study the winds at 500 hPa were considered to determine the movement of the convective cells (steering winds). The UKMO (1997) defines the height of the steering winds at a third above the cloud base height

$$H_{base} + \frac{1}{3} (H_{top} - H_{base})$$

Typical values from the Seeb sounding as well as pilot observations as noted in Table 3-1 indicates that 500 hPa is the appropriate steering wind level.

The storm in Figure 3-6 was chosen for the cloud seeding experiment. The seeding team noticed weak updrafts which improved to medium updrafts later and two seeding cases were done. The cloud base height varied between 3660 and 4115 m. Another research aircraft was present southeast of Al Ain, where some shallow convection started earlier. They noticed a cloud base at 3960 m and a lot of ice was present in the clouds. The storm in Figure 3-8 was investigated for the possibility of seeding but although the cloud base decreased to 3050 m MSL, no updraft was found and the cloud dissipated. They were able to see the gust front of this storm and rain reaching the ground.

### 3.3.3 The 8<sup>th</sup> of July

The storms developed after 1015 UTC at the same location as on the 7<sup>th</sup> of July (Fig. 3-6) to the mountains at about 90 km southeast of Al Ain.

Storm A was weak on the 1027 UTC volume scan with a dBz of 30 (Fig. 3-10). However, it was enough to attract both research aircraft into the area. A few cells developed over the mountains southeast of Al Ain.

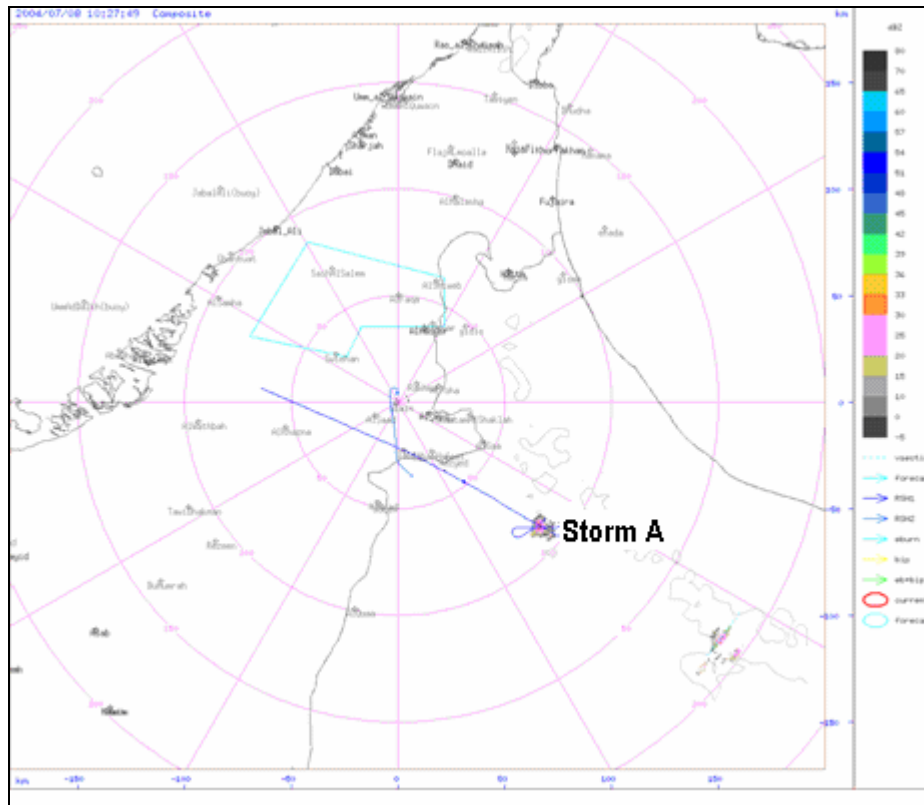
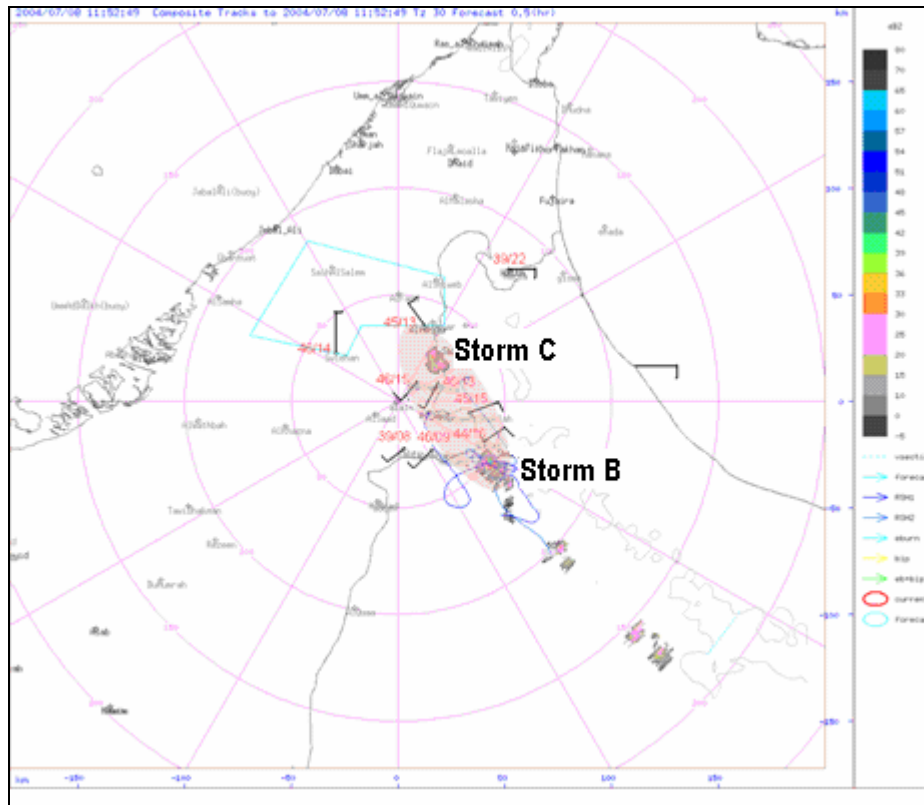


Figure 3-10: Radar reflectivity (dBz) on the 8<sup>th</sup> of July 2004 at 1027 UTC.

The surface wind convergence is shown by the pink color in Figure 3-11. The observations are valid for 1145 UTC, approximately 10 minutes before the radar image.

The Figure shows a 40 dBz storm (storm B) located about 50 km southeast of Al Ain inside the convergence zone and another storm (storm C) about 25 km northeast of the radar centre. Other individual cells also developed inside the shaded area in Figure 3-11.

The storms southeast of Al Ain were treated by the research team. The seeding team noticed that there was a rain shaft present during seeding, weak updrafts and no lightning. The clouds base height varied between 3290 and 3535 m.



**Figure 3-11:** Radar reflectivity (dBz) on the 8<sup>th</sup> of July 2004 at 1152 UTC. The wind vectors, temperature and dew point values are surface observations at 1145 UTC while the pink shaded area indicates the estimated convergence zone.

### 3.3.4 The 9<sup>th</sup> of July

Convective clouds started to develop much earlier on the 9<sup>th</sup> of July with the first storms being noticed by 0800 UTC. This storm intensified to a dBz of 40 about 30 minutes later (Fig. 3-12).

The convergence zones at about 1000 UTC are indicated in Figure 3-13. Storms developed later in these convergence zones (Fig. 3-14 & Fig. 3-15).

The winds at the steering level were light northeasterly at Seeb 1200 UTC sounding, to southeasterly at Abu Dhabi one. So most of the storms developed and collapsed at the same area or drifted slowly to the west or southwest.

Storm A (Fig. 3-13) was chosen for the cloud seeding experiment. The pilots observed a cloud base height at 2440 m ASL. Initially light rain was observed but this increased to heavy rain and lightning. The other research aircraft flew to treat storm B east of Al Ain (Fig. 3-13). They noticed that most clouds had ragged bases with heights varying between 9895 and 3355 m and the updraft was weak to nil.

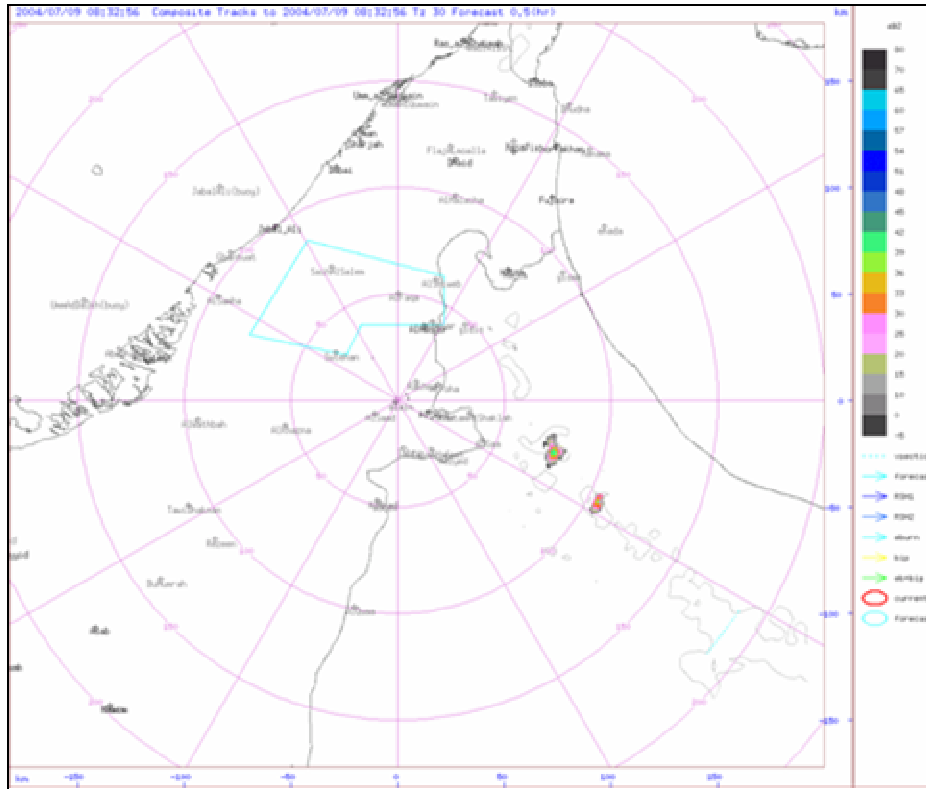


Figure 3-12: Radar reflectivity (dBz) on the 9<sup>th</sup> of July 2004 at 0832 UTC.

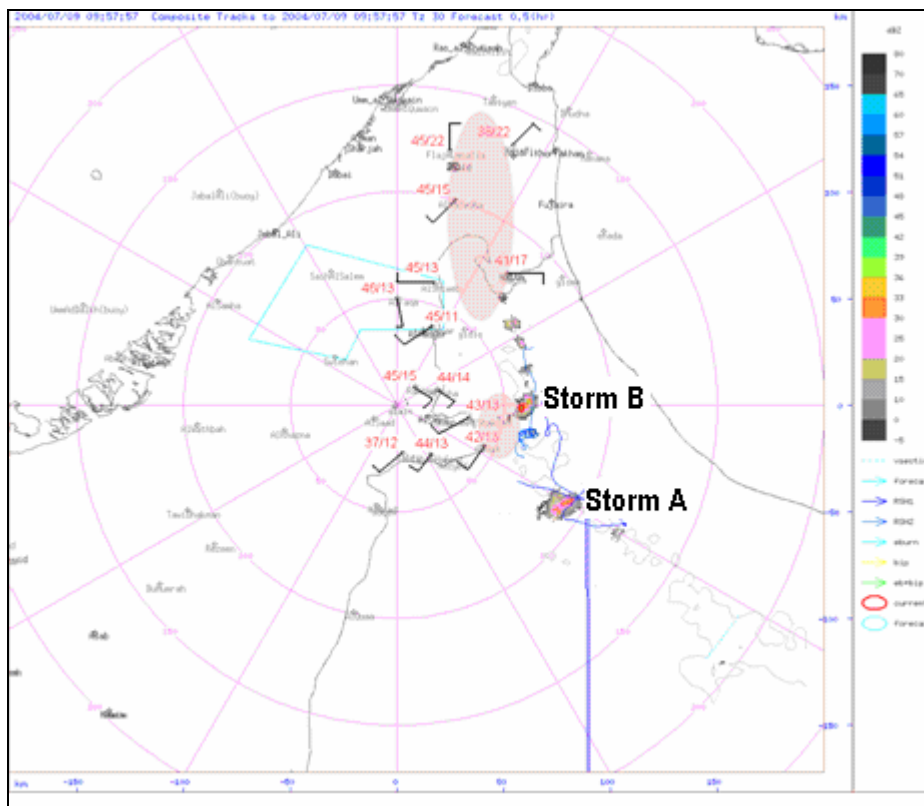


Figure 3-13: Radar reflectivity (dBz) on the 9<sup>th</sup> of July 2004 at 957 UTC. The wind vectors, temperature and dew point values are surface observations at 1000 UTC while the pink shaded area indicates the estimated convergence zone.

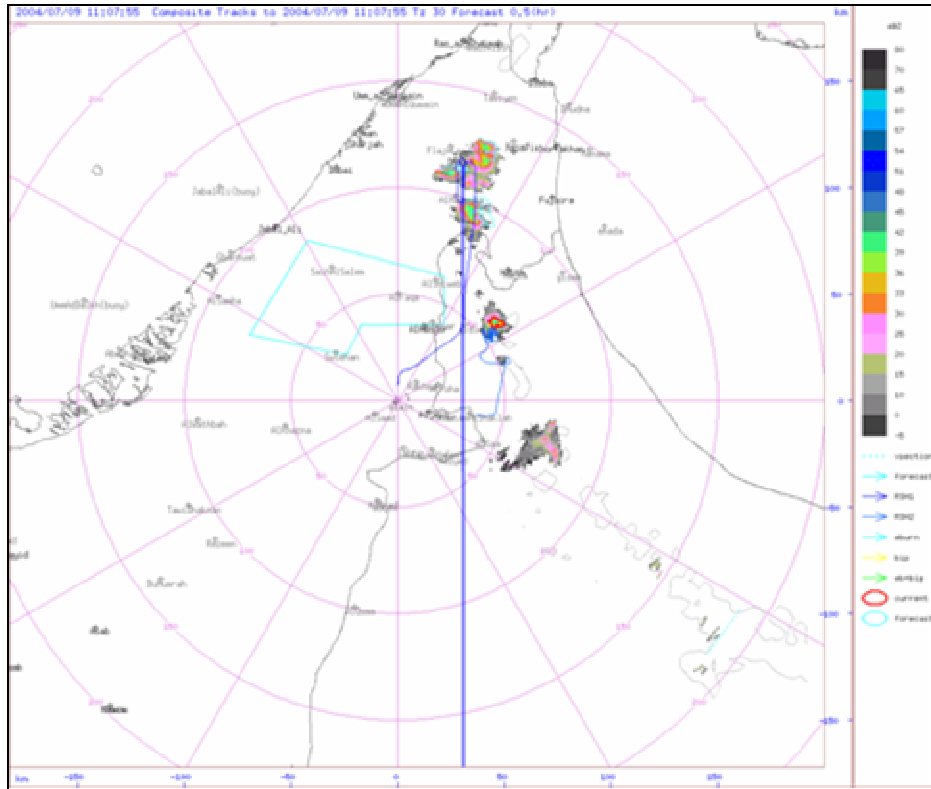


Figure 3-14: Radar reflectivity (dBz) on the 9<sup>th</sup> of July 2004 at 1107 UTC.

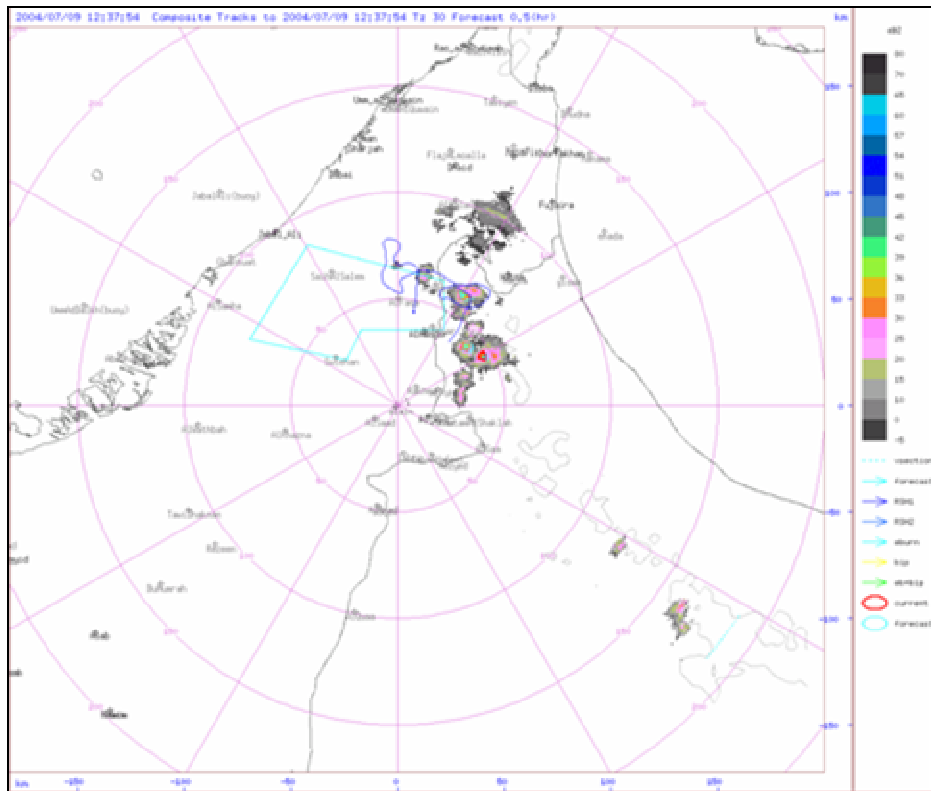
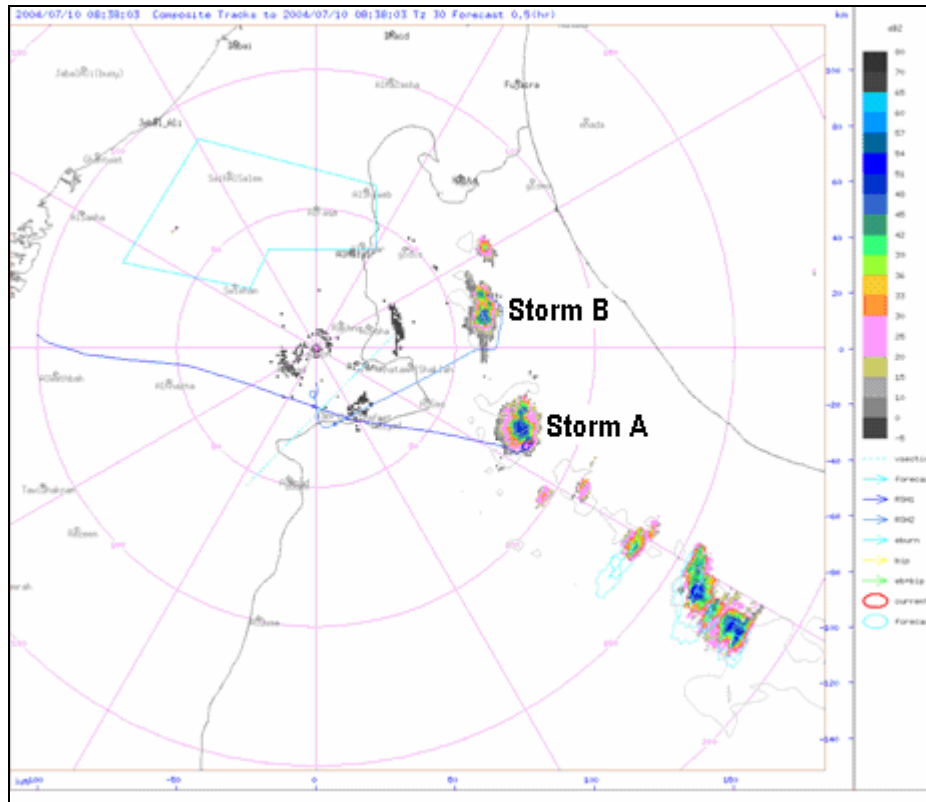


Figure 3-15: Radar reflectivity (dBz) on the 9<sup>th</sup> of July 2004 at 1237 UTC.

### 3.3.5 The 10<sup>th</sup> of July

The radar images confirmed that this was a Very Active day. Storms A and B developed early before 0800 UTC over the peaks of the Al Hajar Mountains as individual cells as seen in the 0838 UTC volume scan (Fig. 3-16). The reflectivity of both storms in Figures A and B were about 50 dBz. Convective cells developed over the entire mountain range on this day.



**Figure 3-16: Radar reflectivity (dBz) on the 10<sup>th</sup> of July 2004 at 0838 UTC.**

Other storms developed quickly and some of the isolated cells then joined to form a multi-cellular system of storms along the mountains as seen at 0918 UTC (Fig. 3-17). Figure 3-17 shows storm C of multiple cells over the mountains extending further south with reflectivity's of more than 50 dBz. Figure 3-17 also shows storm B2 which was probably a secondary development of the storm B shown by Figure 3-16.

Storm D (Fig. 3-18) then developed south of Hatta station at about 0930 UTC and its reflectivity was 40 dBz at 1003 UTC. Storm B2 (Fig. 3-17) became a very intensive cell (storm B3) that expanded with a maximum reflectivity above 55 dBz as seen at 1033 UTC volume scan (Fig. 3-19).

Late convection occurred in the north as storms E and F developed after 1200 UTC. At this time, most of the other cells had already dissipated except storm B3 (Fig. 3-20). Figure 3-20 also shows the convergence zone, shaded area, according to the surrounding stations observations at 1115 UTC.

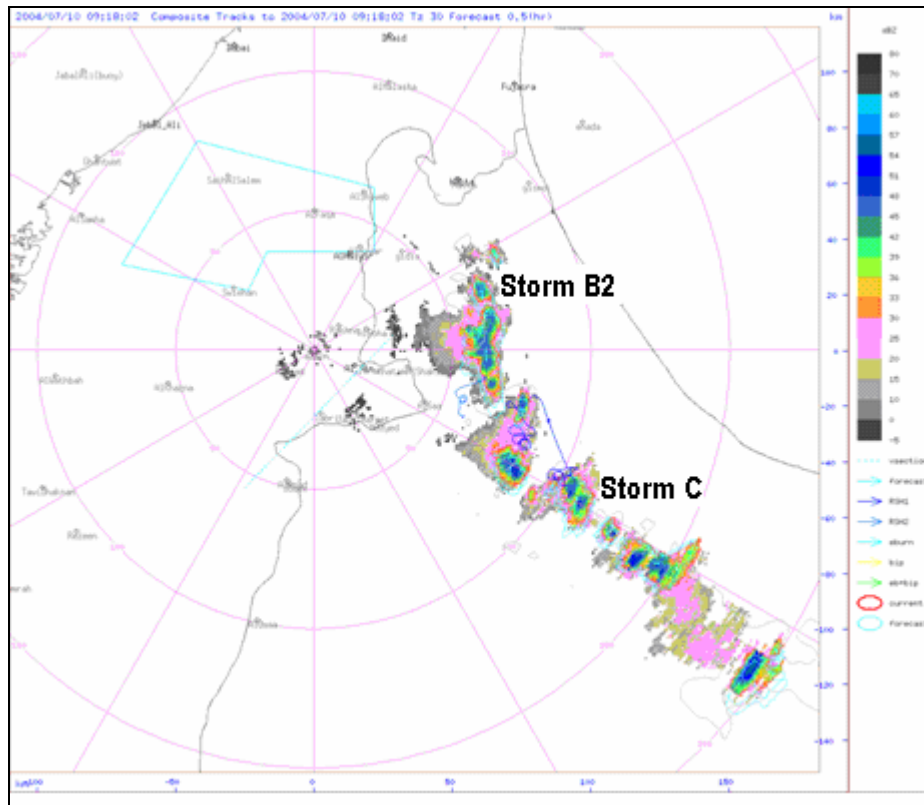


Figure 3-17: Radar reflectivity (dBz) on the 10<sup>th</sup> of July 2004 at 0918 UTC.

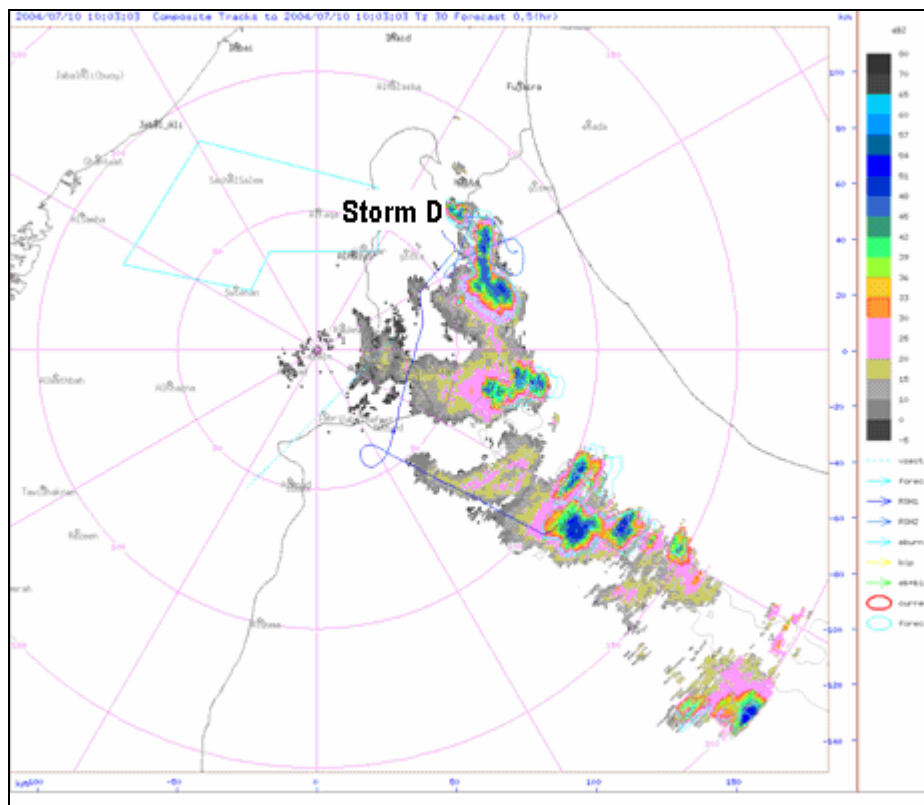


Figure 3-18: Radar reflectivity (dBz) on the 10<sup>th</sup> of July 2004 at 1003 UTC.

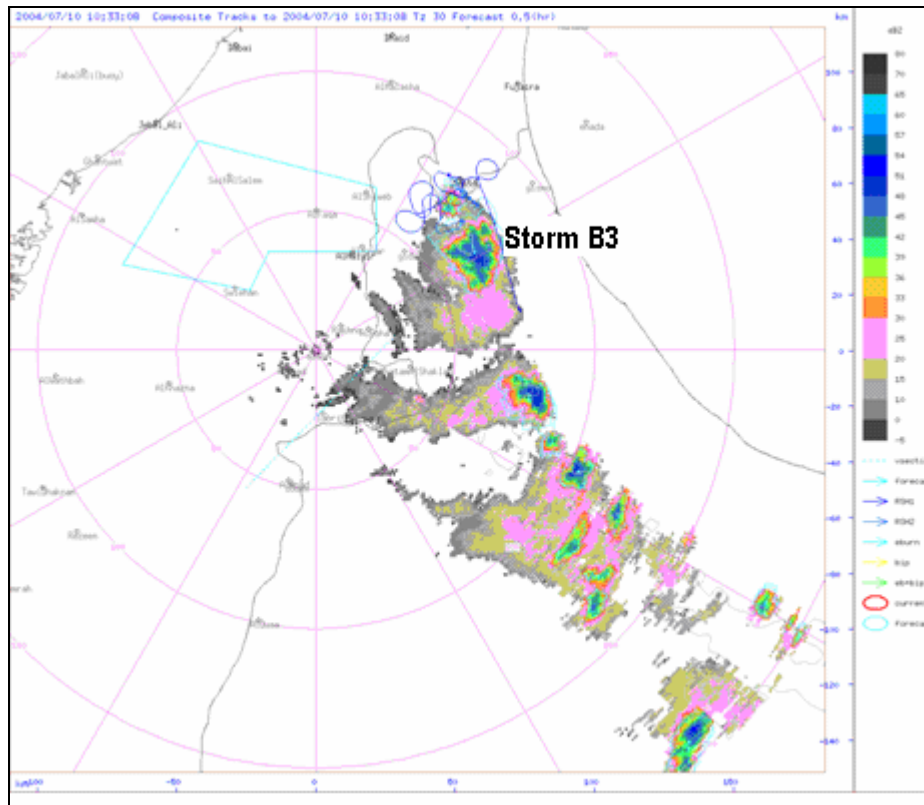


Figure 3-19: Radar reflectivity (dBz) on the 10<sup>th</sup> of July 2004 at 1033 UTC.

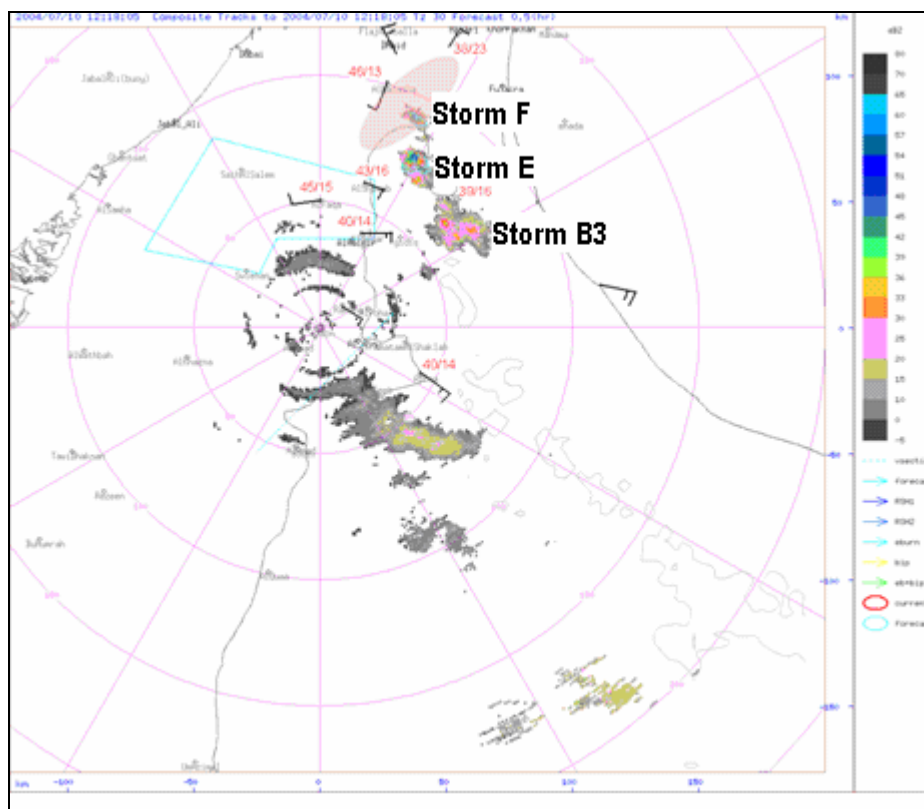
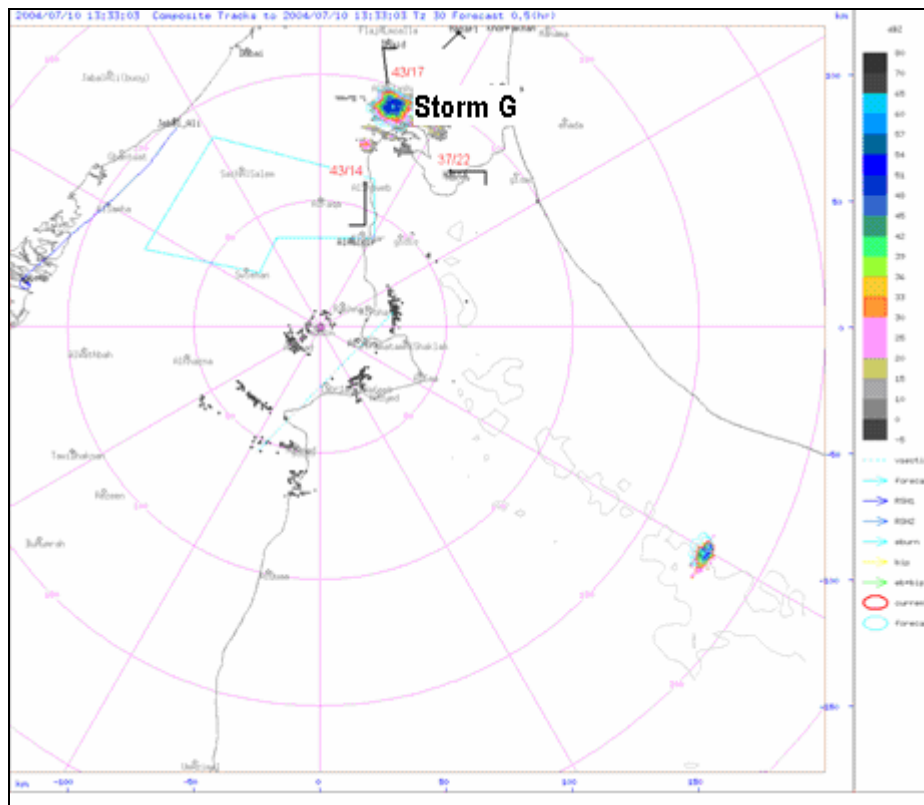


Figure 3-20: Radar reflectivity (dBz) on the 10<sup>th</sup> of July 2004 at 1218 UTC. The wind vectors, temperature and dew point values are surface observations at 1215 UTC while the pink shaded area indicates the estimated convergence zone.



Convective clouds formed over the northern area of the SSA until late afternoon. Storm G (Fig. 3-21) had a reflectivity of almost 60 dBz as seen in the 1333 UTC volume scan and it still existed at 1430 UTC.

The wind circulations, as observed from different stations at 1330 UTC, are also shown in Figure 3-21 and indicate the convergence zone area where storm G developed. The wind was northerly at Al Malaiha , southerly at Al Shiweb and easterly at Hatta (Fig. 3-21). At the same time, the surface temperature was about 43 °C around the area where storm G intensified suggesting strong thermal insulation.



**Figure 3-21: Radar reflectivity (dBz) on the 10<sup>th</sup> of July 2004 at 1333 UTC. The wind vectors, temperature and dew point values are surface observations at 1330 UTC.**

The steering winds were light northerly as shown by Seeb and Abu Dhabi 1200 UTC soundings (Fig. 4-27). So, storms were more likely to be semi-stationary, grow and collapse in the area, or drift slowly to the south. Winds were light, so no wind shear, and thereby enabling easy growth.

The clouds seeding research team executed four operations on the clouds on this day. The pilots noted that there were individual cells that developed a line of convection. While being treated, it was noted that the clouds were thermally induced with non solid cloud bases. The updrafts were moderate and rain was noticed. The clouds base heights varied between 2195 and 2895 m.

### 3.3.6 The 11<sup>th</sup> of July

This was another Very Active day of thunderstorms and convection started even earlier than the day before over the Al Hajar Mountains peaks. Storm A (Fig. 3-22) was noticed first before 0800 UTC and then storm B, in the same Figure, developed to the north with reflectivity of more than 40 dBz at 0803 UTC. Several convective storms developed over the mountain range an hour later (Fig. 3-23). At 0923 UTC, storm C (Fig. 3-24) became more intense with a 50 dBz reflectivity. Storm B (Fig. 3-24) was very intense with a reflectivity of about 60 dBz in its core while storm A (Fig. 3-24) was very active and gathered other cells around it. Storm A (Fig. 3-25) then became more intense while storm B (Fig. 3-24) started weakening. A couple of cells developed over the north like storm D and storm E (Fig. 3-25).

At 1108 UTC, storm A (Fig. 3-26) was still active with reflectivity above 50 dBz and another very intense storm (storm F) formed in the north by the combining of storm D and storm E with other individual cells (Fig. 3-26). The same volume scan also showed storm G developing in the northeast. Storm F (Fig. 3-25) lasted for a long time and was seen to be active even after 1200 UTC. Then, other isolated cells appeared over the northeast and moved to the west of the UAE. No active storms remained over the Al Hajar Mountains and the surrounding area after 1300 UTC. However, there were plenty of active cells located to the west over the UAE area which lasted until late afternoon. Storm H (Fig. 3-27) was located over Al Hiyar at 1328 UTC with a volume scan reflectivity of more than 40 dBz. Then, storm F (Fig. 3-26) moved to the west and lasted until later than 1500 UTC.

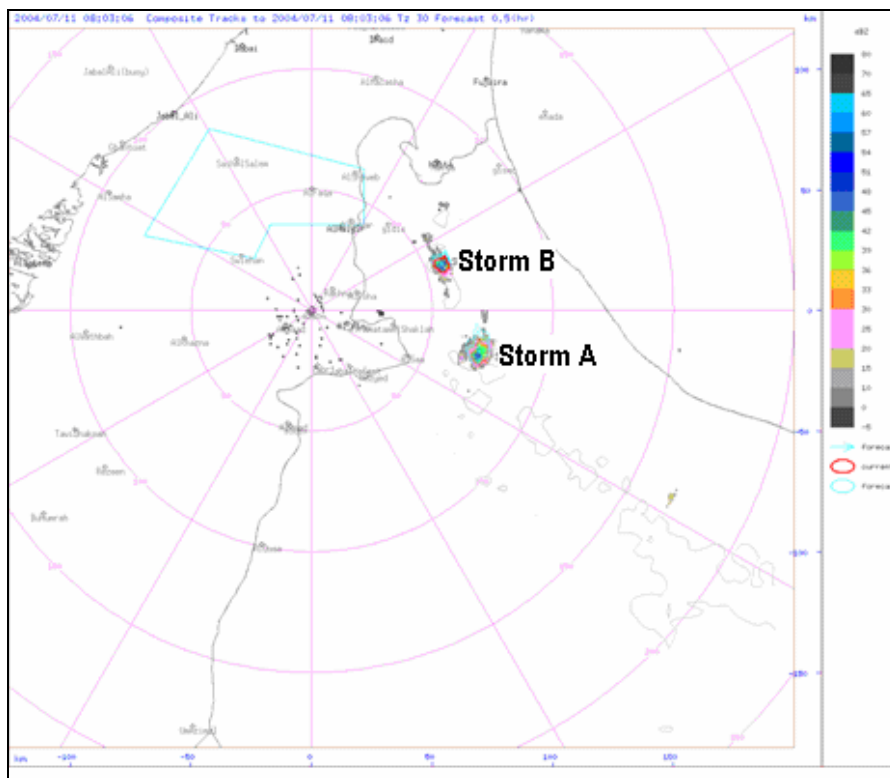


Figure 3-22: Radar reflectivity (dBz) on the 11<sup>th</sup> of July 2004 at 0803 UTC.

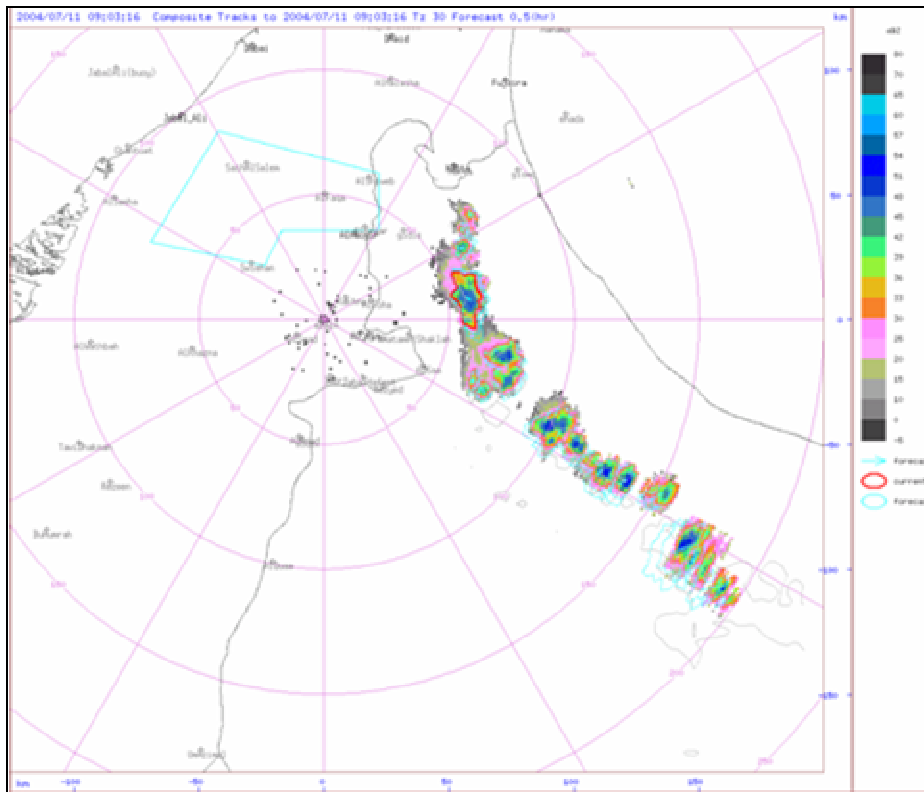


Figure 3-23: Radar reflectivity (dBz) on the 11<sup>th</sup> of July 2004 at 0903 UTC.

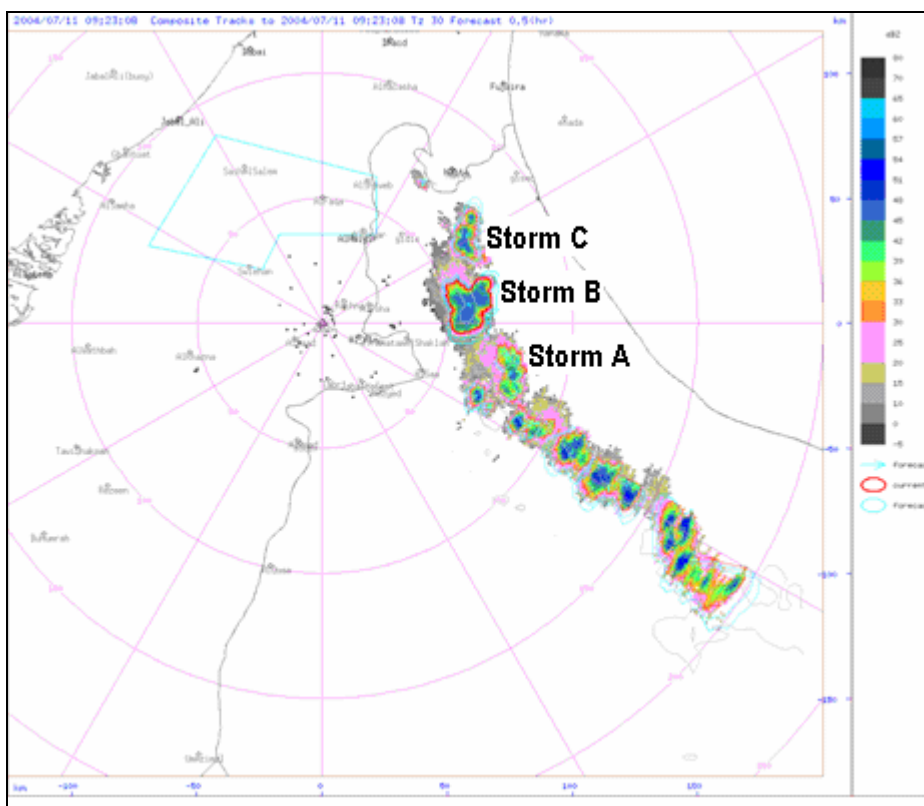


Figure 3-24: Radar reflectivity (dBz) on the 11<sup>th</sup> of July 2004 at 0923 UTC.

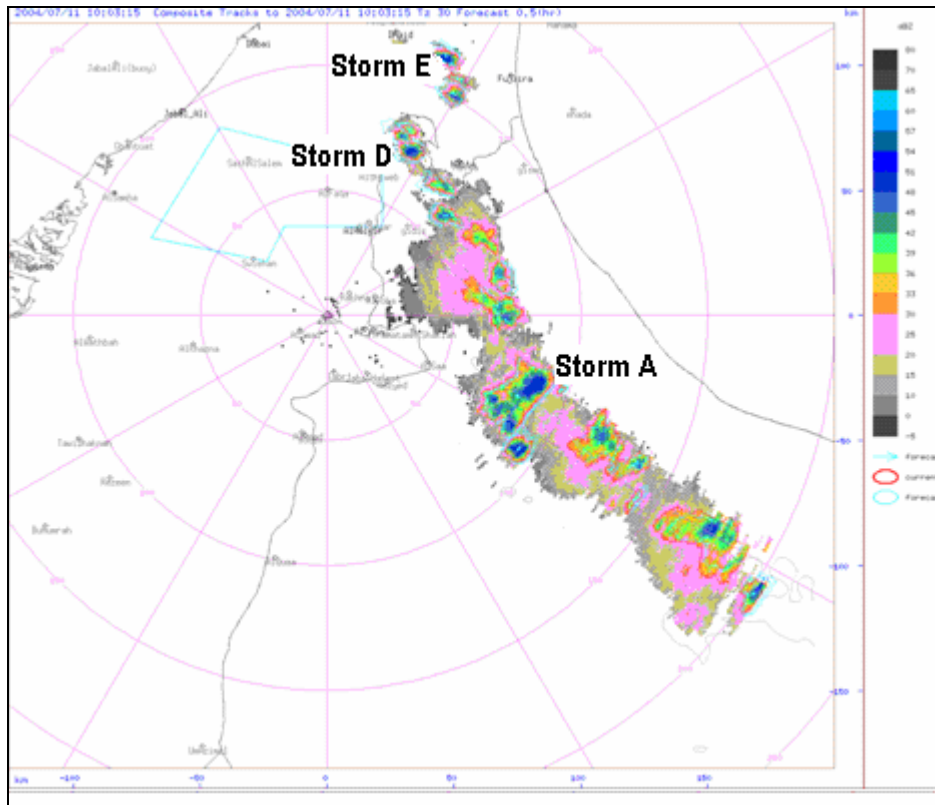


Figure 3-25: Radar reflectivity (dBz) on the 11<sup>th</sup> of July 2004 1003 UTC.

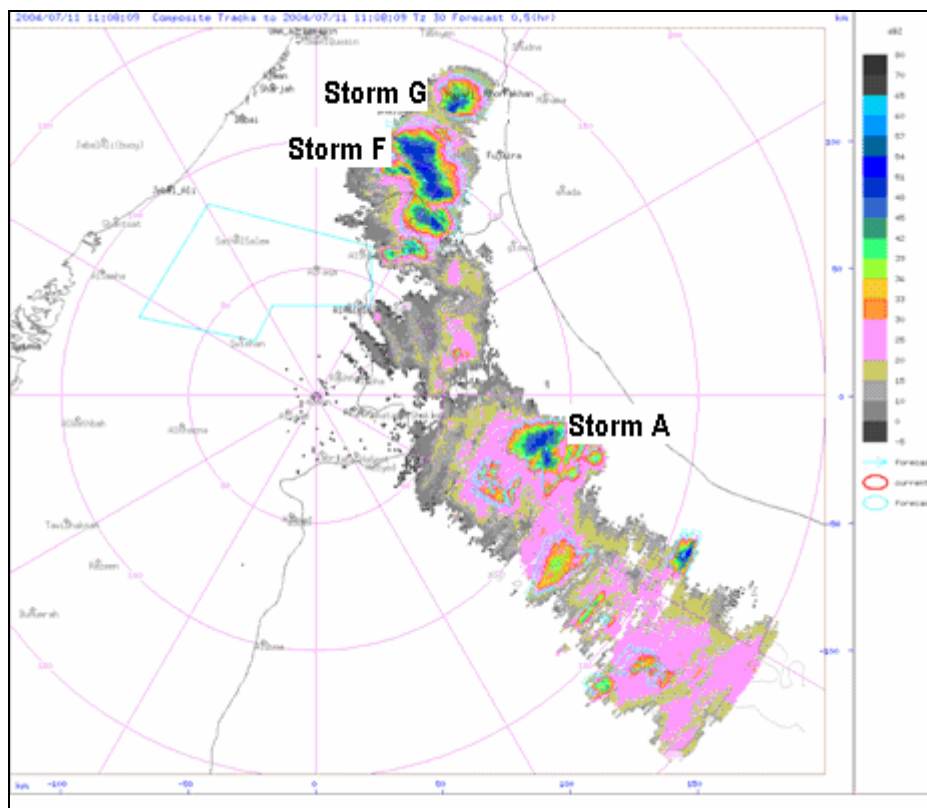
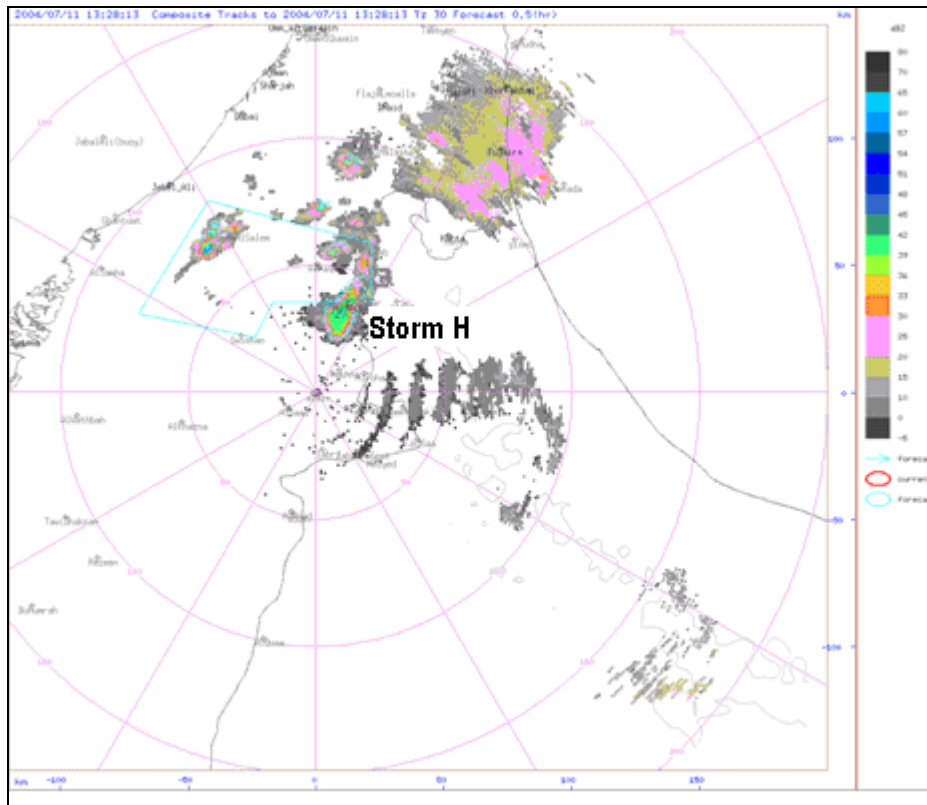


Figure 3-26: Radar reflectivity (dBz) on the 11<sup>th</sup> of July 2004 1108 UTC.



**Figure 3-27: Radar reflectivity (dBz) on the 11<sup>th</sup> of July 2004 at 1328 UTC.**

The wind convergence zones on this day identified the areas of preferred convection accurately. For instance at 0833 UTC (Fig. 3-28) when the storms developed, the winds (three minutes before) were mostly southerly to southwesterly over the southern stations west of the mountains. Yet, the southeasterly wind occurred over the northern stations like Al Malaiha. The southwesterly wind was moist as the dew point temperatures were between 16 and 17 °C. However, the southeasterly wind was much moister as seen over Hatta which had a dew point temperature of 26 °C and Al Malaiha 21 °C. The surface temperatures were mostly above 40 °C. The observations after one hour (Fig. 3-29) indicated the dominance and the strength of the southwesterly winds over the stations west of the mountains including the wind over Al Malaiha which was southeasterly an hour before. This caused the dew point temperature to drop to 16 °C. The mixing of the two different airmasses was partly responsible for initiating a convergence zone marked by pink shadow in Figure 3-29. Most of the storms which developed later (Fig. 3-26) were seen in that marked zone.

A couple of flights with five operations were executed on the clouds by the seeding research team. The team noticed from the aircraft that the clouds over the mountains east of Al Ain had a cloud base at 1525-1980 m and experienced lightning, moderate updraft and rain on the ground. The northern clouds that formed between Hatta and Masafi (storm E on Fig. 3-25 and storms G & F on Fig 3-26) had cloud base closes to the mountain in many cases (2440-2895 m) with strong updrafts and rain. The overcast cloud that formed later to the north of Al Ain had light rain. Their bases were difficult to distinguish and the top was generally between 5790 and 6095 m.

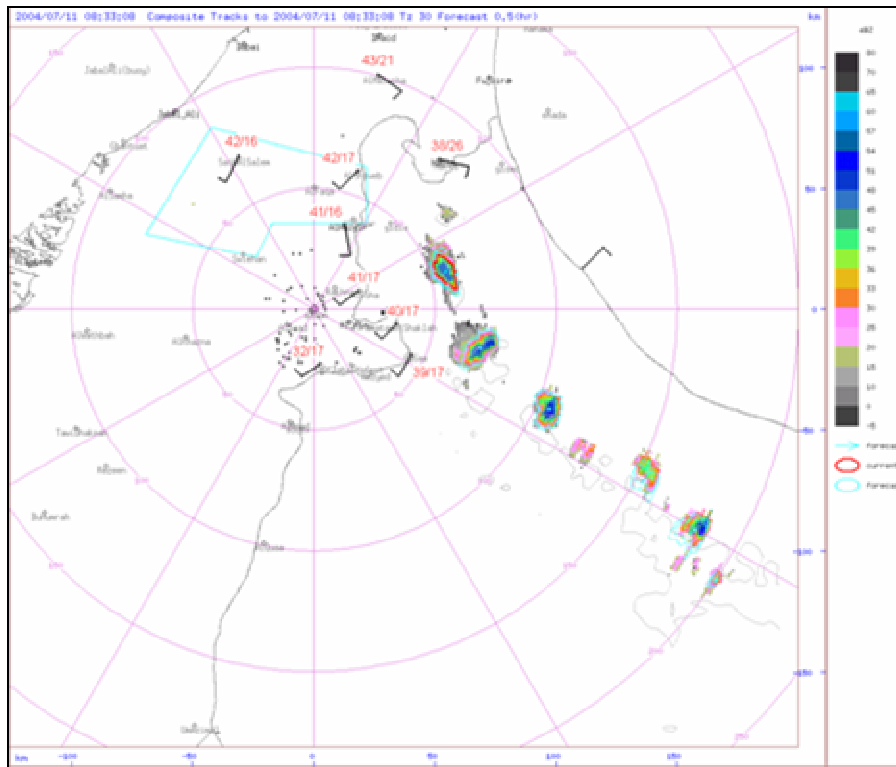


Figure 3-28: Radar reflectivity (dBz) on the 11<sup>th</sup> of July 2004 at 0833 UTC. The wind vectors, temperature and dew point values are surface observations at three minutes before the volume scan time.

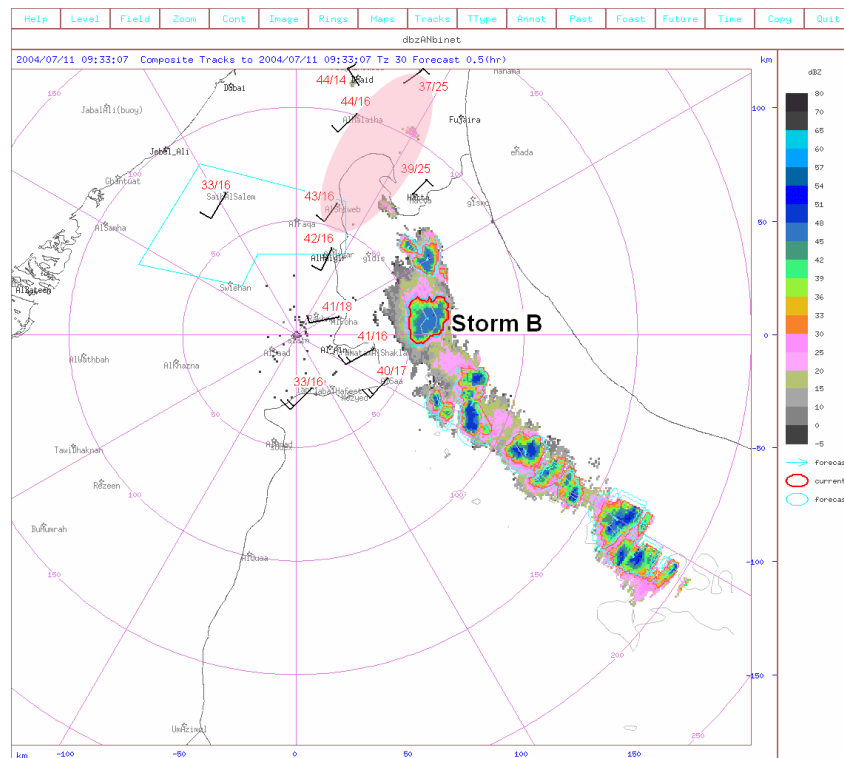


Figure 3-29: Radar reflectivity (dBz) on the 11<sup>th</sup> of July 2004 at 0933 UTC. The wind vectors, temperature and dew point values are surface observations at three minutes before the volume scan time while the pink shaded area indicates the estimated convergence zone.

### 3.3.7 The 12<sup>th</sup> of July

Storms again developed over the Al Hajar Mountains on the 12<sup>th</sup> of July. They started a bit later than the previous day as storm A (Fig. 3-30) developed at 0820 UTC at the same location (southeast of Al Ain) as on the 11<sup>th</sup> of July. The reflectivity was already about 60 dBz in its core on the 0853 UTC volume scan (Fig. 3-30). This Figure also shows other individual cells like storm B developing just to the north. After about half an hour, storm A became very intense and seemed to join with another cell.

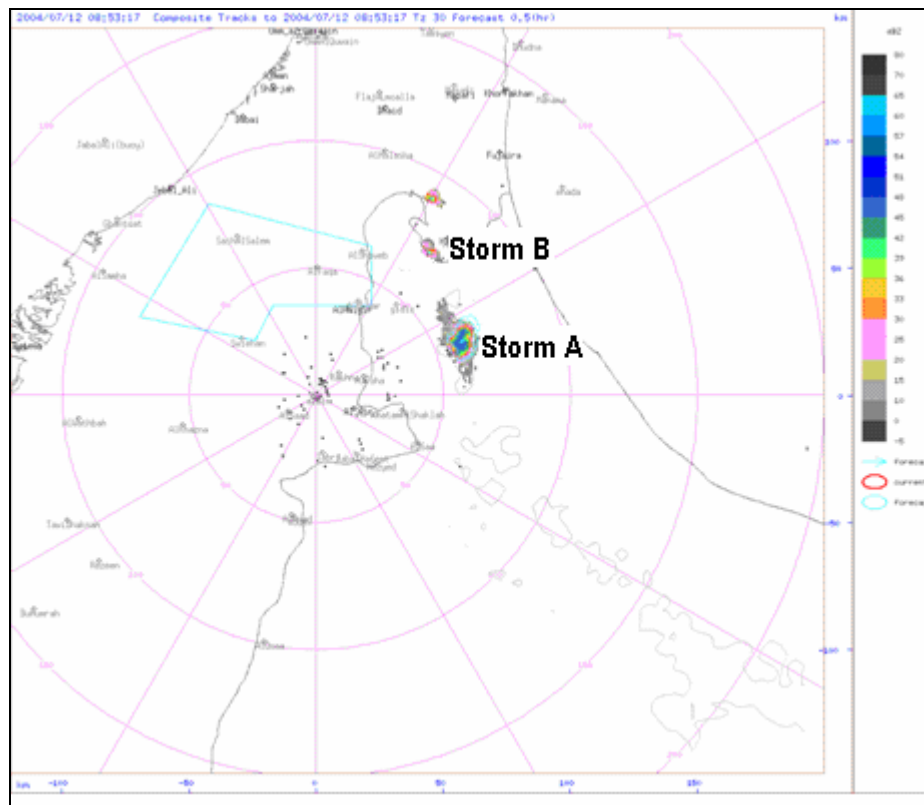


Figure 3-30: Radar reflectivity (dBz) on the 12<sup>th</sup> of July 2004 at 0853 UTC.

Figure 3-31 shows storm B which appeared to join with another cell to form storm B2 while storm C developed at about 0910 UTC over the area where the first storms developed during the previous three days. At 0958 UTC the volume scan (Fig. 3-32), storm A2 was split from the mother cell, storm A, which now moved to the south; however both storms were very intense and their reflectivity was about 60 dBz in the core.

The Figure also shows that storm B2 divided into small cells with less reflectivity but the area there remained active. Storm C was weak and was about to merge with another cell to its northeast and storm A to the north. Figure 3-32 also shows other storms developing over the southeastern mountains at about 100-150 km from Al Ain. After about 25 minutes, storm A became very intense by combining with storm C and other individual cells moved from the south as the steering winds were light to moderate southeasterly at Seeb 1200 UTC



sounding to southerly at Abudhabi one. Storm A2 also moved to the north to influence a wider area and was still intense with a reflectivity of about 60 dBz in its core.

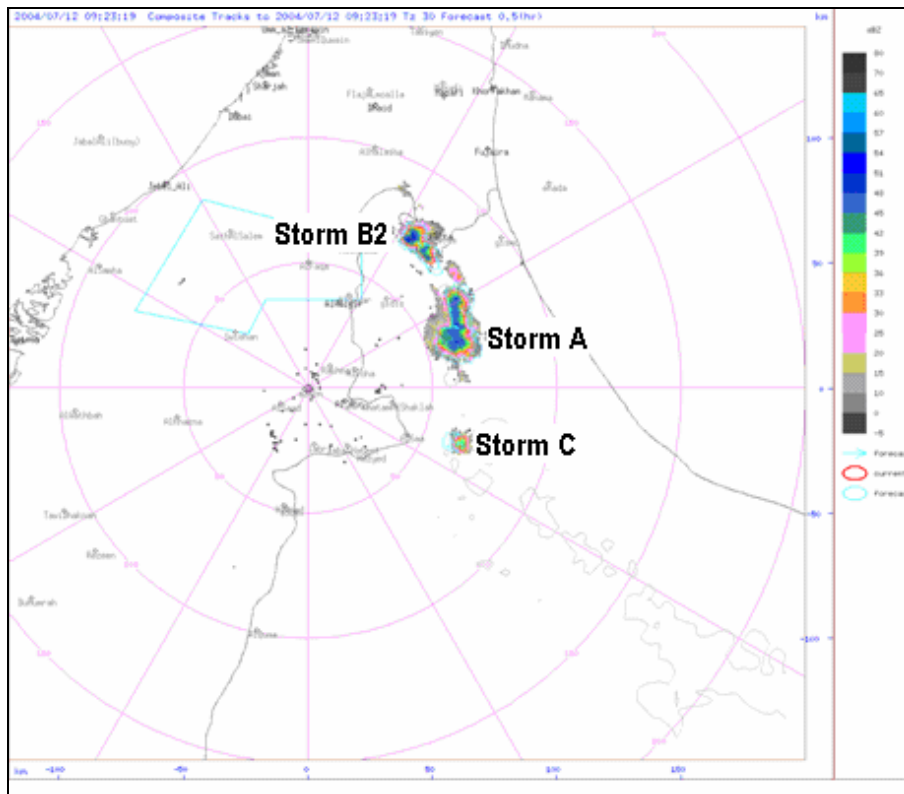


Figure 3-31: Radar reflectivity (dBz) on the 12<sup>th</sup> of July 2004 at 0923 UTC.

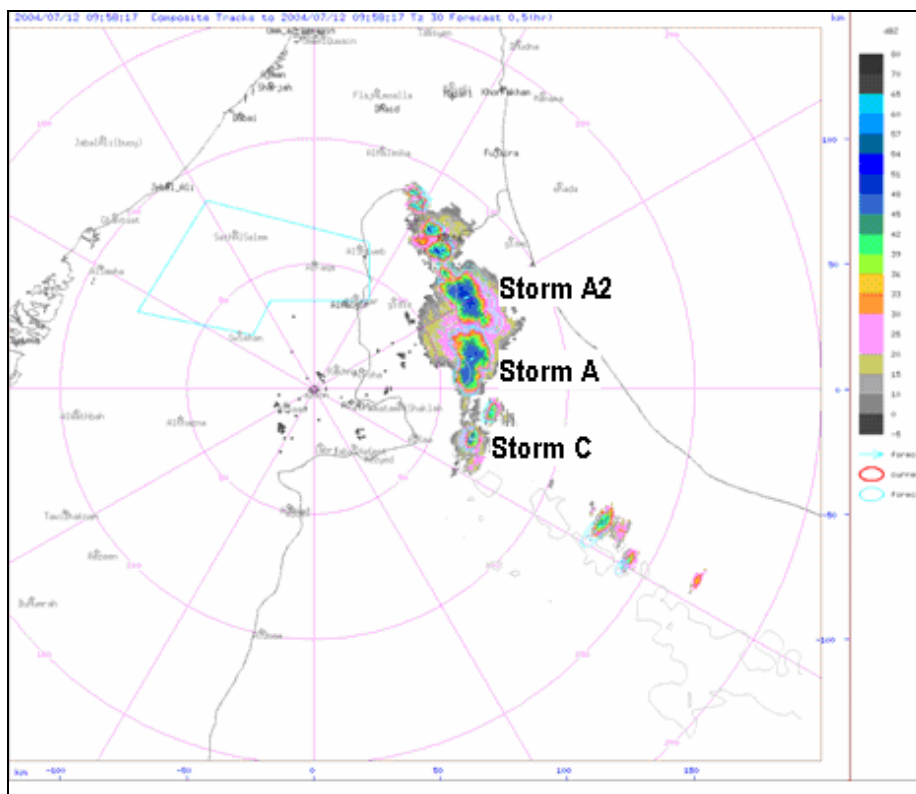


Figure 3-32: Radar reflectivity (dBz) on the 12<sup>th</sup> of July 2004 at 0958 UTC.



The southeastern area was still active with a couple of isolated cells but many more convective cells occurred to the northeast of Al Ain. Storm E (Fig. 3-33) was another huge storm that developed over the southeastern mountains and it was made up of several individual cells which formed earlier over the area and moved northwesterly. Figure 3-33 also illustrates storm A being active while storm A2 (Fig. 3-32) was already over but some isolated storms were developing to the north (west of Fujaira).

At 1123 UTC (Fig. 3-34) a very intense storm (storm F) with a reflectivity of about 60 dBz in its core resulted from the combining of storms A and E (Fig. 3-33) and it was seen covering an area more than 100 km along the mountains and the surrounding areas. The area southeast of this storm was still active while other isolated cells were still developing over the north such as storm G west of Fujaira (Fig. 3-34). Storm F (Fig. 3-34) remained active until about 1230 UTC but the northern area was also active until late afternoon. Storm H developed over the northern area at 1145 UTC. It was seen active at 1303 UTC (Fig. 3-35) and remained until about 1400 UTC when all the storms over the area disappeared.

The research aircraft flew all along the mountains and carried out three seeding operations. The team reported a long line of convective clouds with their base height varying between 1340 and 2745 m. The low cloud bases prevented the seeding experiments from taking place. Heavy rain was also noticed on many occasions.

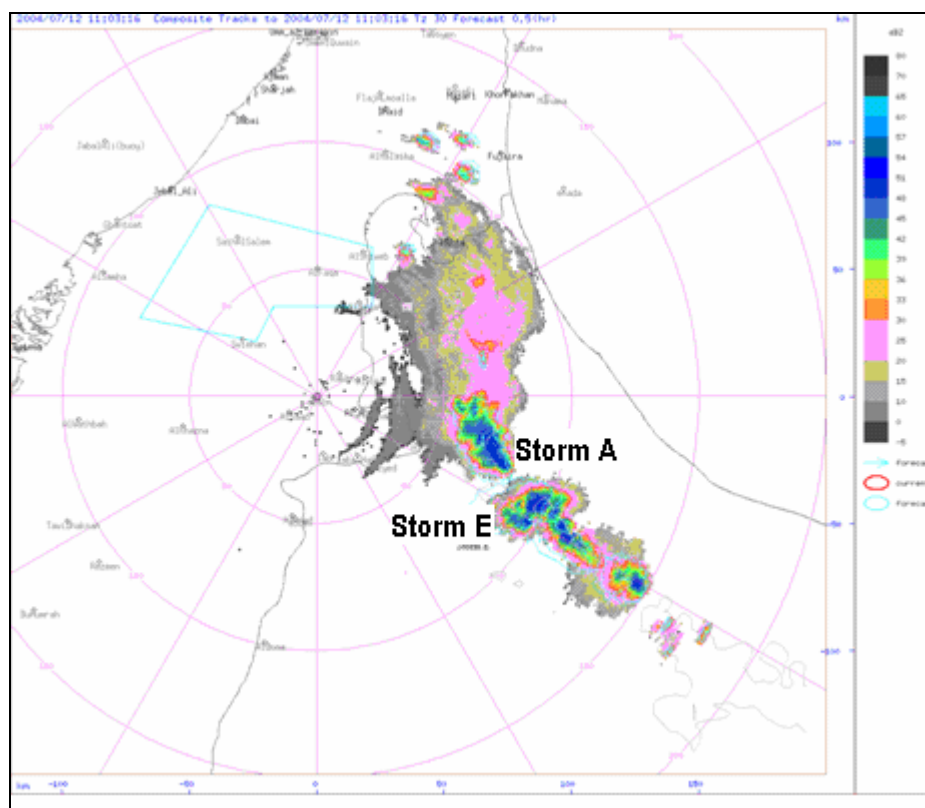


**Figure 3-33: Radar reflectivity (dBz) on the 12<sup>th</sup> of July 2004 at 1103 UTC.**

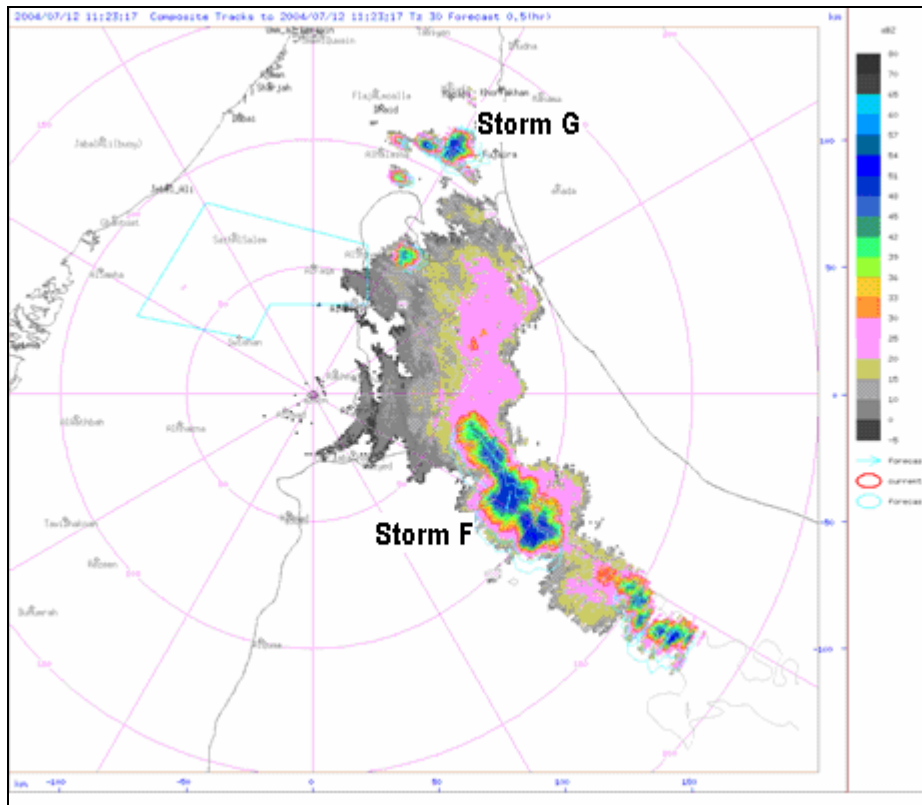


Figure 3-34: Radar reflectivity (dBz) on the 12<sup>th</sup> of July 2004 at 1123 UTC.

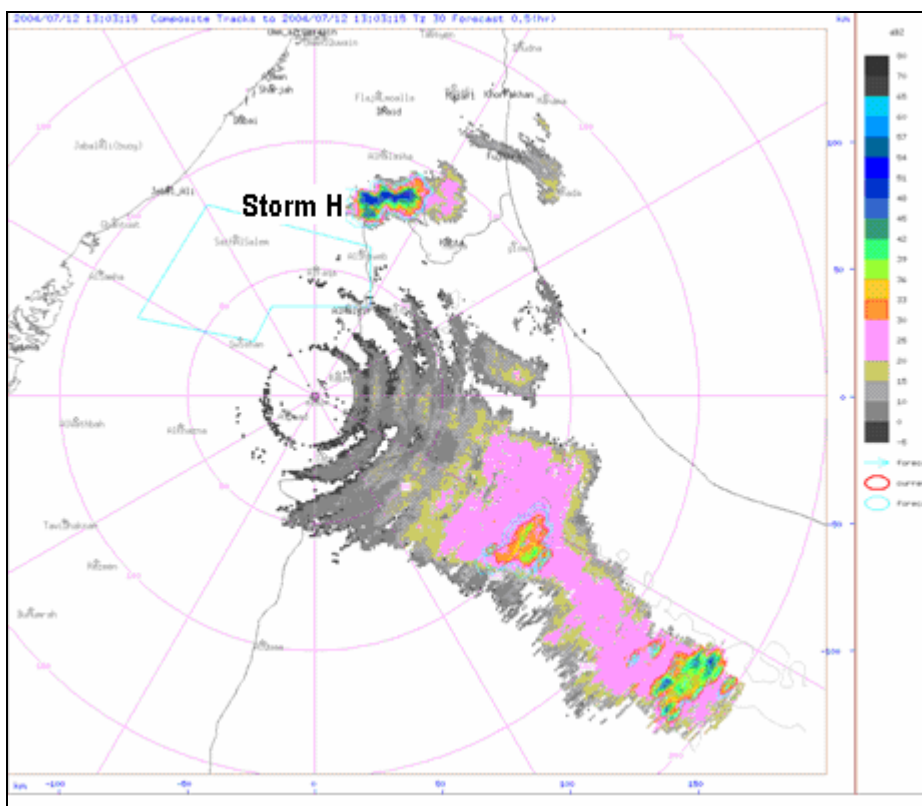


Figure 3-35: Radar reflectivity (dBz) on the 12<sup>th</sup> of July 2004 at 1303 UTC.

### 3.3.8 The 13<sup>th</sup> and 14<sup>th</sup> of July

No radar images were available on these two days and the Aqua true color satellite images available from MODIS were investigated to identify convection.

Generally, the convection started a bit late on the 13<sup>th</sup> of July, after 0900 UTC, and spread over the mountains as seen on MODIS Aqua true color image at 0900 UTC (Fig. 3-36A). Some storms over the eastern Hajar Mountains to the south were present on the 14<sup>th</sup> of July indicated by the satellite image at 0940 UTC (Fig. 3-36B).

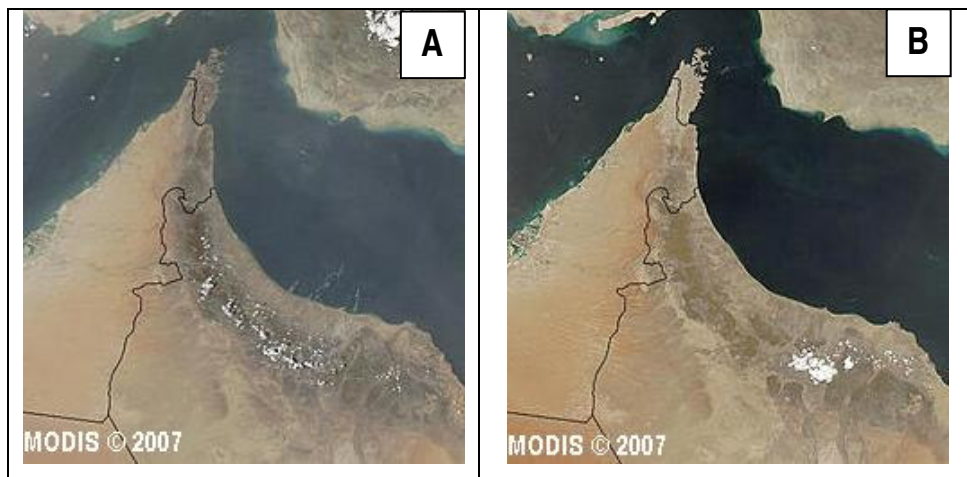
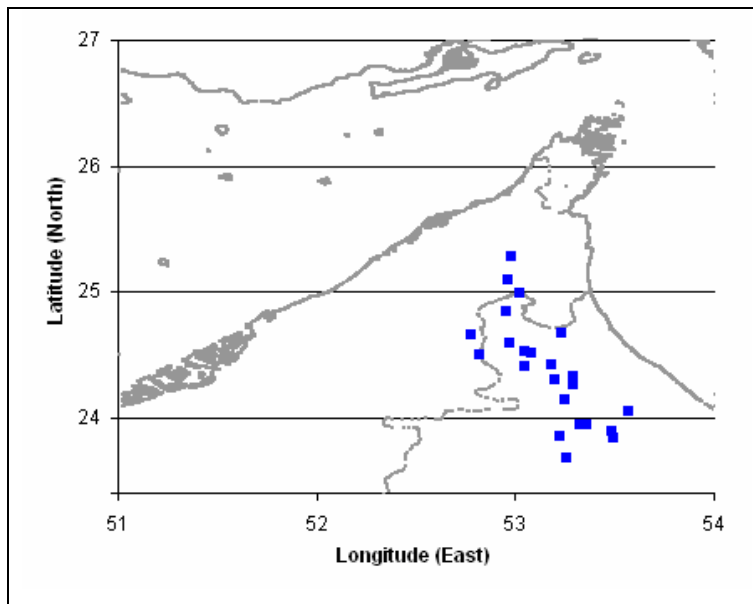


Figure 3-36: Aqua True color image at 0900 UTC on 13<sup>th</sup> (A) & at 0940 UTC on 14<sup>th</sup> (B) of July 2004. (Adapted from: MODIS, 2007)

The research team achieved three seeding operations on the 13<sup>th</sup> of July and noticed that the ideal cells developed with cloud bases at 3200-3355 m. They also noticed moderate updrafts at first with light rain on occasions. No convective storms were observed over the SSA during the 14<sup>th</sup> of July.

### 3.4 Seeding cases during the study period

During the Active and the Very Active days of the study period, there were 23 randomized seeding cases mostly conducted over the Western Hajar Mountains of Oman (Fig. 3-37). The flight information of the 23 cases along with the pilots' comments are listed in Table 3-1. This information includes the case number in the project, position of the operation (longitude and latitude), decision time (the time when pilots decided to start the randomized seeding operation according to the characteristics of the targeted storm), the cloud base and brief pilot comments. About two quarters of the cases were conducted during the Very Active days (10<sup>th</sup>-13<sup>th</sup> of July) where the storms were available for seeding at earlier times compared with the other days. The lowest cloud base was observed below 2000 m in one of the early seeding cases on the 11<sup>th</sup> of July over the mountains east of Al Ain. It was found that there was a relationship between the cloud bases, time of the storm and the number of randomized seeding cases achieved.



**Figure 3-37:** Randomized seeding experiment locations of 23 seeding cases (blue solid squairs) during the period (6<sup>th</sup> -13<sup>th</sup>)of July 2004. (Data from DAS and NCAR).

**Table 3-1:** Flights summary of the 23 randomized seeding cases during the period (6<sup>th</sup> -13<sup>th</sup>)of July 2004.

Case #	Date	Lat.	Lon.	Decision Time	Cloud Base Height (m)	Comments
R2C45	06 Jul 04	24.6	55.974	1123	3660	light to medium rain on ground - moderate updraft
R2C46	07 Jul 04	23.687	56.256	1058	4115	rain on ground when starting - weak updrafts improved to good
R2C47	07 Jul 04	24.416	56.043	1137	3660	moderate updrafts with broken base - rain on ground and windscreen
R2C48	08 Jul 04	23.849	56.222	1056	3320	rain-shaft present after flares 1&2, no lightning, rain reaching ground on flares 9&10
R2C49	08 Jul 04	24.506	55.818	1227	3535	light rain even during flares 1&2, no lightning
R2C50	09 Jul 04	24.146	56.245	956	2895	weak updraft - moderate to heavy rain on ground
R1C17	09 Jul 04	25.278	55.982	1043	2440	updraft died early; strong gust front and lightning
R2C51	09 Jul 04	24.531	56.045	1053	3505	good base & good updraft during middle of seeding
R1C18	10 Jul 04	23.952	56.362	852	3050-3660	good updrafts all the way; rain and lightning at start
R2C52	10 Jul 04	24.337	56.291	904	2195	lightning to begin; rain on ground by flares 3&4, good updrafts
R1C20	10 Jul 04	23.842	56.491	927	3200	lots of rain and lightning - base all precipitation when doing base pass
R1C21	10 Jul 04	24.049	56.569	1112	2590	base eroded while treating then dumped precipitation on us
R1C22	11 Jul 04	24.299	56.2	841	2440-2135	good updrafts; nice solid base; lots lightning; heavy rain
R2C53	11 Jul 04	24.519	56.076	846	1675-1830	good updrafts; lightning visible and rain on ground early
R1C23	11 Jul 04	24.841	55.954	949	2286-2804	good updrafts; rain on ground only during last 2 flares
R1C24	11 Jul 04	25.097	55.962	1028	2895	problems with right flares; strong gust front; no precipitation on ground observed
R2C54	11 Jul 04	24.657	55.777	1258	2745	slight rain on ground to begin with; moderate updrafts; very poor visibility
R2C55	12 Jul 04	24.426	56.179	829	2745	light rain on screen to begin; moderate updrafts; rain on ground; no lightning
R1C25	12 Jul 04	24.992	56.017	1036	3110	good updrafts; on edge of heavy rain-shaft; rain reaching ground
R2C56	12 Jul 04	23.896	56.485	1040	2440	rain on ground at begin; good updrafts; no lightning
R1C26	13 Jul 04	23.945	56.326	913	3355	early in growth; no rain during seeding; moderate updrafts
R2C57	13 Jul 04	24.264	56.288	1054	3050-3200	light rain
R2C58	13 Jul 04	24.673	56.228	1122	3200-3355	light rain

Source: DAS and NCAR, 2004.

Lower cloud bases clouds were the earlier seedable storms which developed the required characteristics of updraft and solid base. However, as discussed in section 3.2, mostly all the summer storms of this area can be amenable to hygroscopic seeding.

### **3.5 General discussion**

In this chapter, the problem of the water resources shortage in Oman was briefly discussed as being the motivation of this study. The hygroscopic seeding project in the UAE including the Omani mountains was highlighted. The characteristics of the regional clouds and their amenability to hygroscopic seeding were discussed. The regional clouds were subdivided into eight cloud types but the boundary layer cumulus and deeper cumulus with relatively high bases were the dominant clouds.

The study period of 10 days, 5<sup>th</sup>-14<sup>th</sup> of July 2004, was selected to include Non Active, Active and Very Active days over the mountains. The radar at Al Ain was used to investigate the development of the convective storms over the Al Hajar Mountains.

The satellite images were also used when no radar data were available on the 13<sup>th</sup> and the 14<sup>th</sup> of July 2004. The images show there was no convection on the 5<sup>th</sup> (Non Active day), isolated convection on the 6<sup>th</sup>-9<sup>th</sup> (Active days), very widespread convection on the 10<sup>th</sup>-13<sup>th</sup> (Very Active days) and limited convection outside of the SSA on the 14<sup>th</sup> (Non Active day over the SSA).

The radar images showed that the storms were seen first semi-stationary over the eastern part of the Al Hajar Mountains or then moved to the west according to the steering wind. Wind convergence zones were identified as favourable areas for convection.

## Chapter 4

## Data Analysis and Results

### 4.1 Introduction

The data used here are the NCEP re-analysis data, prognostic fields of the regional model MM5, surface observations at individual stations and upper air data. The convective clouds over the Al Hajar Mountains are considered to occur on the mesoscale and mostly results from the favorable surface conditions, which in turn are influenced by the synoptic scale flow (Al-Maskari, 2006).

The synoptic conditions are discussed use the geopotential heights from NCEP (as discussed earlier in 2.1.5). The prognoses of the regional model MM5 (mentioned earlier in 2.1.4) are verified in order to ascertain its reliability in predicting the general synoptic conditions. The prognostic fields are then used to describe the atmospheric conditions leading to convection. The impact of the synoptic conditions on the mesoscale circulation is then discussed through the surface observations. The upper air data from Seeb (OOMS) and Abu Dhabi (OMAA) are discussed to investigate the atmospheric instability. Some sounding parameters are also analyzed. Ultimately, a general discussion is provided which includes the results found from the analyzed data.

### 4.2 Synoptic conditions

#### 4.2.1 NCEP data

##### A. 1000 hPa analysis

The 1000 hPa geopotential pattern at 0600 UTC was similar for the two Non Active days of the 5<sup>th</sup> and 14<sup>th</sup> of July. On both days the SSA was influenced by a trough of low pressure located to the northeast of Pakistan and a ridge over Iran (Fig. 4-1A & H). The deep trough extended over the entire eastern part of the Arabian Peninsula causing the dry southwesterly winds to prevail over the area. Another low pressure system was located over the Red Sea. There was no clear closed heat low pressure over the Peninsula, unlike the Active days, from the 6<sup>th</sup> to the 9<sup>th</sup> of July, (Fig. 4-1B-D) and the Very Active days, from 10<sup>th</sup> to 13<sup>th</sup> of July (Fig. 4-1E-G).

On the 6<sup>th</sup> of July, the day of the onset of the convection, the high pressure ridge over Iran deepened to the south and extended a ridge over the Strait of Hurmuz, northern Oman. This forced the trough over Pakistan to split and a closed heat low pressure cell formed over the UAE and the northwestern part of Oman. The geopotential height gradients weakened over the SSA and the westerly wind speed was lighter than on the 5<sup>th</sup> of July. This caused the flow from the Gulf of Oman to propagate westward through the gaps in the mountains. Resulting in an increase in the surface moisture especially over the northern part of the SSA (Fig. 4-1B). The low pressure deepened on the 7<sup>th</sup> of July and remained dominant on the 8<sup>th</sup> of July when it extended to

the south of the Arabian Gulf and caused very tight geopotential height gradients in the west of Oman and the UAE (Fig. 4-1C). These tight gradients insured southwesterly to southerly flow over Oman and SSA and moisture was advected from the Arabian Sea. By the 9<sup>th</sup> of July the low pressure deepened further with the geopotential height in the centre of the low at -20 gpm to the southwest of the UAE, Qatar and the northeastern part of KSA (Fig. 4-1D). Very tight geopotential gradients around it kept the flow over Oman moist southerly to southeasterly, resulting in an increase in the surface moisture over the mountains from the south. Consequently, the convection observed over the mountains started early at about 0800 UTC (see section 3.3). A secondary low pressure developed over Iraq by the 10<sup>th</sup> and the 11<sup>th</sup> of July when the Red Sea low pressure system merged with the heat low in the north of the Arabian Peninsula. This low pressure reached a maximum depth on the 11<sup>th</sup> of July, when the maximum convection also occurred. NCEP showed the centre of the low pressure at -35 gpm (Fig. 4-1E). The trough extended to the south and deepened into the Arabian Sea, resulting in a dominant moist southerly flow over the eastern Peninsula and the northern Al Hajar Mountains. The moist air was orographically lifted over the mountains and converged with the sea breeze from the Gulf of Oman and a multi-cellular storm system developed over the entire mountains. On the 12<sup>th</sup> of July the low pressure over Iraq disappeared and the centre of the heat low was over the northeastern part of the Arabian Peninsula (Fig. 4-1F). The low pressure started to fill in but the flow over the SSA was almost similar to the 11<sup>th</sup> and the convection also started early and was very active. The low pressure system over the centre of the Red Sea redeveloped and another low pressure cell also developed over Pakistan. The dominant heat low over the northeastern part of the Peninsula started to weaken.

The synoptic situation on the 12<sup>th</sup> of July was similar to the 9<sup>th</sup> of July except that the trough was deeper on the former day and extended to the south of the Peninsula up to the Arabian Sea. This allowed a more moist southerly flow over the eastern part of the Peninsula and hence the convection was very active. On the 13<sup>th</sup> of July the heat low pressure system started to fill in (Fig. 4-1G). Slack geopotential height gradients were observed over the SSA. This meant the moist southerly flow became somewhat weaker than it was during the previous two days. However, the flow was still southerly to the south of the mountains. Added to this, the SSA area was still moist from the previous days' rainfall and so the day was Very Active. The Pakistan's low pressure system was deepening and its trough extended over the Gulf of Oman on the 14<sup>th</sup> of July (Fig. 4-1H). A dry westerly air mass now dominated the flow over the area. There was no convection over the SSA on the 14<sup>th</sup> of July but isolated cells were observed to the southern parts of the Eastern Hajar Mountains.

To summarise, the 1000 hPa synoptic conditions favourable for the development of convective clouds over the Al Hajar Mountains are the existence of a closed heat low pressure over the Arabian Peninsula. The position and the depth of this low pressure controls the wind flow over the eastern side of the Peninsula. The Very Active days occurred when the heat low was almost in the centre of the Peninsula and the trough deepened to the southern extremes. This causes the flow over the eastern parts of the Peninsula, including the Al Hajar Mountains, to be moist southerly as the air originated from the Arabian Sea.



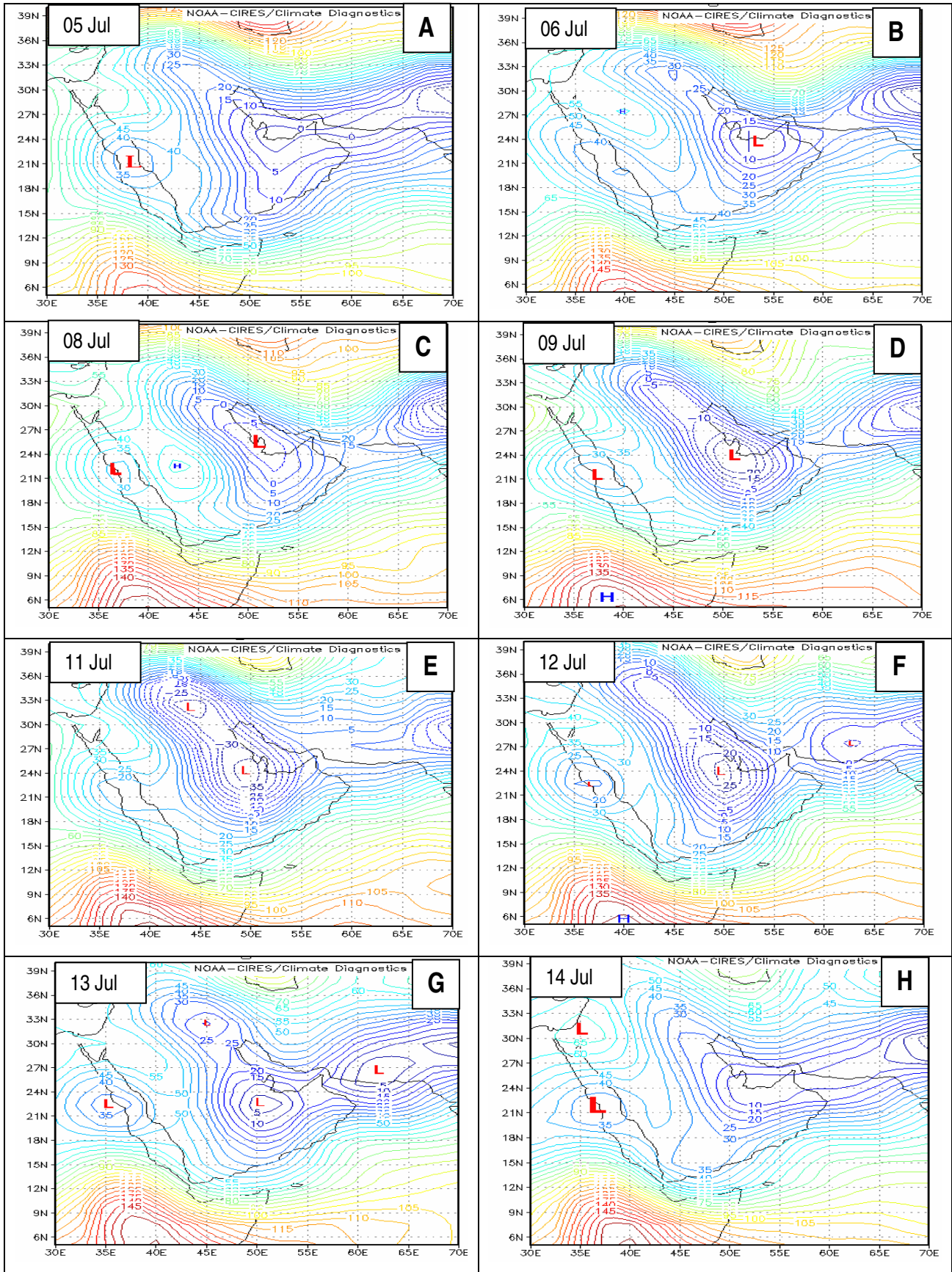


**Figure 4-1:** The geopotential heights (gpm) at 1000 hPa from the 5<sup>th</sup> to the 14<sup>th</sup> of July. (Adapted from: NCEP, 2007).



The deeper the trough is, the more moisture is that advected towards the mountains. This results in earlier daily development of convection over the mountains (10<sup>th</sup>-12<sup>th</sup> of July). If the heat's low position moves from the centre of the Peninsula, the trough in the south will start to fill in, causing less moisture to be advected from the Arabian Sea towards the mountains. This results in less convection over the mountains (6<sup>th</sup>-9<sup>th</sup> of July). The disappearance of the heat low permits the Pakistan trough to dominate over the area with a dry northwesterly flow over the SSA. This happened on the 5<sup>th</sup> and the 14<sup>th</sup> of July over the SSA.

### B. 850 hPa analysis

On the 5<sup>th</sup> of July the geopotential height analysis at 850 hPa indicated that the SSA was influenced by two low pressure systems; one over Pakistan and the other one was over the southeastern Arabian Peninsula (Fig. 4-2A). This kept a dry northerly flow over the eastern part of the Arabian Peninsula and it was a Non Active day. The low pressure system in the southeast extended a trough to the west on the 6<sup>th</sup> of July and a high pressure system developed to the northwest of KSA (Fig. 4-2B). This caused weak geopotential height gradient over the SSA. The flow was still dry northerly but some convection was observed over the SSA.

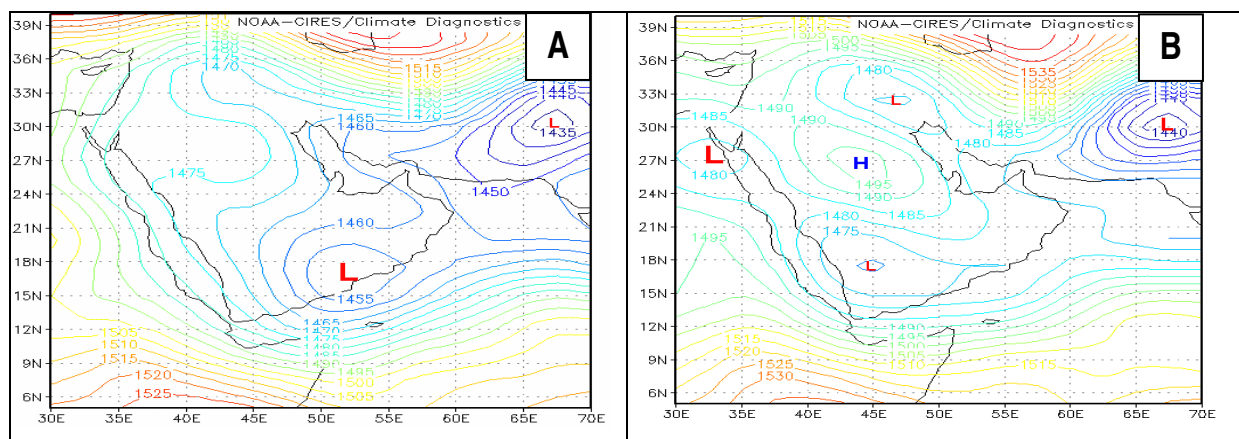


**Figure 4-2: The geopotential heights (gpm) at 850 hPa for the 5<sup>th</sup> (A) & the 6<sup>th</sup> of July 2004. (Adapted from: NCEP, 2007).**

On the 7<sup>th</sup> of July (Fig. 4-3A) the low pressure system centred over southern Iran expanded and extended a trough over the Arabian Gulf to the UAE and Oman. The low pressure system located over Pakistan formed an individual cell and had no effect over the Peninsula. Over the central part of the Peninsula, the high pressure system still dominated, with the low pressure system to the south. The northerly flow was not dominant anymore and the convection was more active than on the 6<sup>th</sup> of July. The low pressure system centred over southern Iran became deeper on the 8<sup>th</sup> of July (Fig. 4-3B) with the second low still prevailing over the SSA suggesting a light southwesterly wind over the SSA and a southeasterly wind in the south. The observed convection was more active than the day before and started later in the day to the west of the mountains (see

section 3.3). The Arabian Gulf and the UAE were still under the influence of the trough from the northern low pressure system.

The high pressure system over the central part of the Arabian Peninsula disappeared on the 9<sup>th</sup> of July (Fig. 4-3C) while the low pressure systems over the Arabian Gulf and the southeastern Peninsula (Fig. 4-3B) merged to form a deep low pressure over the northern Peninsula but extending a trough to the southeast. The position of the low pressure system coincided with the low at 1000 hPa, resulting in a deep moist southerly flow over the eastern Peninsula allowing early convection to develop over the mountains peaks. On the 9<sup>th</sup> of July, a deep low pressure system was located over eastern Iran but with no effect over the Arabian Peninsula. On the 10<sup>th</sup> of July, two low pressure systems were visible (Fig. 4-3D). The entire Arabian Peninsula was under the influence of the trough and the flow was moist southerly over the eastern Peninsula. This day was the beginning of the Very Active period as early convection started in the south and spread over the entire Al Hajar Mountains.

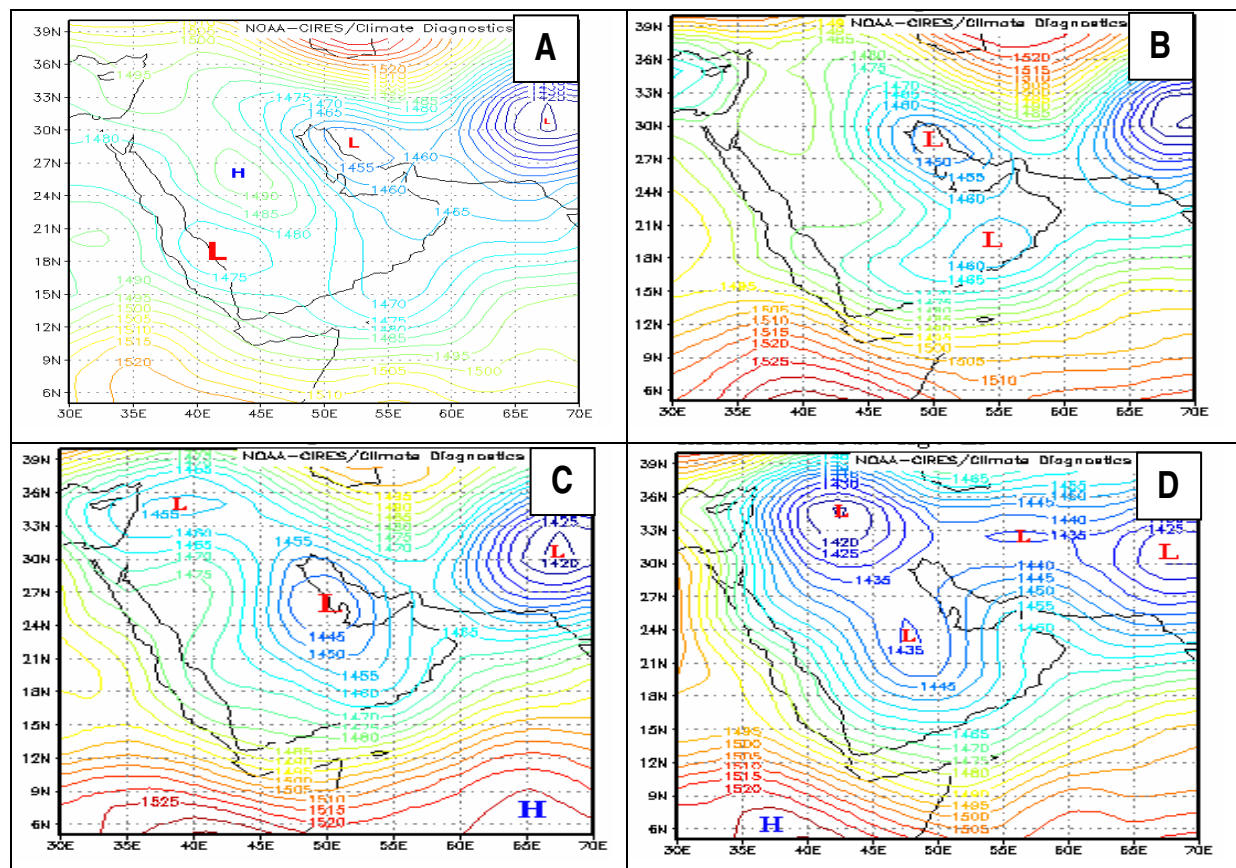


**Figure 4-3:** The geopotential heights (gpm) at 850 hPa for the 7<sup>th</sup> (A), 8<sup>th</sup> (B), 9<sup>th</sup> (C) & the 10<sup>th</sup> (D) of July 2004. (Adapted from: NCEP, 2007).

On the 11<sup>th</sup> of July, the low pressure deepened further to the south into the Arabian Sea (Fig. 4-4A) resulting in tighter geopotential height gradients over the eastern Peninsula. This produced a strong moist southerly flow over the mountains and hence, very active convection occurred. The synoptic pattern remained for the next day (12<sup>th</sup> of July) but with a deepening of the low pressure system over the central Peninsula (Fig. 4-4B).

On the 13<sup>th</sup> of July, the low pressure started to fill up and shifted a little further southwest (Fig. 4-4C). The low pressure system over northern Iraq joined the one east of Iran and the trough extended over the Gulf of Oman. A weak geopotential height gradient prevailed over the eastern Peninsula with the northwesterly wind starting to affect the northeastern parts of Oman.

On the 14<sup>th</sup> of July, the low pressure system over the central Peninsula became wider and moved to the south (Fig. 4-4D). The influence of the heat low diminished over the SSA and the low pressure over Pakistan became more dominant.

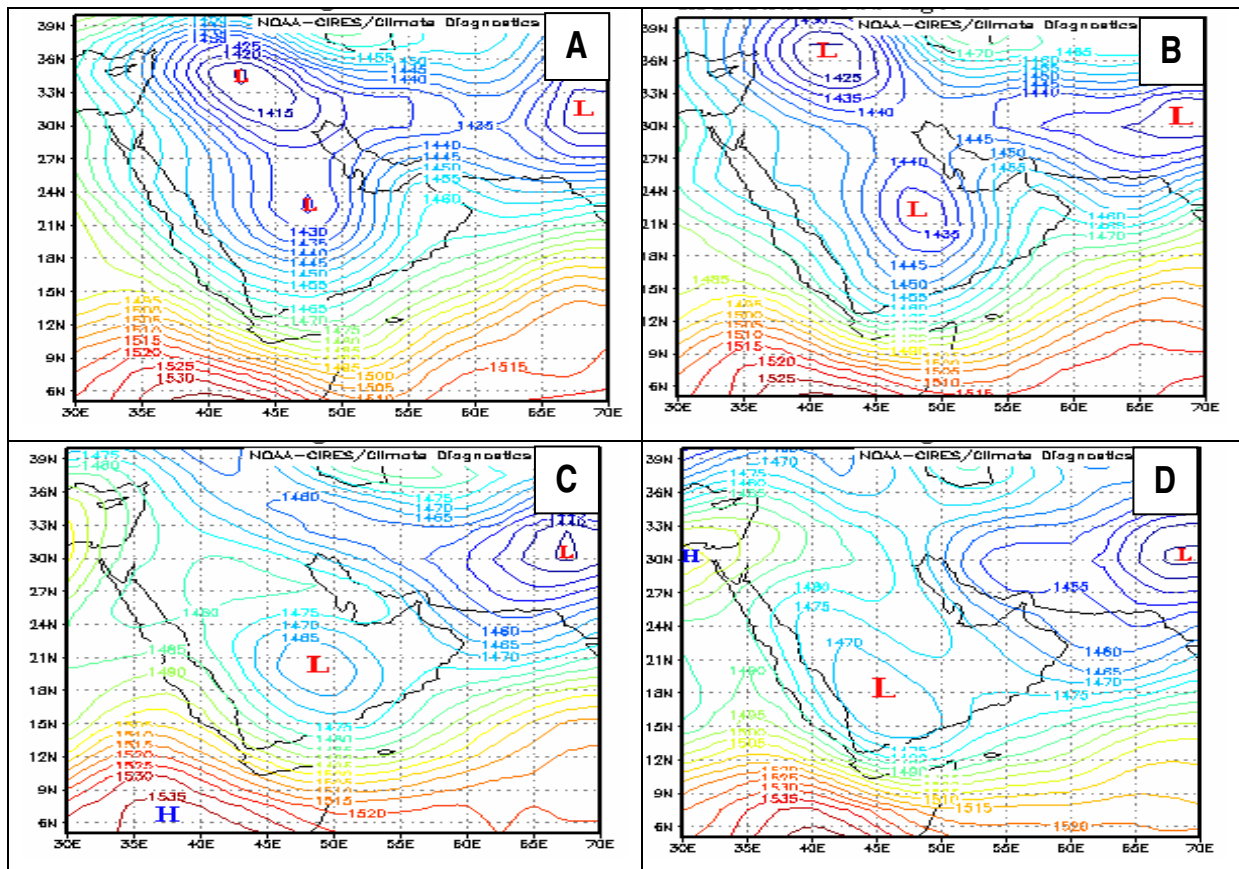


**Figure 4-4:** The geopotential heights (gpm) at 850 hPa for the 11<sup>th</sup> (A), 12<sup>th</sup> (B), 13<sup>th</sup> (C) & the 14<sup>th</sup> (D) of July 2004. (Adapted from: NCEP, 2007).

The synoptic pattern at 850 hPa was similar to the 1000 hPa pattern. The 1000 hPa low pressure system over the Arabian Peninsula extended vertically to the 850 hPa pressure level and was located at approximately the same geographical position.

The synoptic conditions at 850 hPa became favourable for convective development when the heat low pressure was located over the centre of the Arabian Peninsula with a trough deepening to the south as seen on the 10<sup>th</sup>-12<sup>th</sup> of July. This resulted in a moist southerly flow over the eastern part of the Peninsula with moisture advected from the Arabian Sea which enhanced the convection over the Al Hajar Mountains.

The intensity of convection is very sensitive to the position of the low pressure system. A change in the position of the low pressure over the centre of the Peninsula results in a weaker trough in the south and consequently less moisture being advected over the mountains from the Arabian Sea and therefore less convection. The weakening of this low pressure causes a slackening in gradients over the mountains and convection is limited. When the Pakistan's low pressure system dominates, the flow over the Peninsula becomes dry northerly over the mountains and hence no convection results.

### **C. 500 hPa analysis**

The 500 hPa geopotential heights show that the dominant pattern during this period was a strong high pressure system and a ridge affecting the entire area. This semi permanent high pressure kept the upper air dry.

On the 5<sup>th</sup> of July, there was a high pressure system situated west of the Arabian Peninsula and another one located south of Iran extending its ridge over northern Oman (Fig. 4-5A). Between these two systems, a trough extended from the Arabian Sea low pressure system affecting the southeastern part of the Peninsula. The two high pressure systems joined to form a strong high pressure system over the northern parts of the Peninsula by the 7<sup>th</sup> of July (Fig. 4-5B). The SSA was now under the influence of a high pressure ridge which became weak on the 10<sup>th</sup> and propagated westward to the northern parts of the Red Sea with a weak geopotential height gradient over the SSA (Fig. 4-5C).

By the 11<sup>th</sup> of July, a closed high pressure system was over the Arabian Sea and southeastern coast of Oman (Fig. 4-5D). This high pressure moved northward by the 12<sup>th</sup> of July to cover the SSA and the Gulf of Oman (Fig. 4-5E). On the 13<sup>th</sup> of July the high pressure system returned to the central Peninsula extending its ridge over SSA (Fig. 4-5F).

The main synoptic character of the 500 hPa was the dominant high pressure system over the entire area. This was responsible for the prominent dry and stable mid-tropospheric layer normally found (Seeb and Abu Dhabi soundings, see section 4.4) around the 500 hPa level. However, it appears as if the 500 hPa high had very little influence on the convection over the mountains.

In fact, the synoptic circulation on the lower levels such as 850 hPa and 1000 hPa is more important for the development of convective clouds. It is therefore proposed that the 500 hPa pressure level is less important and will not be considered for the forecasting of thunderstorms over the Al Hajar Mountains in summer in this research.

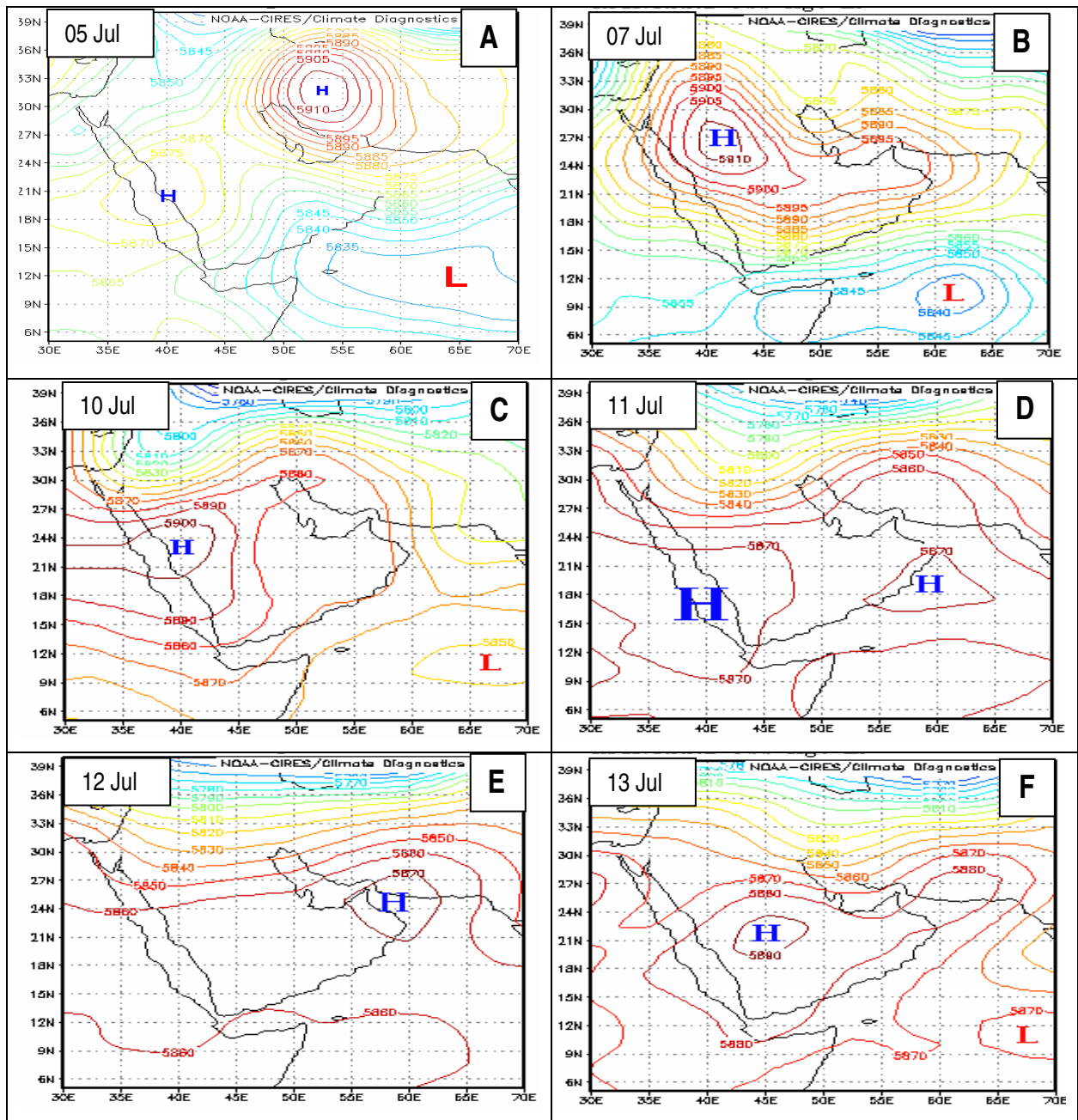


Figure 4-5: The geopotential heights (gpm) at 500 hPa for the 5<sup>th</sup> (A), 7<sup>th</sup> (B), 10<sup>th</sup> (C), 11<sup>th</sup> (D), 12<sup>th</sup> (E) and 13<sup>th</sup> (F) of July. (Adapted from: NCEP, 2007).

#### 4.2.2 The mesoscale model (MM5)

The MM5, as described before in 2.1.4, was used to forecast the development of convection over the SSA during the seeding project. In this part, a short discussion on the capability of this model to predict the general synoptic situation is provided by comparing some of its products to the NCEP data.



The mean sea level prognosis, valid at 0600 UTC, showed that on the 5<sup>th</sup> of July the area was affected by a broad trough extending from the low pressure located over Iran (Fig. 4-6A). The trough was clearly connected to the northern low pressure system and there was no heat low predicted to be present over the Arabian Peninsula. The pressure over the entire Peninsula was generally between 1002 hPa and 999 hPa (Fig. 4-6A).

At the model indicated surface temperatures there was certainly a heat effect. The main aspect is the weak pressure gradient and therefore no moisture inflow. The weak trough suggests that the flow over the SSA should be light westerly to northwesterly with dry desert air present. This is supported by surface temperatures over 40 °C with negative dew point temperatures at most of the observation stations and therefore does not support convective development over the mountains.

On the 7<sup>th</sup> of July, when convection did occur, a closed heat low of 999 hPa was predicted to be west of Oman between the UAE and KSA (Fig. 4-6B). The temperatures in the area between the UAE and KSA were predicted to be above 40 °C. This resulted in the development of the heat low as an independent low pressure system and not connected to the low in the north. The northwesterly wind, reported by most of the observation stations in the south, west of the mountains was not as dry as on the 5<sup>th</sup> of July. A locally generated northwesterly wind off the Arabian Gulf is not as dry as when the synoptic circulation causes the wind to arrive from the northwest from the Arabian Desert, or is drawn from the north from the Iranian desert north of the Arabian Gulf. On the 7<sup>th</sup> of July, unlike the 5<sup>th</sup> of July, the wind was not westerly over the entire SSA area as easterly winds occurred in the north as reported in many stations like Hatta, Al Malaiha and Al Shiweb (see section 4.3.2). It is likely that this wind brought moisture from the Gulf of Oman and as a result, isolated convection was seen over the convergence zones created by the wind circulations (see section 3.3.2).

On the 10<sup>th</sup> of July the low pressure system was predicted to have a central pressure of 996 hPa and enclosed the entire center of the Arabian Peninsula (Fig. 4-6C). The Figure also indicates the deepening of the trough in the south and the southerly flow therefore became dominant over the eastern part of the Peninsula. The position of the heat low and its deepening to the south caused monsoonal moisture from the Arabian Sea to be advected northwards to the Al Hajar Mountains and enhanced moist convection. As a result, this was one of the Very Active days with the convection developing early over the mountains peaks.

On the 14<sup>th</sup> of July the synoptic situation was almost like the one on the 5<sup>th</sup> of July with a return to a weak pressure gradient, the pressure being generally about 1002 hPa (Fig. 4-6D). There was no marked heat low represented over the Peninsula and the trough was connected to the northern system, resulting in dry air. However, there was limited convection far to the south where the moisture was available over the Eastern Hajar Mountains. Otherwise, the atmosphere was dry and no convection was reported over the SSA.

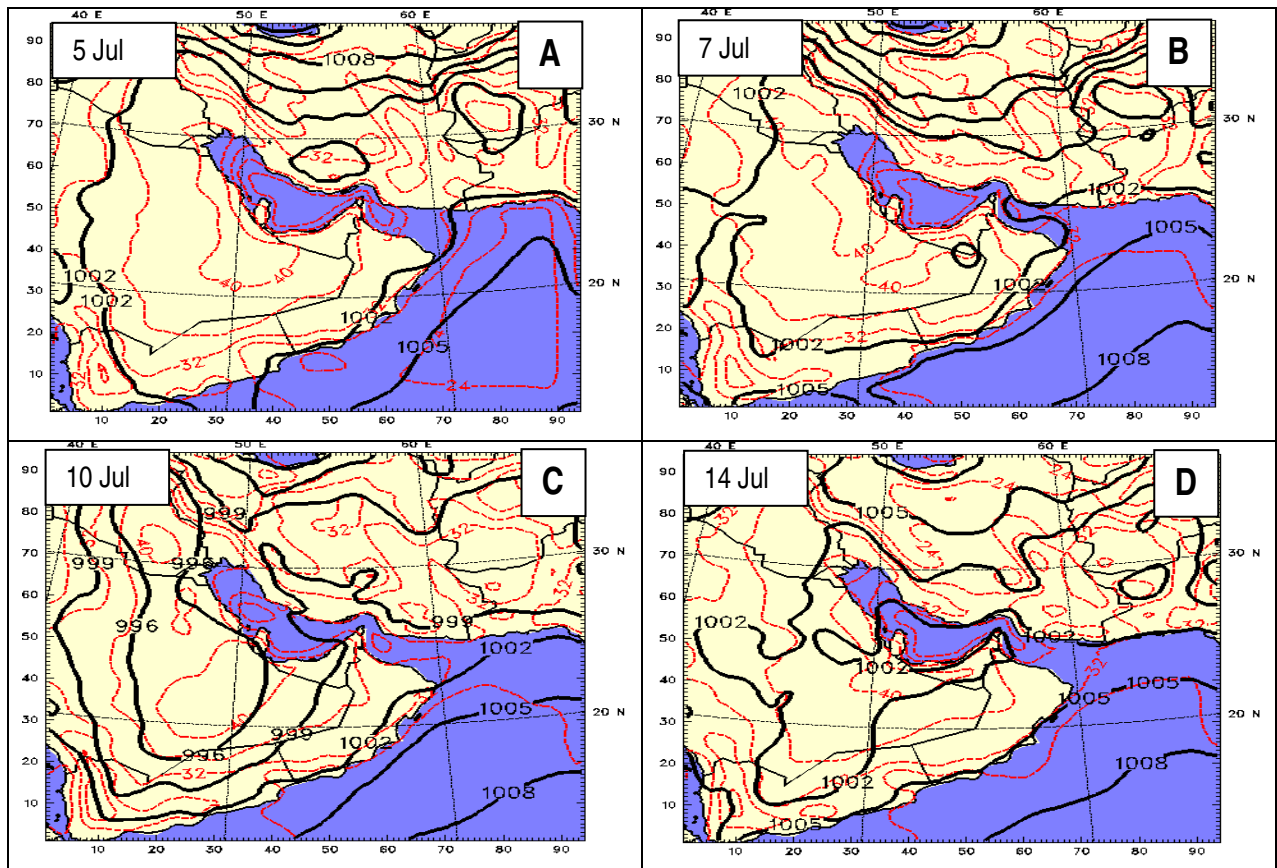


**Figure 4-6:** The MM5 prognosis of mean sea level pressure (hPa) on the 5<sup>th</sup> (A), 7<sup>th</sup> (B), 10<sup>th</sup> (C) and 14<sup>th</sup> (D) July 2004 at 0600 UTC (solid lines) and temperatures in °C (red lines). Contour intervals of the isobars are 3 hPa.

The prognosis of 850 hPa geopotential height on the 5<sup>th</sup> of July indicates the broad trough over the entire area (Fig. 4-7A). The wind vectors showed the westerly to northwesterly winds over the SSA. This brought in dry air and prevented convection. The cyclonic wind circulation indicates the low pressure system located over the southeastern Peninsula.

On the 7<sup>th</sup> of July (Fig. 4-7B) the 850 hPa trough was predicted to extend from the northeast and became a closed low over the eastern part of the Peninsula. However, the cyclonic wind circulation indicated that the trough extended from the low pressure located northwest of the Arabian Gulf. The dry westerly wind was not predicted over the SSA and hence convection developed in some places over the SSA.

On the 10<sup>th</sup> of July, the 850 hPa geopotential height prognosis showed a deep trough of low pressure dominating over the centre of the Peninsula (Fig. 4-7C). The centre of the low pressure was depicted by the cyclonic winds and the wind speed near the centre of the low pressure system was predicted to be 25 kt. The wind vectors also showed the moist southerly flow over the Western Hajar Mountains where strong convection developed.

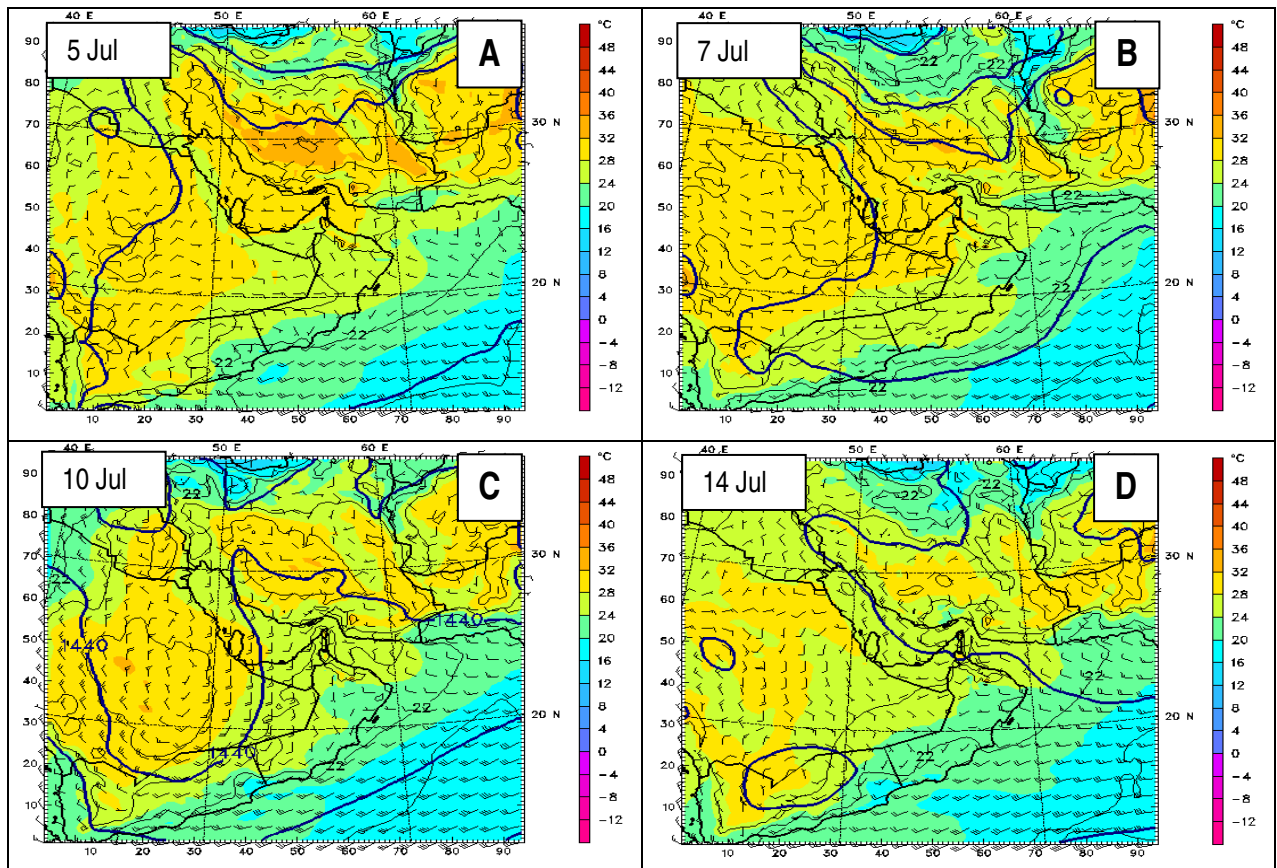


**Figure 4-7: The MM5 prognosis of 850 hPa geopotential heights (blue lines), winds (kt) and air temperatures (°C) on the 5<sup>th</sup> (A), 7<sup>th</sup> (B), 10<sup>th</sup> (C) & the 14<sup>th</sup> (D) of July 2004 at 0600 UTC.**

On the 14<sup>th</sup> of July, the trough moved to the northeast of the governorate of Musandam and the wind vectors indicated the dry westerly wind over the UAE and northern Oman (Fig. 4-7D). Limited convection occurred over the mountains and to the south of the SSA.

In general, the mean sea level pressure, valid at 0600 UTC, showed good correlation with NCEP re-analysis data in predicting the main features of the synoptic situation of the area. The MM5 850 hPa geopotential heights prognosis, valid at 0600 UTC and the NCEP geopotential heights at 850 hPa were also in good agreement if the wind circulation of the MM5 are taken into consideration. The general synoptic situation showed a significant difference between the Non Active, Active and Very Active days. The main feature was the existence of the heat low pressure system over the Arabian Peninsula and its dominance over the area. The position of the low pressure and how it intensified and deepened over the area are other significant factors for the convection development over the Al Hajar Mountains.

The dominance of the heat low over the centre of the Arabian Peninsula with a trough deepening towards the Arabian Sea is considered the most favourable condition for assisting very active development over the Al Hajar Mountains. The deep trough forces the cyclonic wind to flow strong southerly over the eastern part of the Peninsula. The southerly flow over the region is associated with the monsoon it assures the advection of



moisture from the Arabian Sea. The influence of the southerly winds on moisture over the SSA can be seen in Figure 4-8. On the 10<sup>th</sup> of July, MM5 predicted water vapour mixing ratio (WVMR) values of 14-15 g/kg over the SSA (Fig. 4-8A). On the 14<sup>th</sup> of July, as the winds became southwesterly, the WVMR values plummeted to less than 11 g/kg (Fig. 4-8B). In the south, where isolated convection occurred on the 14<sup>th</sup> of July, the WVMR remained close to 13 g/kg.

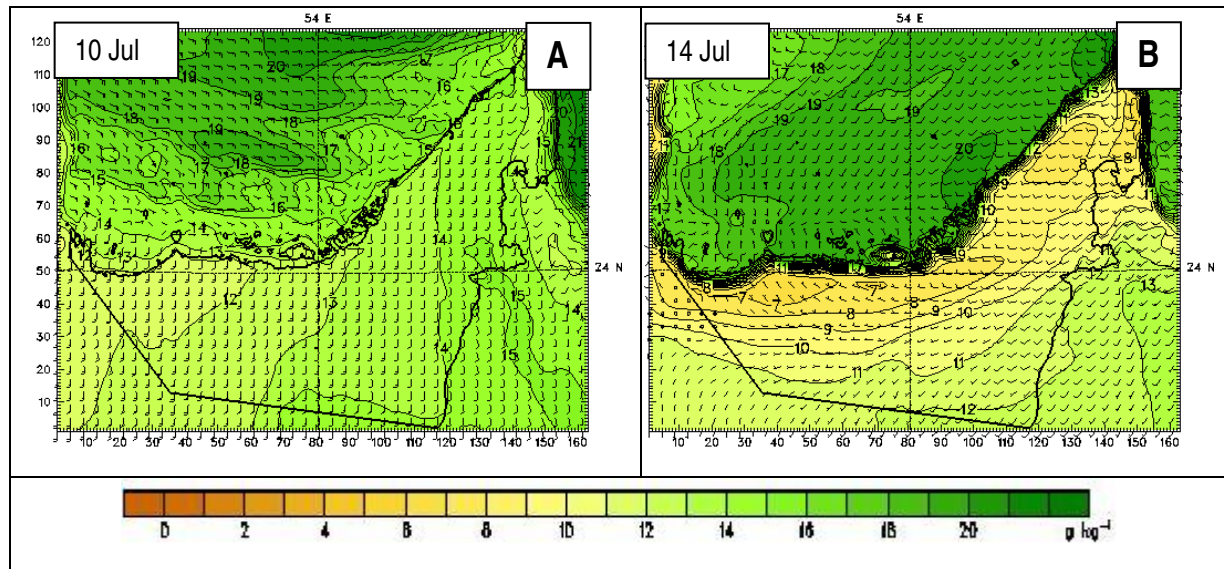


**Figure 4-8:** The MM5 prognosis of the surface water vapor mixing ratio in g/kg (color contours) and the wind (kt) on the 10<sup>th</sup> (A) and 14<sup>th</sup> (B) of July 2004 at 0600 UTC.

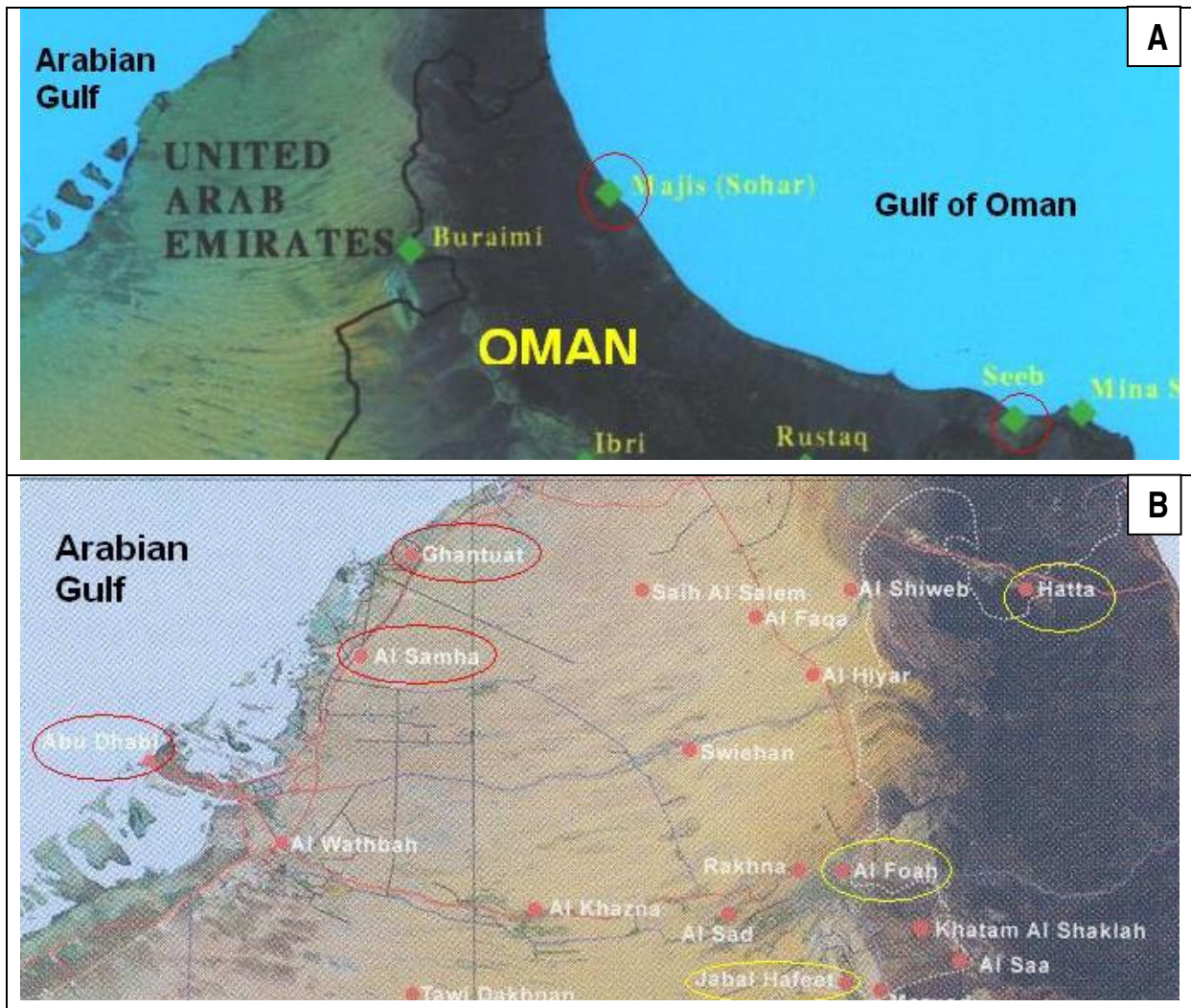
### 4.3 The Impact of the synoptic conditions on the mesoscale development

#### 4.3.1 Coastal stations

As discussed in chapter 2, the coastal stations used in this study were divided into two categories. They are divided to represent stations east of the SSA, Sohar and Seeb (Fig. 4-9A) and west of the SSA, Ghantuat, Al Samha and Abu Dhabi (Fig. 4-9B).

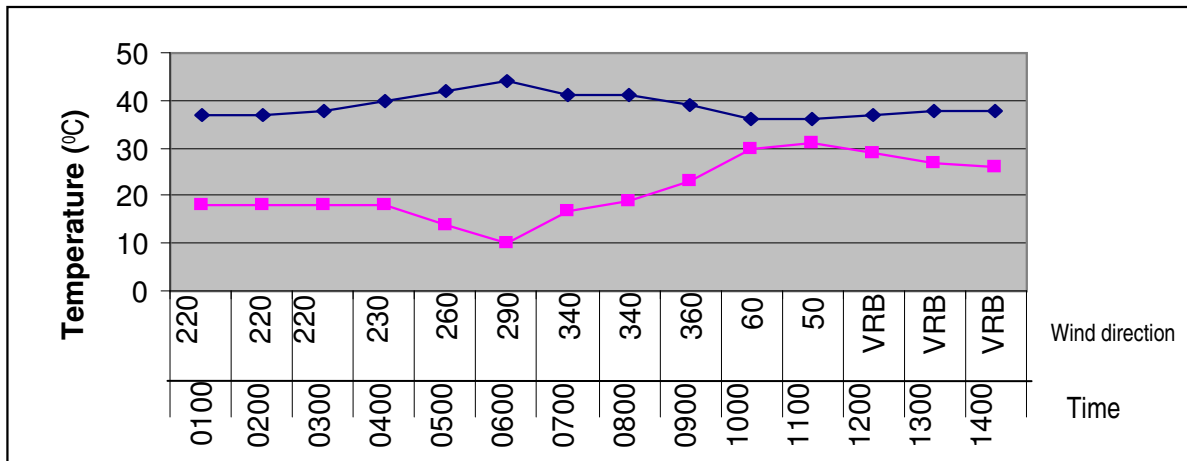
During this study period, the wind at Seeb was generally on-shore (northeasterly) with a wind speed of 5-15 kt. This wind normally starts at 0600 UTC unless delayed by a synoptically generated opposing southwesterly wind. On the 5<sup>th</sup> of July the trough of low pressure situated over Pakistan caused fresh southwesterly winds to blow over the station from early morning. The southwesterly wind was also observed for a couple of hours before it turned into northeasterly on the 12<sup>th</sup>, 13<sup>th</sup> and 14<sup>th</sup> of July. Normally, the southwesterly or westerly winds at Seeb and Sohar stations are very dry and hot and cause the surface temperature to rise suddenly with an accompanying dramatic drop in the dew point temperature. Westerly winds originate over the mountains and as the air is forced to descend towards the coast, it warms at the dry adiabatic lapse rate. This

happened on the 5<sup>th</sup> of July when the maximum temperature at Seeb was 44 °C and was recorded early at 0600 UTC.



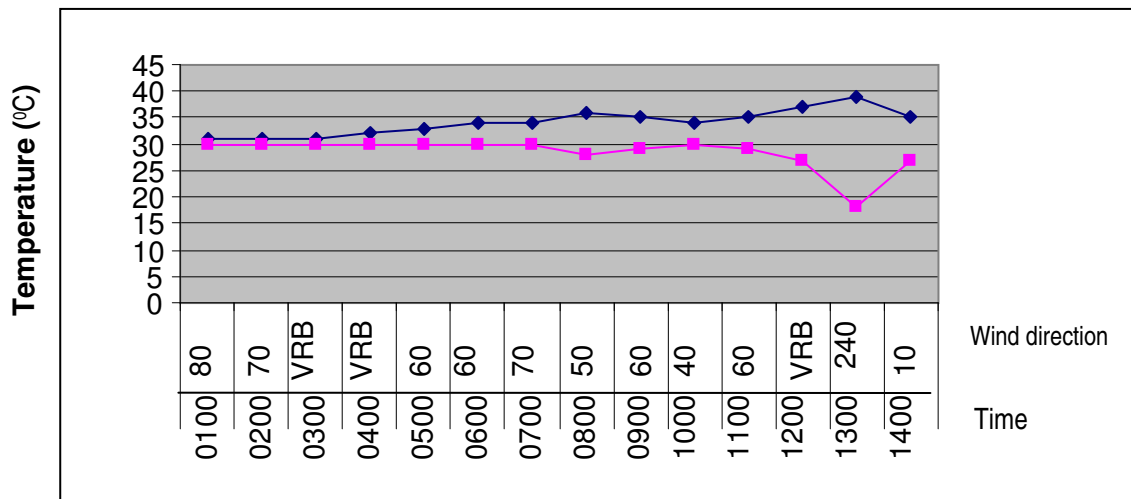
**Figure 4-9:** Regional maps showing the eastern coastal stations (A) and the western coastal stations (B) marked by red circles/ellipsoids. The three inland analyzed stations are marked by yellow circles/ellipsoids (B).

Figure 4-10 shows the dry hot air at 0600 UTC while it became moist and cooler at 1000 UTC as the wind turned northeasterly. Figure 4-10 indicates the relationship between the wind direction and the surface temperature and moisture. At 1000 UTC the flow become on-shore from the Gulf of Oman, the surface temperature dropped and the dew point temperature increased. The synoptically generated southwesterly wind was dominant, but eventually the flow became on-shore as the sea breeze became strong enough to oppose the southwesterly wind, but without any effect on convective development. The implication is that the dry westerly wind in the morning restricted the sea breeze to the coast until it was too late to aid convection, resulting in the 5<sup>th</sup> of July being a Non Active day.



**Figure 4-10:** The hourly temperature (blue) and dew point temperature (pink) in °C on the 5<sup>th</sup> of July 2004 at Seeb from 0100 UTC to 1400 UTC. The wind direction in degrees and time (UTC) is given below.

After the 5<sup>th</sup> of July, there were no prevailing southwesterly winds during this study period and the maximum surface temperature was not reached early. For example, the maximum temperature on the 6<sup>th</sup> of July was only 35 °C and occurred at 0900 UTC. Another example is the 11<sup>th</sup> of July which was a Very Active day (Fig. 4-11). The day started cooler with much higher dew point temperatures than on the 5<sup>th</sup> of July as the wind was an on-shore easterly to northeasterly from the onset.



**Figure 4-11:** The hourly temperature (blue) and dew point temperature (pink) in °C on the 11<sup>th</sup> of July 2004 at Seeb from 0100 UTC to 1400 UTC. The wind direction in degrees and time (UTC) is given below.

At Sohar, to the north of Seeb (Fig. 4-9A), the flow was generally on-shore during this study period and the wind strength between 5-15 kt during the Active Day Period (ADP). This was also true for the Non Active days of the 5<sup>th</sup> and the 14<sup>th</sup>. The maximum surface temperature varied between 35-39 °C and the maximum dew

point temperature was 26- 30 °C. The on-shore flow at this station did not always reach the mountains to aid the development of the convection.

The observations from the three western coastal stations along the Arabian Gulf, Ghantuat, Al Samha and Abu Dhabi (Fig. 4-9B) experienced an increase in the dew point temperature with a westerly on-shore wind. However, there were some notable differences. At Ghantuat the air became very moist when the wind direction veered beyond 200°. More moisture is advected when the wind blows from west or northwest than from the south, which is off the desert. A good example was on the 5<sup>th</sup> of July when at the start of the ADP the winds were almost southerly (190°), resulting in a minimum dew point (11 °C) and a maximum temperature (41 °C) recorded at 0745 UTC. After 15 minutes, the wind turned southwesterly (220°) and the dew point temperature increased by 7 °C. However, on the 6<sup>th</sup> of July when the wind direction was westerly (270°) the maximum surface temperature at Ghantuat was 6 °C cooler than on the 5<sup>th</sup> of July.

### **4.3.2 Inland stations**

The observations of three different inland stations are analyzed here in order to find the main characteristics of the temperature, dew point and the wind on Non Active, Active and Very Active days during this study period. The stations are Al Foah, Jabal Hafeet and Hatta (Fig. 4-9B).

On the 5<sup>th</sup> of July, at Al Foah, situated west of the mountains, the wind was southwesterly at the beginning of the ADP but then turned to northwesterly after 1000 UTC, causing the dew point temperature to drop to negative values (Fig. 4-12A). The Figure indicates the dry air over the station as the temperature was mostly around 45 °C and accompanied by negative dew points. A northwesterly wind at this station is generally dry as the air originates over the mountains of Iran. However, it is occasionally associated with a sea breeze circulation and therefore with higher dew point temperatures (as discussed in section 4.3.3). In Figure 4-12B the dew point temperature increased by 13 °C in 15 minutes, just after 1400 UTC as the wind turned northwesterly and the influence of the sea breeze became apparent. The trough associated with the Pakistan low pressure started weakening by the 6<sup>th</sup> of July (Fig. 4-1B) and the synoptically induced influx of dry air mass into the SSA decreased. However, the increase in dew point temperature happened late on the 6<sup>th</sup> and was not associated with convective development in the area (see section 3.3.1). The northerly/northwesterly wind continued on the 7<sup>th</sup> of July, causing the dew point temperature to drop gradually at the beginning of the ADP but not reaching negative values this time (Fig. 4-12B). Some convection was observed after 1100 UTC over the area east of the station. The wind turned northeasterly at 1300 UTC and probably reached the mountains after propagating through the valleys in the mountains. The mixing of the two air masses, the northwesterly and the northeasterly, created a convergence zone which helped the convection to take place and some convective clouds were observed after 1330 UTC (see section 3.3.2).

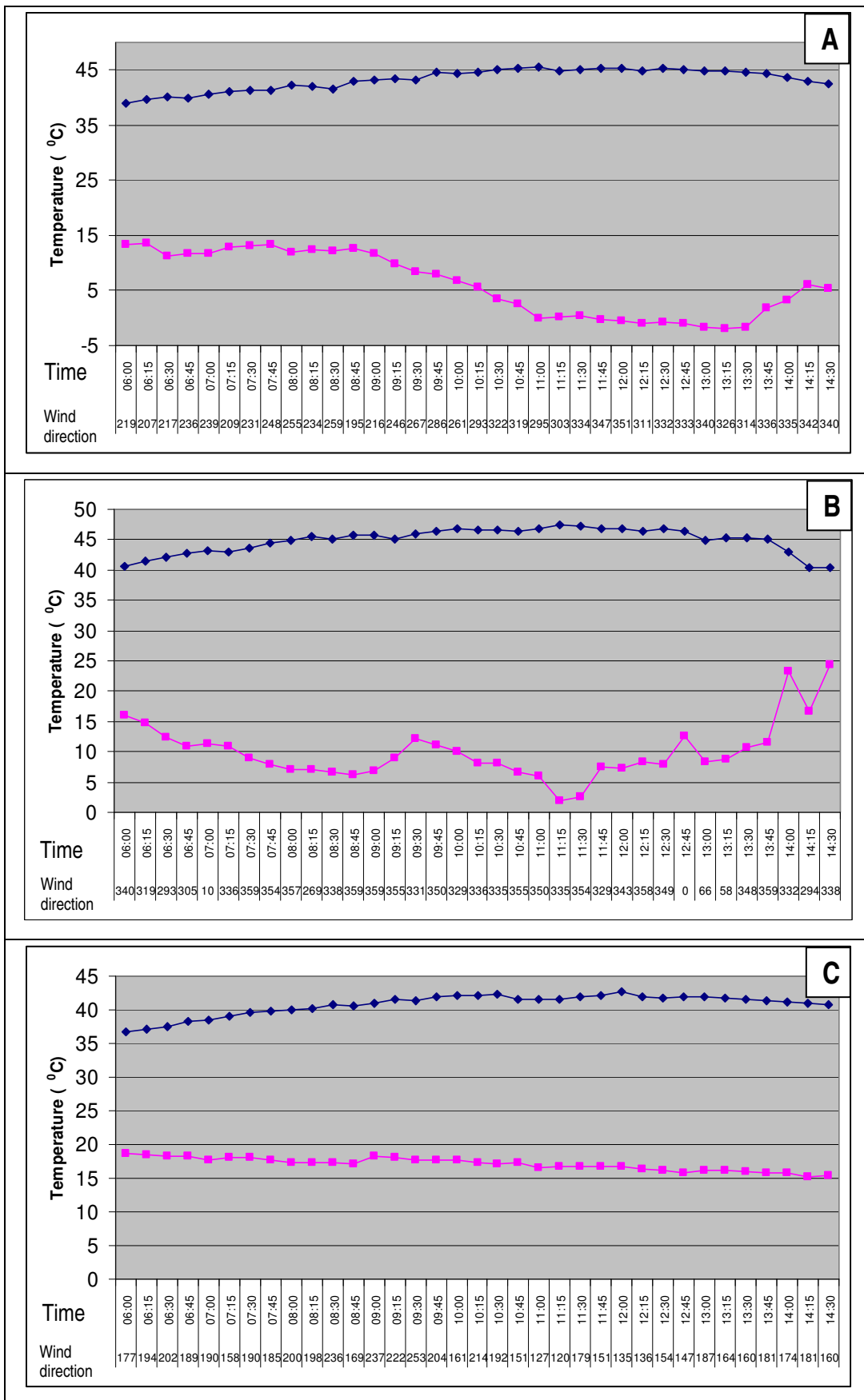


Figure 4-12: The temperature (blue) and dew point (pink) in °C on the 5<sup>th</sup> (A), 7<sup>th</sup> (B) and 11<sup>th</sup> (C) at Al Foah from 0600 UTC to 1400 UTC. The wind direction in degrees and time (UTC) is given below.



At 1400 UTC, a northwesterly wind of 19 kt arrived at the station and replaced the northerly 7 kt wind observed 15 minutes before, resulting in an increase in the dew point temperature by more than 10 °C. This increase occurred in association with the sea breeze, but the moisture did not aid convective development as it arrived late in the afternoon (after 1400 UTC). During the following three days, the wind direction was mostly westerly with occasional intrusion of easterly winds. The air remained relatively moist with dew point temperatures above 13 °C. There was no abrupt increase in the dew point temperature indicating the sea breeze arrival like the one on the 6<sup>th</sup> and the 7<sup>th</sup> of July. Most of the moisture was advected from the dominant synoptic southeasterly flow during the night and the morning and was moist enough to keep the atmosphere from drying during the day. Again on the 8<sup>th</sup> of July, the convection was observed over the station at about 1245 UTC after the intrusion of the easterly wind. However, prior to that, a storm was observed at 1130 UTC to the north of the station. Although the air was moist, there was no convective development at this station in consequent days. This is most likely due to the absence of the convergence zone discussed above.

On the 11<sup>th</sup> of July, the dew point temperature was mostly between 15-20 °C (Fig. 4-12C). The southeasterly wind along with the occasional southwesterly had no significant effect on altering the dew point temperatures. This situation was the same on the 12<sup>th</sup> and the 13<sup>th</sup> of July with generally westerly winds. On the 14<sup>th</sup> of July, the situation was mostly the same as on the 5<sup>th</sup> of July. The dew point temperature dropped gradually to negative values with a dry northwesterly air mass.

At this station, a westerly wind is not necessarily a dry wind unless it occurs in association with a synoptic flow originating from Iran or the central parts of the Arabian Peninsula.

Jabal Hafeet station is situated on the Hafeet Mountain, which is west of Al Hajar Mountains on the border between Oman and the UAE (Fig. 4-9B). The observations from this station on the 5<sup>th</sup> of July showed a dry northwesterly wind prevailing with negative dew point temperatures (Fig. 4-13A). The same happened on the 6<sup>th</sup> of July before the fresh northwesterly sea breeze reached the station after the end of the ADP at about 1445 UTC. This caused the dew point temperature to climb by more than 12 °C in 30 minutes. On the 7<sup>th</sup>, the northwesterly wind was not as dry as before and the sea breeze again reached the station again after 1400 UTC, increasing the dew point temperature by more than 7 °C (Fig. 4-13B). On the 8<sup>th</sup> of July, the flow was southerly to southeasterly overnight, but in early morning it became southwesterly then northwesterly during the ADP with no significant effect on the moisture as the dew point temperature remained above 7 °C. There was not any abrupt increase in the dew point temperature on this day. The southwesterly wind on the 9<sup>th</sup> of July was not dry as the peninsula was already filled with moisture originating from the southeast (Fig. 4-13C). During the night of the 13<sup>th</sup>, the moisture over the peninsula decreased due to the lack of the moist southeasterly flow.

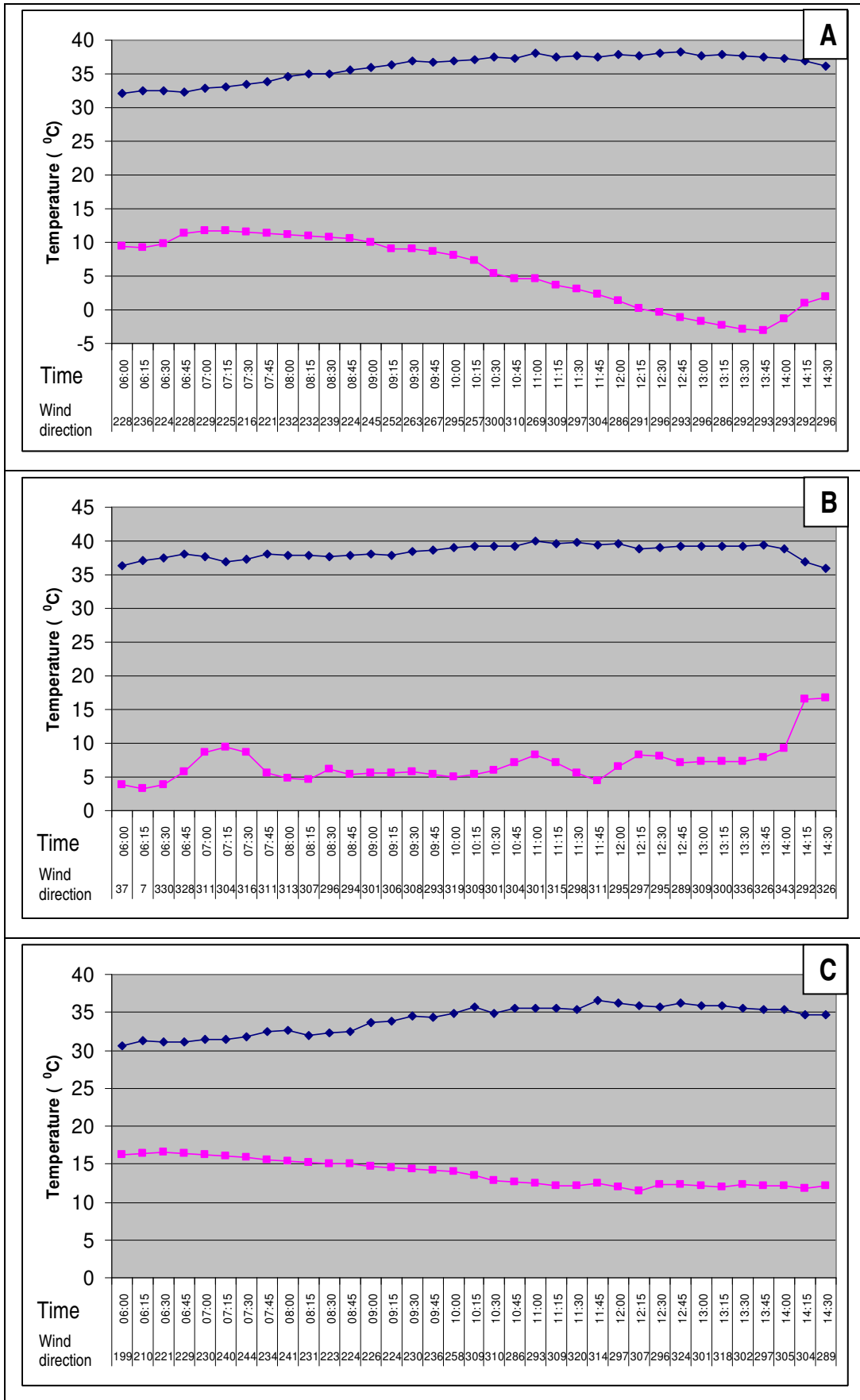


**Figure 4-13:** The temperature (blue) and dew point (pink) in °C on the 5<sup>th</sup> (A), 7<sup>th</sup> (B) and 13<sup>th</sup> (C) at Jabal Hafeet from 0600 UTC to 1400 UTC. The wind direction in degrees and time (UTC) is given below.



This resulted in a gradual decrease in dew point temperature which reached negative values on the 14<sup>th</sup> as the dry airmass intruded the area. Although there was no convection observed over the station during this period, the observations indicated moist air even at this elevated station (1059 m) on the mountain on Active days. This is a true indication of the moisture depth at the SSA and the moisture alone is not enough to initiate convection.

Hatta is located in between the mountains bordering the UAE and Oman (Fig. 4-9B). On the 5<sup>th</sup> of July, the wind direction was westerly at a speed of 4-13 kt. The atmosphere was very dry with high surface temperatures (Fig. 4-14). The surface temperature was above 40 °C during the ADP with a maximum of 46 °C recorded at 1200 UTC. The dew point temperature was very low and never exceeded 6 °C with negative values during most of the ADP. The observations at this station clearly differentiate between the dry air prevailing on the 5<sup>th</sup> of July and the moist air on the following days.

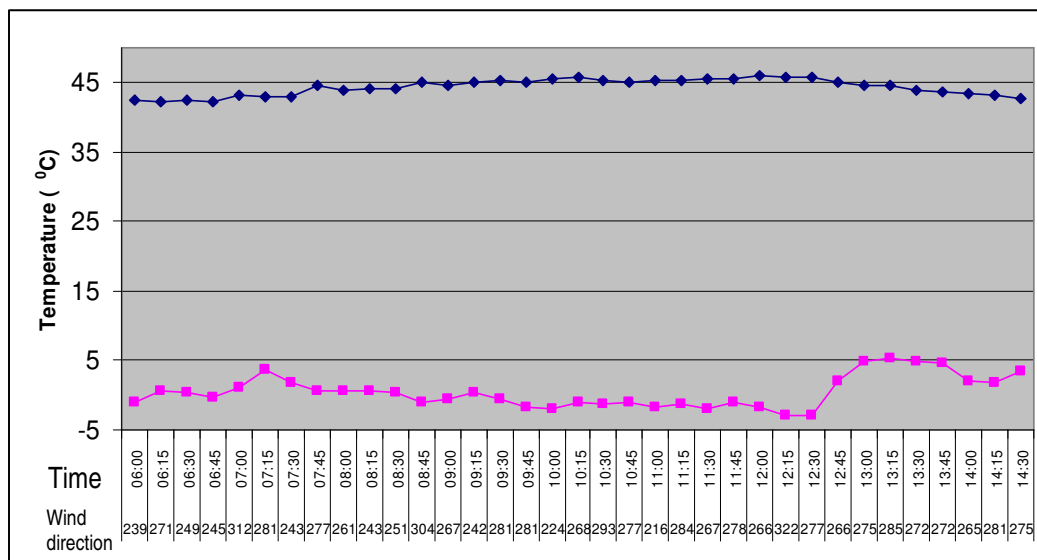


**Figure 4-14:** The temperature (blue) and dew point (pink) in °C on the 5<sup>th</sup> of July 2004 at Hatta from 0600 UTC to 1400 UTC. The wind direction in degrees and time (UTC) is given below.

The situation changed rapidly on the 6<sup>th</sup> of July when the maximum temperature did not reach 40 °C as moist easterly winds blew at the station from the early hours of the day. The temperature was much lower than the previous day with a maximum of 39 °C and the dew point temperature was above 25 °C (Fig. 4-15).

In general, westerly winds over this station were dry and easterly winds were moist. The easterly flow from the Gulf of Oman seems to reach Hatta with ease. However, the dominant easterly flow with no intrusion of a westerly wind indicates the lack of wind convergence zones over the area and hence convection at this station was rare. Most of the wind convergence occurred north and west of the station where convection occurred. The easterly flow continued for the next three days with considerable moisture being advected from the Gulf of Oman.

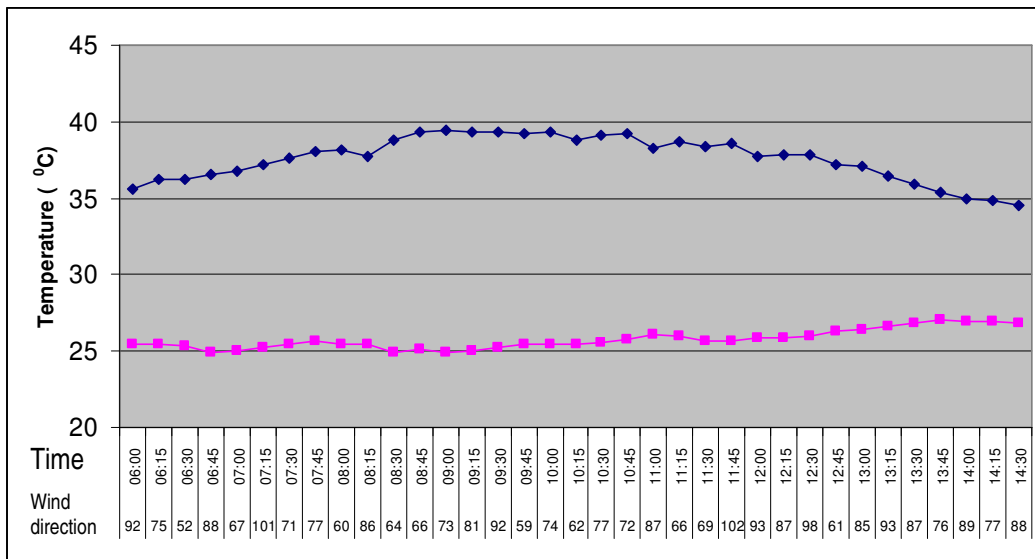


**Figure 4-15:** The temperature (blue) and dew point (pink) in °C on the 6<sup>th</sup> of July 2004 at Hatta from 0600 UTC to 1400 UTC. The wind direction in degrees and time (UTC) is given below.

On the 10<sup>th</sup> of July, a drop in dew point temperature of 5 °C was observed in 15 minutes when the wind direction changed to the northwest at 0800 UTC (Fig. 4-16). However, the dew point temperature increased to about 9 °C in 15 minutes when the wind returned to the east at 0915 UTC. This day was Very Active with convection being observed over the entire mountain range. The intrusion of a different air mass borne by the westerly wind helped the convection to develop over the station at about 1030 UTC (see section 3.3.5).

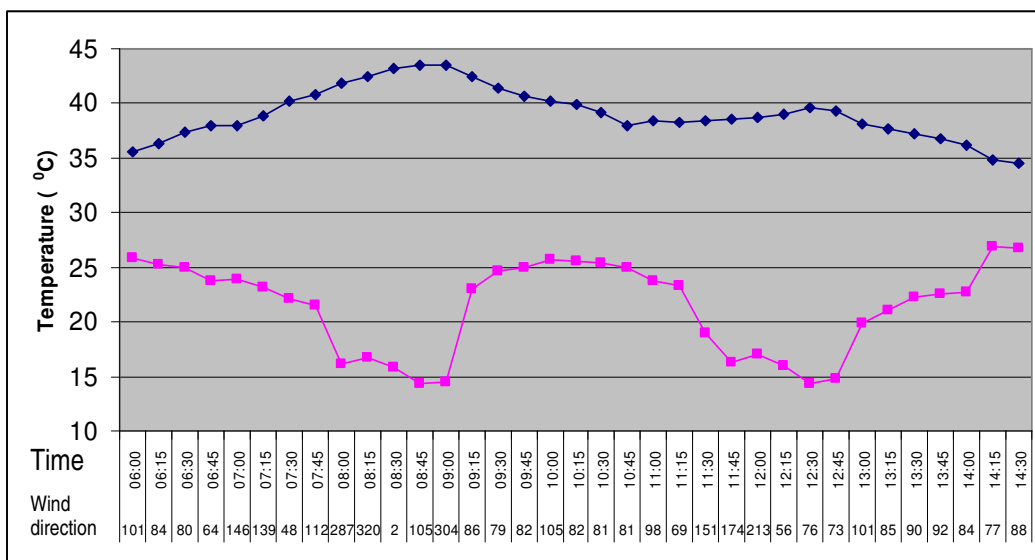


**Figure 4-16:** The temperature (blue) and dew point (pink) in °C on the 10<sup>th</sup> of July 2004 at Hatta from 0600 UTC to 1400 UTC. The wind direction in degrees and time (UTC) is given below.

On the 11<sup>th</sup> of July, the dew point dropped from 26 °C at 1045 UTC to 17 °C at 1100 UTC when the northwesterly wind arrived over the station. This mixing of the wet and dry air masses aided the convection to develop immediately over the station.

The same phenomenon was observed on the 12<sup>th</sup> of July after 1000 UTC when the wind direction changed to southwesterly instead of southeasterly and hence the dew point temperature dropped dramatically by 13 °C in 15 minutes (Fig. 4-17). The dew point remained below 15 °C until 1245 UTC when the wind became northeasterly and the dew point increased by 20 °C. The convection over the station was observed after 0900 UTC. By the evening, the dominant wind became westerly and remained the same during the last two days of the period. The atmosphere dried gradually and the dew point temperature was back to negative values on the 14<sup>th</sup> of July as started on the 5<sup>th</sup> of July.

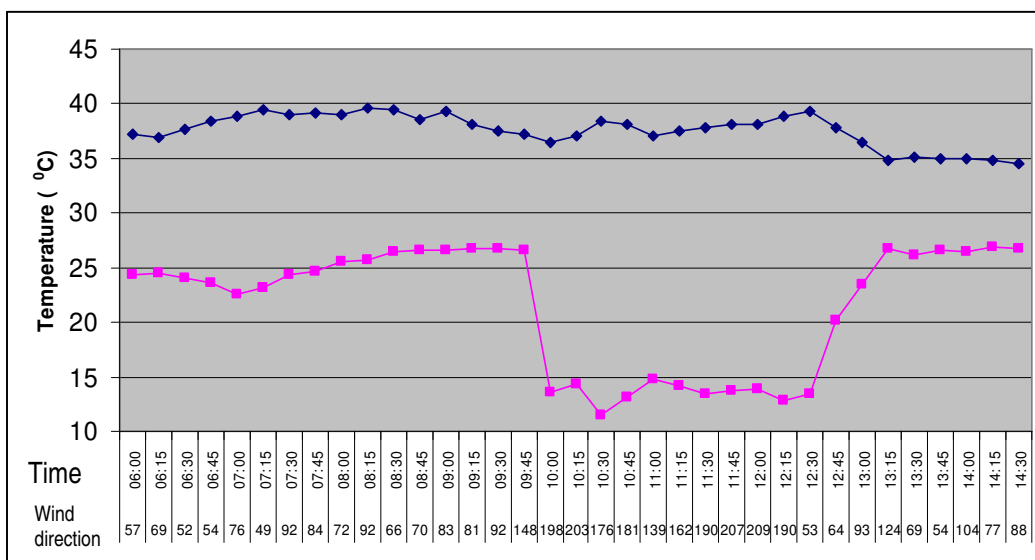


**Figure 4-17: The temperature (blue) and dew point (pink) in °C on the 12<sup>th</sup> of July 2004 at Hatta from 0600 UTC to 1400 UTC. The wind direction in degrees and time (UTC) is given below.**

In general the inland stations received high amount of insolation that cause the maximum temperature to rise above 40 °C. The synoptic northwesterly wind is a dry source unless associated with sea breeze circulation which could arrive in the late afternoon. However, the synoptic southeasterly flow is moist and the moisture is not limited to the lower level but may extend into the vertical. The northeasterly local winds are usually moist and might mix with the northwesterly winds in a convergence zone. This causes the possibility of the convection to develop in such places.

The dry air mass blown by the 14<sup>th</sup> of July limited the convection over the SSA and the atmosphere became dry as the 5<sup>th</sup> of July's situation.

### **4.3.3 Sea breeze**

The sea breeze is defined as a coastal local wind that blows from sea to land resulting from the difference in the temperature between the air mass over water and land. The sea has high thermal conductivity and a small variation in the surface temperature while the adjacent land has a smaller thermal conductivity and thus exhibits a larger variation in temperature during the day. According to Clarke (1955, cited in Du Preez, 2006) pressure gradients between sea and land develop due to the temperature difference. This results in a low-level on-shore flow during the day in the form of sea breeze and a weaker off-shore flow during the night, the land breeze. The leading edge of the intrusion of cooler, moist air carried by the sea breeze is called the sea breeze front, normally marked by horizontal discontinuity in temperature and humidity (AMS, 2007).

According to Simpson (1994, cited in Du Preez, 2006) for the sea breeze to start blowing over the land, the temperature difference between the sea and the land must be large enough to overcome any large-scale circulation. The Arabian Peninsula receives a large amount of the solar heat during the summer (see chapter 1). For example, the absolute maximum temperature at Sohar (Fig. 4-9A) in July 2004 was 40.4 °C while the average sea surface temperature of the Gulf of Oman in the same period, recorded by Sohar Marine station (Just off coast), was 30.8 °C (DGCAM, 2005). The absolute maximum temperatures well inland are much higher than at Sohar and very high temperature difference between the sea and the land can easily develop as pointed out by Simpson (1994).

In the north, Oman is bounded by the Gulf of Oman to the east and the Arabian Gulf to the northwest and the sea breeze can reach the SSA from the Gulf of Oman and the Arabian Gulf. Normally the sea breeze in this area is well known as fresh northeasterly to easterly wind from the Gulf of Oman or northwesterly to northerly wind from the Arabian Gulf.

A sudden and significant increase in the dew point temperature occurred in 15 minutes at many stations. The abrupt increase varied with time and intensity according to the geographical location of the stations. The focus here is on some inland stations which were often influenced by the sea breeze effect. Considering the northwesterly flow from the Arabian Gulf, the northern stations (Fig. 2-2) are affected by the sea breeze before those in the south or southeast. A sudden increase in the dew point temperature was generally noticed when the wind direction is northwesterly with occasional increase in its speed. The passage of the sea breeze is also normally indicated by an increase in moisture and when the wind direction changes to the northwest. However, when the prevailing wind is northwesterly the passage of the sea breeze front may only be noticed by an increase in moisture as the wind speed does not necessarily increase. Generally, the sudden and significant increase in moisture along with the northwesterly wind is the clearest indication of the arrival of the sea breeze to the station from the Arabian Gulf during the ADP.

Figure 4-18 shows the sudden increase of dew point temperature with time at some selected stations (Fig. 2-2) from the north to the south on the 5<sup>th</sup> of July. The sudden increase of the dew point in 15 minutes started at the northwestern stations, as expected. The dew point increased to about 5 °C at 0900 UTC in Falaj Al Moalla (blue), 13 °C at 1030 UTC in Al Malaiha (pink), 5 °C at 1200 UTC in Al Shiweb (yellow), 7 °C at 1300 UTC in Al Hiyar (turquoise) and 4 °C at 1430 UTC in Khatam Al Shaklah (violet). The wind was northwesterly with the wind strength slightly more than 10 kt when the sudden increase in the dew point temperature occurred.

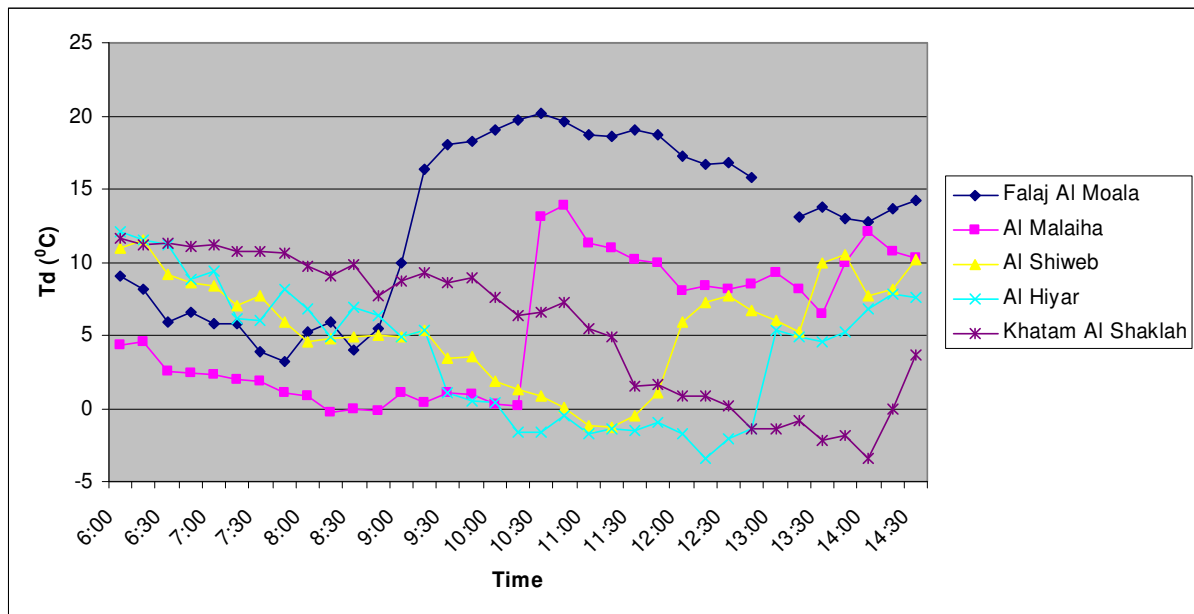
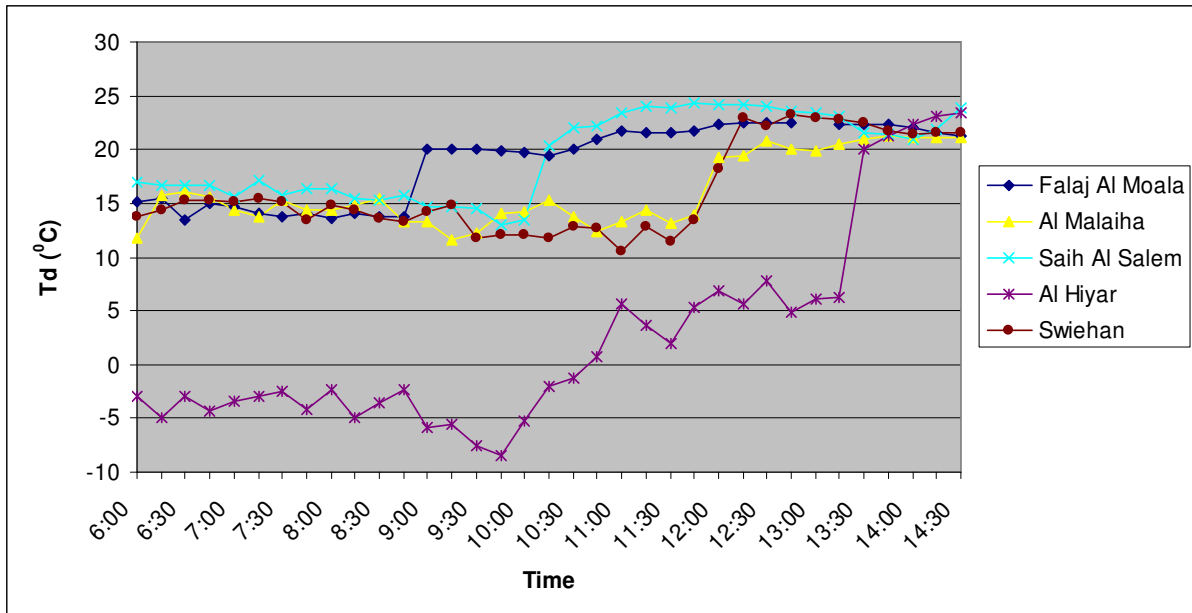


**Figure 4-18: Significant increase of dew point temperature over some stations during the day according to the northwesterly sea breeze on the 5<sup>th</sup> of July 2004.**

On the 6<sup>th</sup> of July (Fig. 4-19), the air was more moist as all the stations started the ADP with dew point temperature above 10 °C, except for Al Hiyar (violet) which had negative value.

The abrupt increase of the dew point in 15 minutes generally also started from the northwestern stations. The dew point increased to about 6 °C at 0900 UTC in Falaj Al Moalla (blue), 7 °C at 1015 UTC in Saih Al Salem (turquoise), 5 °C at 1200 UTC in Al Malaiha (yellow), 5 °C at 1200 UTC in Swiehan (dark red), 14 °C at 1330 UTC in Al Hiyar.

Generally, the dew point temperature decreased during the day until the moist northwesterly sea breeze reached the station. It is clear that the arrival of the sea breeze occurred later during the ADP over Al Hiyar and Khatam Al Shaklah. They are situated further to the southeast and further from the sea (Fig. 4-9).



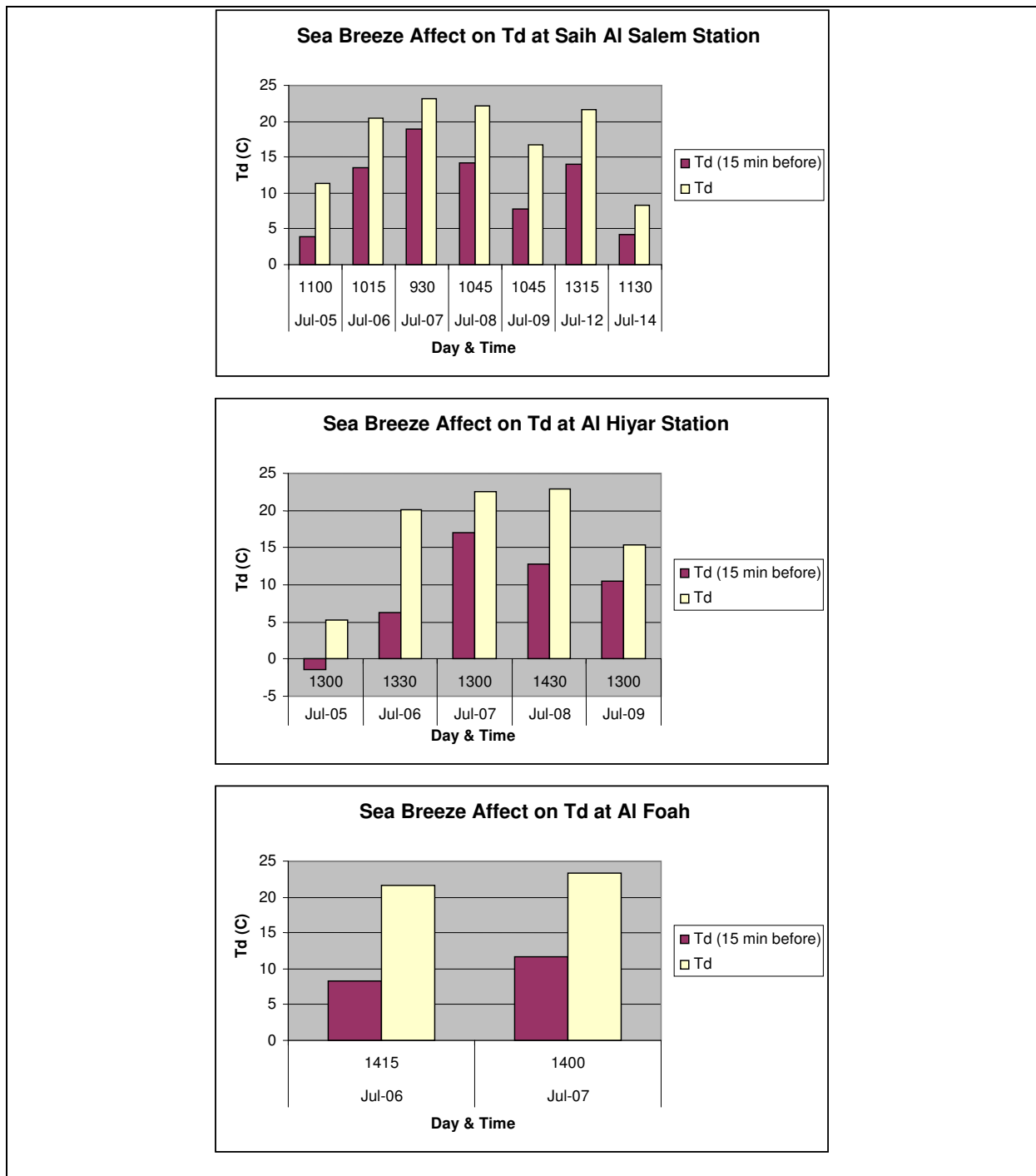
**Figure 4-19: Significant increase of dew point temperature over some stations during the day according to the northwesterly sea breeze on the 6<sup>th</sup> of July 2004.**

Figure 4-20 depicts the effect of the sea breeze on the dew point temperature during the study period over selected stations from north to south (Saih Al Salem, Al Hiyar and Al Foah). The X-axis indicates the day with the exact time of the sudden increase in the dew point temperature of 4 °C or more in 15 minutes caused by the northwesterly sea breeze, if it reached the station. Both the increased dew point temperature value and the one recorded 15 minutes earlier are represented in the graphs. The effect of the sea breeze was most frequently evident at Saih Al Salem during the study period except on the 10<sup>th</sup>, 11<sup>th</sup> and 13<sup>th</sup> of July and reached the station between 0930 UTC to 1130 UTC except on the 12<sup>th</sup> of July when it arrived after 1300 UTC. Al Hiyar Station, which is located to the southeast, received the sea breeze only on the 5<sup>th</sup> to the 9<sup>th</sup> of July and it was not observed before 1300 UTC. Further to the southeast and closer to the mountains, the sea breeze reached Al Foah only on the 6<sup>th</sup> and the 7<sup>th</sup> of July and it was after 1400 UTC.

The passage of the leading edge of sea breeze is marked by a near simultaneous drop in temperature and rise in relative humidity (Du Preez, 2006; Estoque *et al.*, 1976; Physick, 1992). The sea breeze arrival at the surface is also indicated by a sharp shift in wind direction (Estoque *et al.* 1976) and an increase in wind speed (Bonnardot *et al.* 2001, Asimakopoulos *et al.* 1998).

In this research, it was found that the increase in moisture was the clearest indication of the passage of the sea breeze. The decrease in the temperature was not as significant since the sea breeze mainly reached the area after the temperature reached its maximum and already started its gradually decrease. The sharp shift in

the direction and the increase in the speed of the wind were on occasion indicative of the passage of the sea breeze.



**Figure 4-20: The effect of the sea breeze (if any) on the dew point temperature during the study period at three selected stations.**

According to Physick (1980, cited in Du Preez, 2006:16) the sea breeze system extends over land and sea and expands in both directions during the day. The distance of inland penetration of the sea breeze fluctuates over different parts of the world. Simpson (1994) found that many factors like temperature differences



between land air and sea air and the Coriolis force influence the distance the sea breeze penetrates inland (Du Preez, 2006). Here it is also found that the efficiency and the arrival time of the sea breeze are not only the wind speed and direction, but the distance of the station from the sea as well. The northwestern stations, which are closer to the Gulf, are influenced by the northwesterly sea breeze earlier than those in the southwest.

Simpson *et al.* (1977) indicated that the synoptic wind affected not only the formation of the sea breeze but also its subsequent movement inland (Du Preez, 2006). Generally the northeastern stations such as Hatta, Al Malaiha, Al Manama and Masafi (Fig. 2-2) are located in the mountain passes and are open to receive the flow from both the east and the west. The synoptic circulation determines the wind strength to a larger extent than the sea breeze circulation. The effect of the easterly sea breeze from the Gulf of Oman can be clearly seen over these northeastern stations, if there was no opposing stronger wind (as discussed earlier in section 4.3.2).

Moreover, it can propagate through the mountains gaps to reach western stations such as Al Shiweb, Khatam Al Shaklah and Al Saa. Likewise, the northwesterly breeze can also reach the stations through the mountains if it is strong enough. In general, the western stations follow similar wind regime as seen through the observations except those closer to the coast of the Arabian Gulf. They clearly represent the general synoptic and local circulations of the wind and become moist quickly as soon as the sea breeze or wet air mass arrives. The observations in general indicated a dominant southeasterly wind after the 9<sup>th</sup> of July, especially the southern stations and they lasted until the morning of the 13<sup>th</sup> of July. The southeasterly winds were seen as the main moisture source that kept feeding the regional area, including the SSA. The dry westerly air mass replaced the wet one gradually from the northwest to the southeast on the 14<sup>th</sup> of July (Fig. 4-21).

Bechtold *et al* (1991) found that the maximum breeze intensity and the propagation speed of the sea breeze front is hampered by a large scale contradictory flow, so that the sea breeze front may remain stationary with respect to the coastline. This was the case on the 5<sup>th</sup> of July when the southwesterly wind was dominant at the beginning of ADP. The dry southwesterly delayed the flow of the sea breeze over the land and when it did change to the northwest it was late in the ADP and most of the moisture evaporated due to the very warm and dry air mass. Consequently, it was some time before there was a notable rise in moisture. Clark (1983, 1984) found that when the sea breeze was supported by an on-shore component of a large scale flow, it can rise over mountain ranges and can still be detected hundreds of kilometres inland (Du Preez, 2006). A modest assisting wind causes sea breeze surge to move well inland in the day and move faster than when there is no presence of assisting wind (Clark, 1983). In fact, Clark's findings were also observed in this study. Here the strongest sea breeze was observed by the 7<sup>th</sup> of July when the sea breeze reached the stations earlier (at 0930 UTC in Saih Al Salem, 1300 UTC in Al Hayar and 1400 UTC in Al Foah).

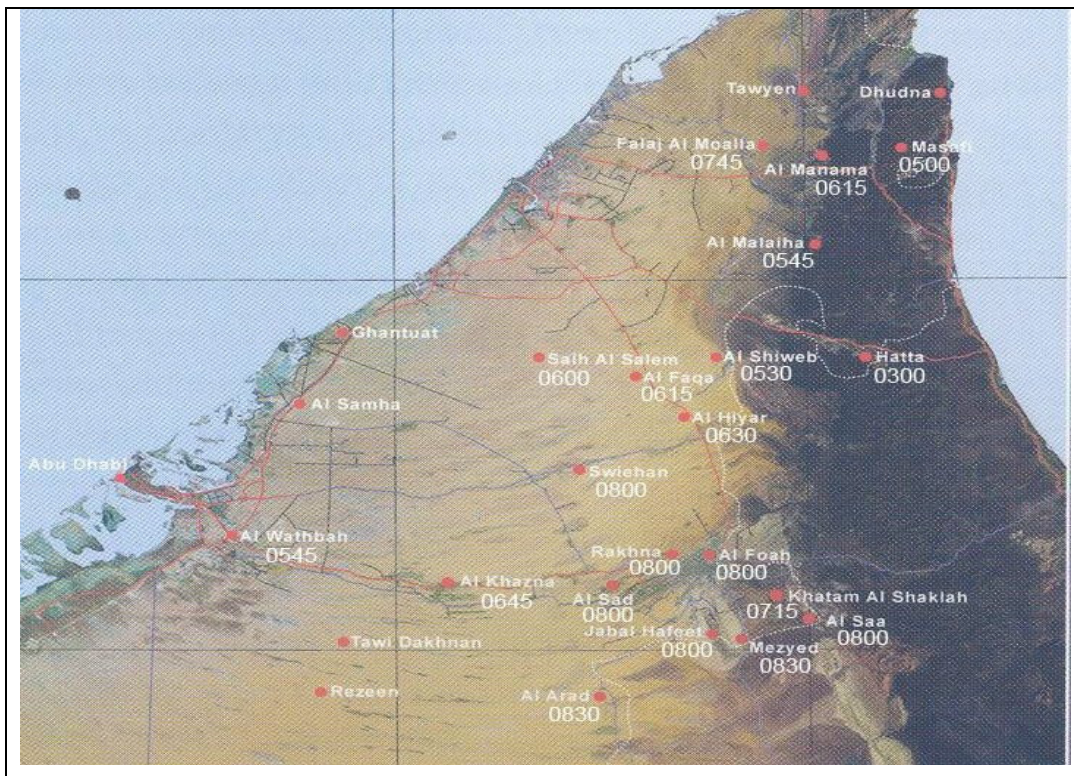


**Figure 4-21:** The observed time (UTC) of the dry air mass movement over the stations (from the northwest to the southeast) marked under the stations name.

This was the earliest time of arrival of the sea breeze during this study period with a wind strength of 20 kt at some stations. Unlike the 5<sup>th</sup> of July, the northwesterly wind started earlier on the 6<sup>th</sup> of July and was also seen at the beginning of the ADP on the 7<sup>th</sup> of July without a dry southwesterly effect or opposing southeasterly flow, over the stations close to the Gulf coast. This made the sea breeze much more effective and it travelled quicker than before. As the southeasterly wind started to propagate over the area by the 8<sup>th</sup> and the 9<sup>th</sup> of July, the northwesterly sea breeze became weaker and it was seen only over the northern stations.

According to Pielke and Simpson *et al.* (1974, 1980 cited in Du Preez, 2006) the sea breeze from the east and west coasts of the Peninsula in Florida, USA, strongly influences the development of deep cumulus convection. That could also happen over this area if two sea breezes, one from the Gulf of Oman and one from the Arabian Gulf, converge strongly in case of absence of synoptically disturbed conditions like the dry westerly flow. Then areas of convergence could develop with the different circulations of the two air masses encouraging convection to develop. This was the case when convection developed over these convergence zones and shown later on during the study period (see section 3.3).

The sea breeze alone was not the key ingredient for triggering the thunderstorms over the Al Hajar Mountains. In a dry synoptic condition, the sea breeze, even if it reached the mountain area, could not assist the convection to develop. A good example occurred on the 5<sup>th</sup> of July when the SSA was under a trough of low pressure located over Pakistan. The influence of the synoptic circulation was clearly reflected in the 15 minutes

observations at the inland stations as the wind tends towards a geostrophic wind. As a result, most of the stations reported southwesterly wind in the early hours of the ADP but then turned to the northwesterly. The southwesterly along with the following northwesterly winds were very dry, causing the dew point temperature to drop to negative values at most of these stations. The sea breeze developed later and reached the mountains in the late afternoon. At Seeb (Fig. 4-9A), the sea breeze started to flow from the Gulf of Oman at about 1000 UTC at 5-7 kt and remained for only two hours. To the north, at Sohar (Fig. 4-9A), the northeasterly sea breeze was observed at 0700 UTC after a light variable wind. The northeasterly was from 30 to 50 degrees from true north at 7-10 kt until 1200 UTC, then became easterly 5-7 kt. On the western side, the sea breeze started to flow from the Arabian Gulf after 0800 UTC. So, the coastal stations show that there was no lack of the on-shore flow on the 5<sup>th</sup> of July. However, most of the moisture either did not reach the mountain area or arrived late after the ADP. In fact, no moisture reached the mountains from the Arabian Gulf during the Very Active days (10<sup>th</sup>-13<sup>th</sup> of July). It was easterly moisture that was generally dominant from the Gulf of Oman during the whole period of study. This supports the existence of a stronger synoptic scale on-shore flow other than the sea breeze itself, which was present during the Very Active days.

In general, the synoptic conditions were clearly reflected over the local conditions in this area. The development of the heat low pressure over the northeast of the Arabian Peninsula played a key role in the wind circulations over the area. Deepening of the low pressure to the south, caused the wind regime over the SSA to become moist southerly to southeasterly which extended to the western coast and delayed the northwesterly sea breeze. As a result, an off shore flow at the beginning of the ADP was clearly observed by the western coastal stations from the southeast since the 9<sup>th</sup> of July. This off-shore flow was dominant at Abu Dhabi (Fig. 4-9B) until the 12<sup>th</sup> of July. This means that the synoptic conditions made a direct impact on the surface moisture distributed over the area and hence the initiation of the thunderstorms over the Al Hajar Mountains.

#### **4.4 Upper air and sounding parameters**

##### **4.4.1 Upper air**

The upper air data, from Seeb and Abu Dhabi sounding (see section 2.1.2) will be discussed here. Three days were selected for this discussion. They are the 5<sup>th</sup> of July (Non Active day), the 7<sup>th</sup> of July (Active day) and the 10<sup>th</sup> of July (Very Active day). On the 5<sup>th</sup> of July at 0000 UTC, the upper air at Seeb (Fig. 4-22A) was very dry for the whole layer with a shallow layer of moisture between 450 and 500 hPa. A small surface inversion was present but with a more pronounced inversion at 470 hPa. The convective inhibition (CIN) was -601 J/kg and the convective available potential energy (CAPE) of 141 J/kg and hence the atmosphere was under 'pseudolent instability'. Shohoni and Paranjpe (1937) used the term pseudolent instability for the situation, when ignoring the negative sign, the CIN exceeds the CAPE. The pressure of the lifting condensation level (LCL) was at 679 hPa.

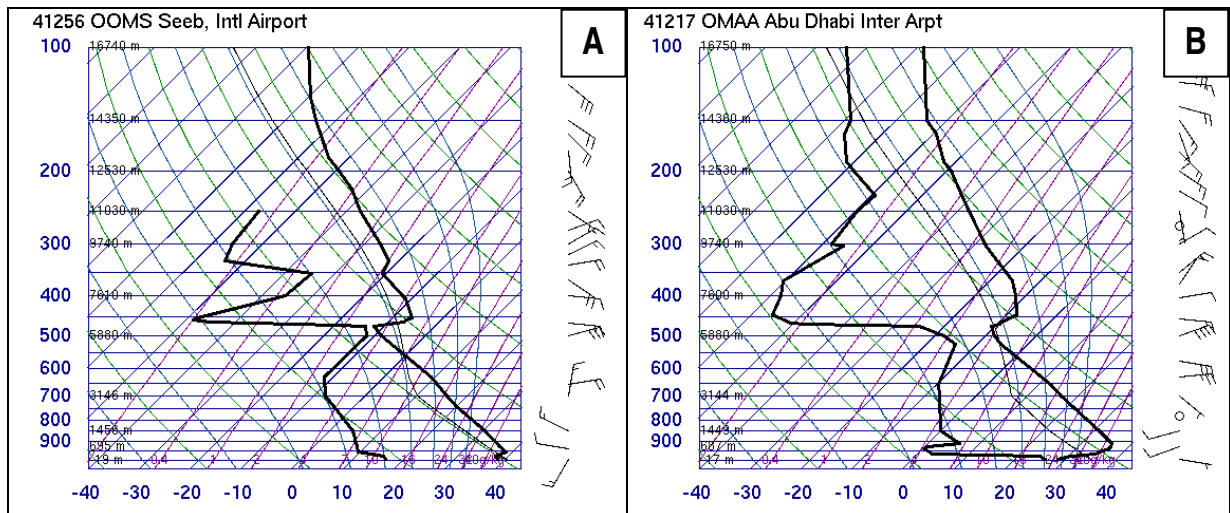


**Figure 4-22: Skew T diagrams at 0000 UTC on the 5<sup>th</sup> of July 2004 (A) for Seeb & (B) for Abu Dhabi. (Adapted from: University of Wyoming, 2006).**

The Abu Dhabi 0000 UTC sounding (Fig. 4-22B) indicated a high surface dew point temperature (26 °C) with a strong temperature inversion at the surface and a very dry layer above the inversion, up to the 500 hPa level. There was a slight increase in relative humidity at around the 500 hPa level with a temperature inversion above this. The pressure of the LCL was at about 720 hPa. Both Seeb and Abu Dhabi 0000 UTC soundings indicated conditional pseudolent instability of the atmosphere over that area and relatively high LCL heights. They indicate the difficulty for convective cloud to develop past the mid level inversion.

The 1200 UTC sounding at Abu Dhabi (Fig. 4-23) showed that the surface moisture and the inversion no longer existed by the midday; however the upper stable layer dominated the upper air. The LCL pressure was at about 720 hPa.

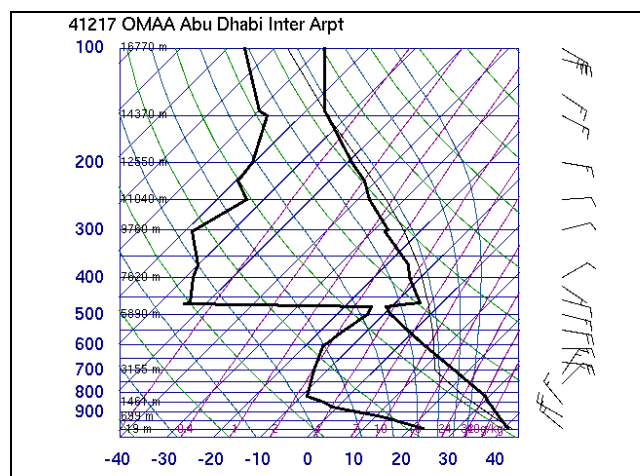


**Figure 4-23: Abu Dhabi sounding (Skew T diagram) at 1200 UTC on the 5<sup>th</sup> of July 2004. (Adapted from: University of Wyoming, 2006).**



The CAPE was 1207 J/kg and the CIN was -389 J/kg and according to Schults, *et al.* (2000), this indicates that the atmosphere was latently unstable. An atmosphere is considered to be latently unstable when the CAPE exceeds the CIN and therefore must produce positive buoyancy as the atmosphere was real latently unstable. Although the stable layer at 500 hPa was still present at midday (Fig. 4-23), the convection had the potential of pushing through the 500 hPa level to approximately as high as the 200 hPa level. This did not happen and the day was totally dry without any convection seen over the SSA.

On the 7<sup>th</sup> of July, the Seeb 0000 UTC sounding (Fig. 4-24A) showed a high dew point temperature at the surface caused by the northeasterly surface wind. The surface dew point temperature increased from 17 °C on the 5<sup>th</sup> to 29 °C on the 7<sup>th</sup>. The surface inversion extended up to 900 hPa and then the dry bulb temperatures were isothermal up to 810 hPa. Above that, the typical dry adiabatically lapse rate was present up to 550 hPa.

The relative humidity in the mid levels (above 550 hPa) was higher than on the 5<sup>th</sup> and the mid tropospheric inversion largely disappeared. The atmosphere was under real latent instability as the CAPE (1672 J/kg) exceeded the CIN (-749 J/kg). Both the surface moisture and the conditionally real latent instability prevailed during the day and are clearly represented on the 1200 UTC sounding (Fig. 4-25A).

The LCL pressure was at 832 hPa on the midnight sounding and dropped to 862 hPa at 12000 UTC. The 7<sup>th</sup> of July was an Active day but the convection was limited to isolated cells over the mountains.

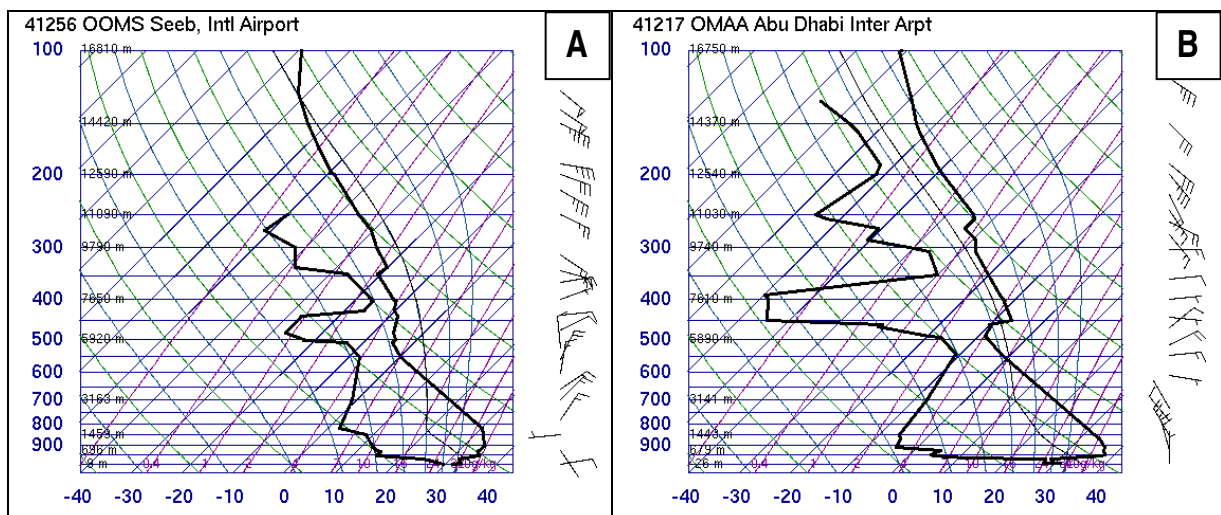
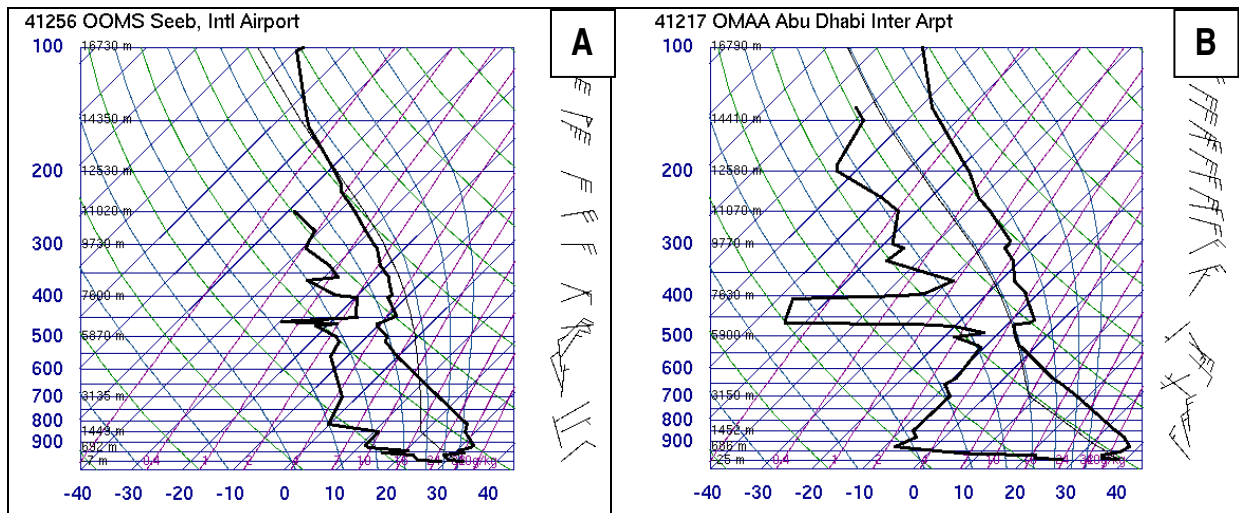


Figure 4-24: Skew T diagrams at 0000 UTC on the 7<sup>th</sup> of July 2004 (A) for Seeb & (B) for Abu Dhabi. (Adapted from: University of Wyoming, 2006).



**Figure 4-25: Skew T diagrams at 1200 UTC on the 7<sup>th</sup> of July 2004 (A) for Seeb & (B) for Abu Dhabi. (Adapted from: University of Wyoming, 2006).**

Both of Abu Dhabi soundings (Fig. 4-24B & Fig. 4-25) indicated that the LCL pressure was still low at about 700 and 770 hPa respectively. The potential for convection did exist if considering the heights of the LCL alone but the other atmospheric parameters did not support the formation of convective cloud. The Abu Dhabi 0000 UTC sounding (Fig. 4-24B) showed the pseudolent instability, but at 1200 UTC (Fig. 4-25B) the atmosphere was stable to all vertical displacement as no CAPE was present.

The 10<sup>th</sup> of July was one of the best convective days during this period (see section 3.3.5). The Seeb sounding at midnight (Fig. 4-26A) showed high surface dew point temperatures and the real latent instability of the atmosphere (CAPE: 2913 J/kg and CIN: -457 J/kg). Unlike the 7<sup>th</sup> of July, the mid troposphere inversion redeveloped and the higher layers were drier.

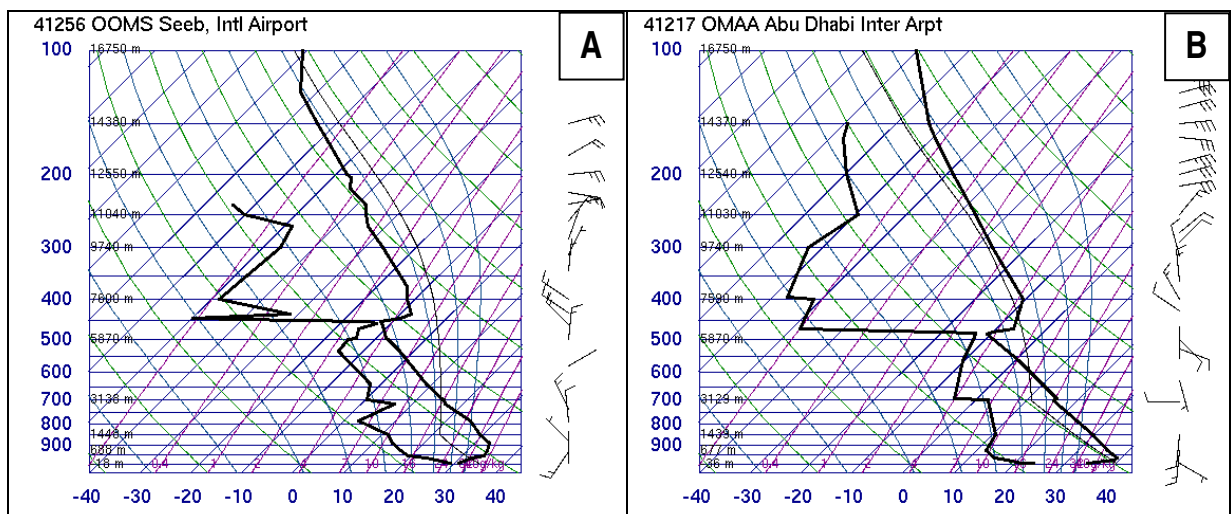


**Figure 4-26: Skew T diagrams at 0000 UTC on the 10<sup>th</sup> of July 2004 (A) for Seeb & (B) for Abu Dhabi. (Adapted from: University of Wyoming, 2006).**

The 1200 UTC sounding at Seeb (Fig. 4-27A) was not as favorable as the 0000 UTC sounding (Fig. 4-26A) for convective development. The CAPE was only 438 J/kg and by using the parcel method, the pressure of the cloud top was 400 hPa. The atmosphere was pseudolent unstable. The pressure of the LCL was approximately 850 hPa at 0000 UTC but at 790 hPa at 12000 UTC. The average clouds base, as noticed by research pilots (Table 3-1) was about 700 hPa and therefore closer to LCL pressure in 1200 UTC (Fig. 4-27).

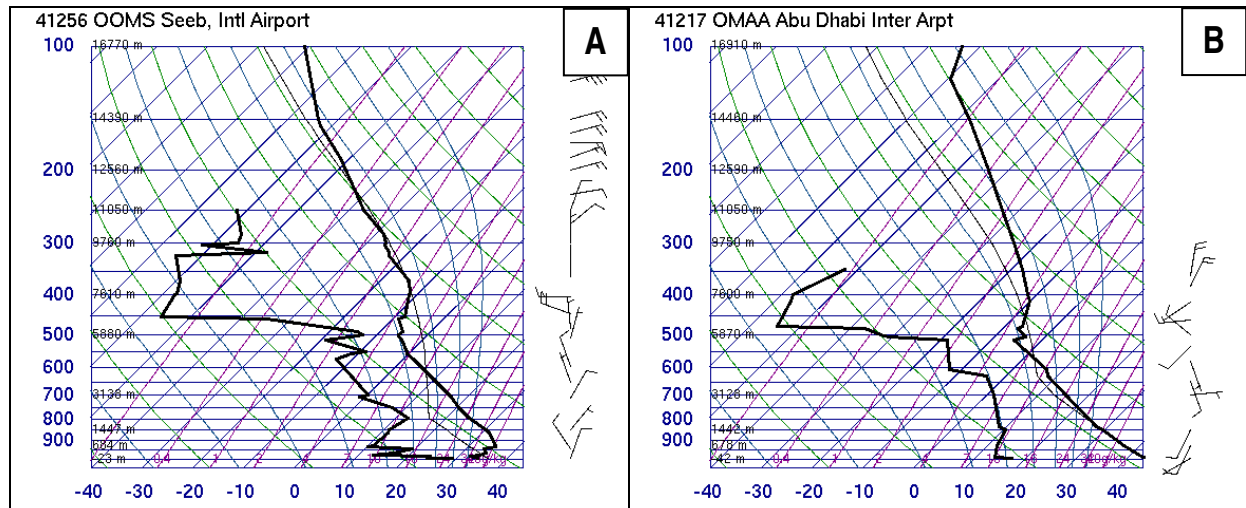


**Figure 4-27: Skew T diagrams at 1200 UTC on the 10<sup>th</sup> of July 2004 (A) for Seeb & (B) for Abu Dhabi. (Adapted from: University of Wyoming, 2006).**

The Abu Dhabi soundings at 0000 UTC (Fig. 4-26) and at 1200 UTC (Fig. 4-27B) were pseudolent unstable with lower surface dew point temperatures compared with the Seeb one. Although the stable layer at 500 hPa (Fig. 4-26B) was not particularly strong in the afternoon (Fig. 4-27B), this Skew T diagram is not conducive for convective development. The pressure of the LCL was at 650 hPa at 0000 UTC.

Considering the upper air data for these three days, the mid level inversion accompanied by dry stable layer above it, is a semi-permanent feature on both the Seeb and Abu Dhabi Skew T diagram and occurs in association with the upper level high. Breed *et al.* (2005) concluded that the strength of this layer determines the formation of storms and their intensity. However, it was noticed here that the convection did not require this layer to disappear or even to weaken in order for convective development to take place. Thunderstorms may develop in the presence of the mid tropospheric inversion as illustrated on the 10<sup>th</sup> of July.

Factors which are considered to be more valuable to forecast convective cloud in the mountains are the availability of surface moisture and the pressure/height of the LCL. The Seeb sounding was dry at the surface on the 5<sup>th</sup> (dew point temperature of 16.6 °C) while on the 7<sup>th</sup> of July, the dew point temperature increased to 29.4 °C and was 29.2 °C on the 10<sup>th</sup> of July. The upper data considered in these case studies suggest that the Seeb sounding is more appropriate to use to forecast convective cloud over the mountains than the sounding at Abu Dhabi.



The height to which a parcel of air, if heated sufficiently from below by surface heating and thermal convection, will rise adiabatically until condensation starts is typically used to identify the base of cumuliform clouds. Rasmussen (2003) showed that, climatologically, higher LCL levels were associated with insignificant supercells over the Great Plains. Significant convective weather (*i.e.* tornados) are normally associated with relatively high boundary layer moisture and thus lower LCL heights (Craven *et al.*, 2002). In the case studies done in this research, the pressure (height) of the LCL was also a good indicator for convective clouds development over the mountains. The LCL pressure at the Seeb midnight sounding increased with about 100 hPa on the 10<sup>th</sup> of July compared with the previous day to reach about 850 hPa (confirmed by pilot's notes in Table 3.1). In other words the height of the LCL became lower. This was associated with significant convective development. In contrast to the 5<sup>th</sup> of July (Non Active day), and at the same station, the LCL pressure was at about 680 hPa which is much lower (*i.e.* higher height). However, the pressure of the LCL from the Abu Dhabi soundings was high on both days, the 5<sup>th</sup> and the 10<sup>th</sup> of July (>750 hPa) and did not give a clear indication of any associated convective development. Therefore, the midnight sounding of Seeb was better in identifying convection over the Al Hajar Mountains. The upper air data, for only the Seeb soundings, will therefore be analyzed further.

#### 4.4.2 Sounding parameters

Some selected parameters from the Seeb soundings at 0000 UTC were analyzed. These include the K-index (KI), mean mixed layer mixing ratio (MXR), precipitable water (PW) for the entire sounding and the Lifted Condensation Level (LCL).

A statistical study was done for some of these parameters for 835 days since 1983 until. Most of the upper air data of June and July were collected from the website of the University of Wyoming. Data for Seeb was available from this website since 1983. The long term average values as well as the average, maximum and the minimum values were calculated and the results are shown in Table 4-1.

**Table 4-1: The long term average, minimum and maximum values of the KI, Mean mixed layer mixing ratio (MXR) and Precipitable Water (PW) for the Seeb soundings at 0000 UTC.**

	KI	MXR (g/kg)	PW (mm)
<b>Average</b>	20.25	13.67	33.38
<b>Minimum</b>	-18.3	3.09	8.59
<b>Maximum</b>	43.5	26.11	80.09

The values of these parameters for the Seeb soundings at 0000 UTC during this study period are presented in Table 4-2. This table also includes the height of the LCL above the ground level in meters (m)

calculated by using the average temperature and dew point of the lowest 50 hPa. The conditional instabilities according to the values of CIN and CAPE for the 10 days are also included in the table.

**Table 4-2: Sounding parameters of KI, Mean mixed layer mixing ratio (MXR), Precipitable water (PW) and the lifting condensation level (LCL) of Seeb sounding at 0000 UTC for the days 5<sup>th</sup>-14<sup>th</sup> of July 2004. The conditional instability for each day is also included along with the values of convective inhibition (CIN) and the convective available potential energy (CAPE).**

Date	KI	MXR (g/kg)	PW (mm)	LCL Level (m)	CIN (J/kg)	CAPE (J/kg)	Conditional Instability
5 <sup>th</sup> of July	19.5	10.2	26.3	3085	-601	141.4	Pseudolent
6 <sup>th</sup> of July	18.5	13.2	26.2	-	-959	54.7	Pseudolent
7 <sup>th</sup> of July	25.5	18.7	39.6	1198	-749	1672	Real latent
8 <sup>th</sup> of July	29.1	23.1	46.2	410	-452.1	4626	Real latent
9 <sup>th</sup> of July	17.3	12.7	32.2	2103	-1031.7	8.40	Pseudolent
10 <sup>th</sup> of July	33.1	20.1	43.4	1065	-457.8	2913.7	Real latent
11 <sup>th</sup> of July	32.3	15.7	40.9	1707	-510.0	851	Real latent
12 <sup>th</sup> of July	27.7	13.7	37.4	1826	-571.9	266.3	Pseudolent
13 <sup>th</sup> of July	33.7	18.5	45.4	1196	-370.2	2571.6	Real latent
14 <sup>th</sup> of July	29.7	12.0	38.4	2704	-433.8	348.6	Pseudolent

#### 4.4.2.1 The K-index (KI)

This KI (George 1960) is given by

$$KI = (T_{850} - T_{500}) + D_{850} - (T_{700} - D_{700}) \text{ (}^{\circ}\text{C)}$$

Where  $T_{850}$ ,  $T_{500}$  and  $T_{700}$  are the 850, 500 and 700 hPa temperatures, respectively,  $D_{850}$  and  $D_{700}$  are the 850 and the 700 hPa dew point temperatures, respectively. All temperatures are in  $^{\circ}\text{C}$ .

A thorough discussion of the KI and its three terms is included in Chapter 5. In general, if this index is more than 20, the likelihood of showers and thunderstorms increases (AMS, 2007). However, note that the long term average value of the KI at Seeb is 20. The KI is often used by forecasters in Seeb to predict convection over the mountains and a value of 20 or more is considered favorable.

For these case studies (5<sup>th</sup>-14<sup>th</sup> of July) the KI as calculated from the 0000 UTC Seeb sounding showed values above the average for the Very Active days (10<sup>th</sup>-13<sup>th</sup> of July), but it was also high during the dry days (5<sup>th</sup>

and 14<sup>th</sup> of July). Moreover, it shows that the value of the 14<sup>th</sup>, which was a dry day, was higher than the values on the Very Active days like the 12<sup>th</sup> of July. The value on the 5<sup>th</sup> of July (no convection) was higher than on the 6<sup>th</sup> and the 9<sup>th</sup> of July when the convection was observed (Table 4-2). It can be concluded that the KI was misleading in predicting the convection over the mountains during this study period when considering the 0000 UTC soundings at Seeb.

#### **4.4.2.2 Mean Mixed Layer Mixing Ratio (MXR)**

The mixing ratio is defined as the ratio of the mass of water vapor to the mass of dry air which is assumed to contain no water vapor (AMS, 2007).

The mixed layer is a type of atmospheric boundary layer which is characterized by strong turbulence that tends to fold and regularly mix, primarily in the vertical, quantities such as conservative tracer concentrations, potential temperature, and momentum or wind speed (AMS, 2007). The long term average value of MXR for June and July at Seeb is 13.7 g/kg (Table 3-1). During the Active days in the case study, the MXR was higher than the long term average except for the 9<sup>th</sup> and the 6<sup>th</sup> of July (Table 4-2). The lowest values (below the long term average) occurred on the 5<sup>th</sup> and the 14<sup>th</sup> of July. An analysis of Table 4-2 suggests that a threshold of 12 g/kg is appropriate to use as a guide to aid in the prediction of convective storms over the mountains. It should be noted from Table 4-2 that high MXR values are not indicative of the severity of thunderstorms especially when comparing the values of the 8<sup>th</sup> and the 12<sup>th</sup> of July. The MXR on the 12<sup>th</sup> of July, which was a more Active day than the 8<sup>th</sup> of July, was 13.7 g/kg while it was 23.1 g/kg on the 8<sup>th</sup> of July (Table 4-2).

#### **4.4.2.3 Precipitable Water (PW)**

The total Precipitable water (PW) is the amount of water produced when all the water vapor in a column of air, of unit cross section, condenses (AMS, 2007). PW is one of the parameters that provide an indication of the atmospheric moisture. Yet, the actual amount of rain is generally higher than the PW. As water vapor is brought into the storms from a surrounding area, there is a correspondence between precipitation amounts in given storms and the PW vapor of the air masses involved in those storms (AMS, 2007).

The long term average of PW values at 0000 UTC at Seeb is about 33.4 mm (Table 4-2). During the case study days, the PW was above the average during most of the Active days. However, a very high value (38.4 mm) occurred on the 14<sup>th</sup> of July when no convective development took place. The PW on the 5<sup>th</sup> was below the long term average and similar to the 6<sup>th</sup> of July. The PW of the 9<sup>th</sup> of July was just below the long term average, so the PW was gave high values for the Very Active days (10<sup>th</sup>-13<sup>th</sup>). The values of PW on the 5<sup>th</sup>, 6<sup>th</sup> and 14<sup>th</sup> indicate that this value does not necessarily distinguish between convective and non convective days.

#### **4.4.2.4 Height of the Lifting Condensation Level (LCL)**

The Lifting Condensation Level (LCL) is the level at which a parcel of moist air lifted dry adiabatically would become saturated (AMS, 2007). Earlier, at 4.4.1 it was discussed how the pressure of the LCL at Seeb at 0000 UTC gave a good indication of distinguishing between Active and Non Active days and it was found that there was a directly proportional relationship between the pressure level of the LCL and the instability. Consequently the average temperature and dew point at the lowest 50 hPa were used to find the LCL height above the ground level and these values are listed in Table 4-2. From the table, it is clear that the lower LCL heights result in higher instability and vice versa. An example is on the 10<sup>th</sup> (Very Active day) when the LCL height was 1065 m while it was more than 2000 m higher on the 5<sup>th</sup>, at 3085 m. In this study period, it was also found that the CAPE was larger than CIN (*i.e.* real latent instability) when the LCL height was lower than 1800 m (Table 4-2). This implies that any LCL height lower than 1800 m may result in the atmosphere to become latently unstable and enhance the chance for convective development provided other favorable atmospheric conditions are present.

Generally, the parameters listed in Table 4-2 were not all useful to determine if the atmospheric conditions were favorable for the development of the convective clouds over the Al Hajar Mountains and they were misleading on some occasions. On the 6<sup>th</sup> and 9<sup>th</sup> of July convection did occur, however, the parameters listed in Table 4-2 failed to identify the convection. However, they did show some skill in predicting Very Active days (10<sup>th</sup>-13<sup>th</sup> of July) as the values were all above the long term average. The height of the LCL was relatively lower during all the days when the storms were present over the SSA and can be used as one of the keys for forecasting convective cloud development over this area.

### **4.5 General discussion**

In this chapter, a study period of 10 case study days, 5<sup>th</sup>-14<sup>th</sup> of July 2004, was selected to represent Non Active, Active and Very Active days over the mountains. The atmosphere was extremely dry (no convection) on the 5<sup>th</sup> of July, moist (isolated convection) on the 6<sup>th</sup>-9<sup>th</sup> of July, very moist (widespread convection) on the 10<sup>th</sup>-13<sup>th</sup> of July and dry again (limited convection out of the SSA) on the 14<sup>th</sup> of July. Both the synoptic and the local conditions were analyzed and the influence of the large scale flow on thunderstorm development was identified.

The critical discrepancy between the Active and the Non Active days was an increase in surface moisture. The main source of the moisture is the moist flow from east of the mountains. Although the sea breeze was seen reaching the mountains on a number of occasions, it was when the wind was driven by the synoptic flow (southeasterly/southerly) and the moist air was associated with the monsoon and originated over the Arabian Sea that convective development over the mountains reached a maximum. The convergence of the sea breeze, from the Gulf of Oman, and the southerly moist wind allowed convective clouds to develop earlier with stronger convection over the mountains on the 9<sup>th</sup>-12<sup>th</sup> of July. The radar images showed that the storms were

predominantly seen first over the eastern part of the Al Hajar Mountains then drifted westwards with the steering wind. On days with very light steering winds the storms remained semi-stationary, as they grew and collapsed in the area. Principally, the convection developed on the northern mountains after the easterly wind propagates through the mountains gaps and mixed with westerly wind in convergence zones created by the wind circulation. In the event of the absence of a southeasterly/southerly wind on the mountains, the convective development was delayed and occurred west of the mountains as isolated and short-lived storms (6<sup>th</sup>-8<sup>th</sup> of July). These storms were generally initiated where the convergence zones were created to the west of the mountains.

The synoptic conditions influenced the local conditions by controlling the wind flow. The position of the heat low over the Arabian Peninsula is critical in the wind circulations over the eastern part of the Peninsula. Normally, a deep low pressure over the centre of the peninsula extending a deep trough to the south allowed the wind to flow unobstructed southerly to southeasterly over the Al Hajar Mountains and enhanced the moist convection. The movement of the low pressure to the north, or dissipating caused the wind flow to be dry westerly and limited the convection over the mountains.

The upper air characteristics were analyzed. The results showed that Seeb soundings are more appropriate to use than Abu Dhabi's. The lowering of the height of the LCL during the Active days was the most important factor distinguishing Active and Non Active days. Although the stable layer was dominant in the upper air, it was not significant to inhibit the convective development.

## Chapter 5

## The Oman Convection Index (OCI)

### 5.1 Introduction

The KI is often used by the forecasters in Oman to predict convective clouds over the Al Hajar Mountains. In this chapter the KI is discussed, analyzed and evaluated as a convection forecasting tool for the case study period of 5<sup>th</sup> to 14<sup>th</sup> of July 2004. The limitations of the KI are discussed and a new index is proposed to forecast convective cloud over the mountains of Oman. The new index is referred to as the Oman Convection Index (OCI) and to a large extent utilises the same variables contained in the conventional KI but with some differences relevant to the specific area. The OCI is also discussed and analyzed and statistical results are compared with the results for the KI. It is shown how the OCI forecasts convection better than the KI.

Many indices have been developed to aid forecasting convective cloud. Some of the most commonly used indices are the Total of Total Index, the Showalter Index and the KI (Henry, 1999). All of these indices aim to give representation of the static stability of the atmosphere. Static stability (as discussed by Henry, 1999) is the tendency of the atmosphere to either oppose or increase small-scale vertical displacements, due to buoyancy forces developing from temperature differences between the ambient air and the displaced parcel. Most of these indices rely mainly on temperature differences between two or more levels in the troposphere to measure the potential for convection, based on a set of experimental threshold values (Henry, 1999). One of the simplest indices, which consider only the ambient temperature and dew point temperature, is the KI developed by George (1960). This chapter will concentrate on the KI because it is one of the most widely used convection indices in Oman.

In order to form an understanding of the stability of the atmosphere thermal profiles are required over a large area and at a time scale relevant to the onset of convection. This is often not viable (Henry, 1999). In this chapter the upper data from Seeb at 0000UT are utilized to forecast convection over the Al Hajar Mountains. The onset of convection is usually some 10-hours later and more than 200 km away. However, due to the scarcity of upper air assents, this data are used in the analysis.

### 5.2 The KI

The KI was defined previously at section 4.4.2.1. Physical and statistical analysis of its three terms are discussed here.

#### 5.2.1 Physical analysis of KI

The first term of the KI,  $(T_{850} - T_{500})$ , is a lapse rate term and represents the decrease of the atmospheric temperature with height. Large values of this term indicate a large lapse rate, tending towards a dry

adiabatic lapse rate. If the atmospheric lapse rate was dry adiabatic the value of this term will be around 40 °C. This term dominates the KI on the Seeb soundings as a prevailing feature during the summer is the close to dry adiabatic lapse rate found between 850 hPa and 500 hPa. The upper air data on the 7<sup>th</sup> of July 2004 will be used here (Fig. 5-1) to illustrate the KI. In Figure 5-1 the 850 hPa temperature is 31.6 °C and at 500 hPa the temperature was -4.3 °C, the contribution of the first term of the KI was therefore 35.9.

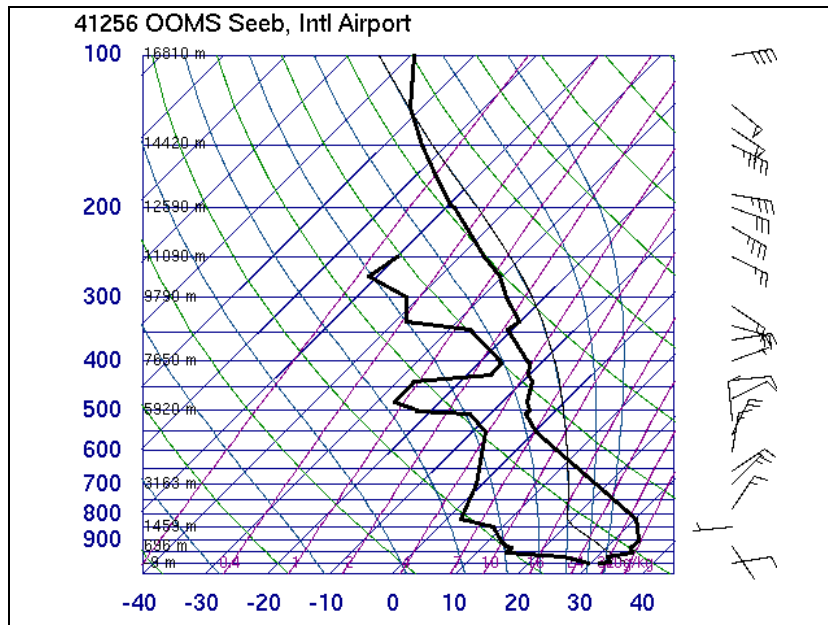


**Figure 5-1:** The Skew T diagram at Seeb at 0000 UTC on 7<sup>th</sup> of July 2004. (Adapted from: University of Wyoming, 2006)

The second term,  $D_{850}$  is the dew point temperature at 850 hPa and is therefore indicative of the amount of water vapor in the atmosphere. High (low) dew point temperature values at 850 hPa increases (decreases) the value of the KI. According to George (1960) this term was initially included in the KI to amplify the contribution of a moist layer just above the ground which would minimize the entrainment of dry air into the parcel. The 850 hPa dew point temperature on the 7<sup>th</sup> of July 2004 was 8.6 °C (Fig. 5-1) and the long term average value is 5.6 °C (Table 5-1).

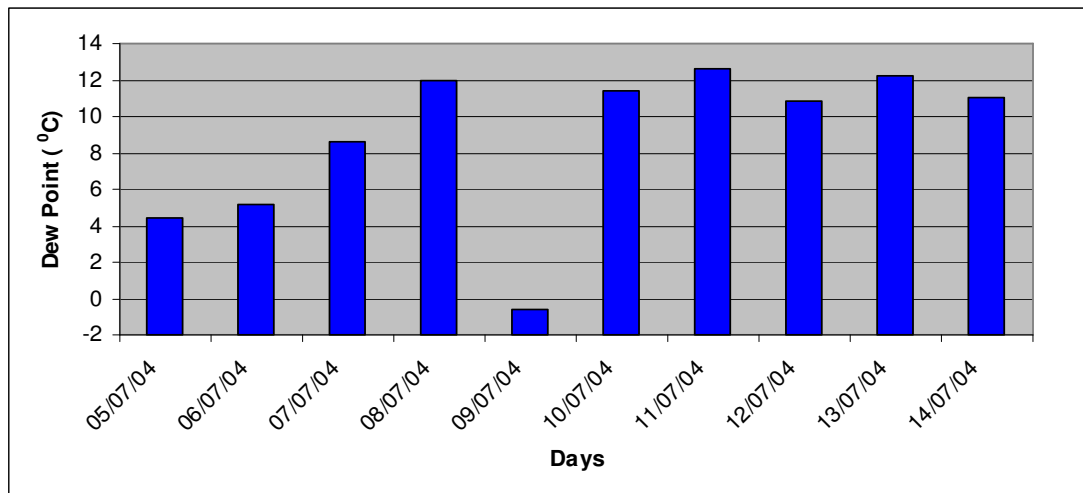
Figure 5-1 depicts a typical profile of dew point temperature at Seeb at 0000 UTC. The air dries considerably just above the surface, in this instance the dew point temperature decreased by 15 °C from the surface to 950 hPa. This rapid decrease in moisture often results in relatively low 850 hPa dew point temperatures at Seeb and therefore penalizes the value of the KI. However, as discussed in Chapter 4, convective clouds nevertheless develop on occasion, even with this rapid decline in dew point. For this reason the 850 hPa dew point is not ideal to use to forecast convection.

Figure 5-2 depicts the 850 hPa dew point temperatures from the 5<sup>th</sup> to 14<sup>th</sup> of July 2004. Convective development started on the 6<sup>th</sup> and continued to the 13<sup>th</sup> of July. There was a general increase in dew point



temperatures during this period, with the exception of the 9<sup>th</sup> when the dew point plummeted to below 0 °C. On the Very Active days (10<sup>th</sup>-13<sup>th</sup> of July) the 850 hPa dew point temperature was above 10 °C. For example the dew point temperature on 10<sup>th</sup> and 11<sup>th</sup> of July were 11.5 °C and 12.5 °C respectively. However, it was also above 10 °C on the 14<sup>th</sup> of July when no convection occurred over the SSA.

The 850 hPa dew point temperature may therefore be misleading in forecasting convection over the Al Hajar Mountains.



**Figure 5-2: The 850 hPa dew point temperature at 0000 UTC at Seeb from the 5<sup>th</sup> to 14<sup>th</sup> of July 2004.**

The third term,  $(T_{700} - D_{700})$  is the dew point depression at 700 hPa. The lower the value, the more moist the air and the higher the KI will be. The rationale behind the inclusion of this term (George, 1960) is to penalize the KI if the mid-tropospheric air is dry. However, careful analyses of the Seeb sounding reveals that the atmosphere is dry at 700 hPa on most days, also days when convection occurs over the mountains. The long term average dew point depression at 700 hPa is 19.5 °C (Table 5-1). On the 7<sup>th</sup> of July (Fig. 5-1) when convective cloud did develop over the mountains the 700 hPa dew point depression was 19 °C.

The 700 hPa dew point depression therefore also seems to be inappropriate to forecast convective cloud over the Hajar Mountains. This is emphasized when considering the dew point depression values at 700 hPa from the 5<sup>th</sup> to 14<sup>th</sup> of July 2004 (Fig. 5-3).

Although the lowest dew point depression occurred on the 13<sup>th</sup> of July (Very Active day) with a value below 15 °C and the highest value was 25 °C on the 5<sup>th</sup> of July (Non Active day), values were between 15-20 °C on all other days.

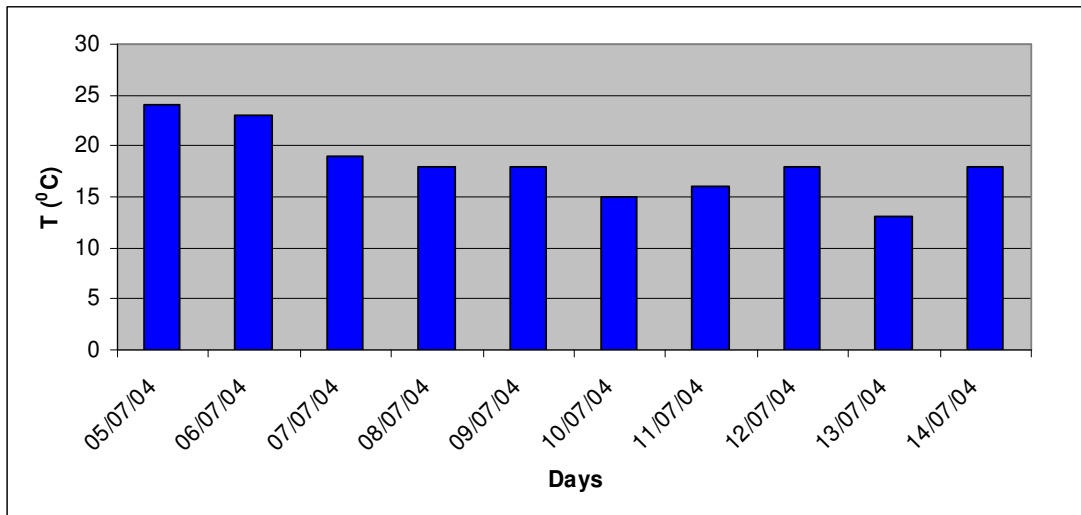


**Figure 5-3:** The 700 hPa dew point depression at 0000 UTC at Seeb from the 5<sup>th</sup> to 14<sup>th</sup> of July 2004.

### 5.2.2 Statistical analysis of KI

In order to investigate the significance of the contribution of each of the terms in the KI, average daily values were calculated for each of the terms for the summer months of June and July. Seeb has upper air data available from July 1983 and all available 0000 UTC upper air data from 1983 to 2006 were used to calculate the average daily values. Most of the data were obtained from the web site of the University of Wyoming ([www.weather.uwyo.edu](http://www.weather.uwyo.edu)). Some data was collected from the climate section at the Department of Meteorology in Oman. There were 835 June and July days available for analysis.

The long term average, maximum and minimum values for the months of June and July for the three terms of the KI are shown in Table 5-1. The long term average 850 to 500 hPa lapse rate was about 34°C.

**Table 5-1:** The long term average, maximum and minimum of the KI and its three terms.

	First term ( $T_{850} - T_{500}$ )	Second term ( $D_{700}$ )	Third term ( $T_{700} - D_{700}$ )	KI
<b>Average</b>	34	5.6	19.5	20.1
<b>Maximum</b>	42	21	49	44
<b>Minimum</b>	18	-17	0	-21

The long term average value for the KI (Table 5-1) is 20.1. The maximum value is 44 and the lowest value during the period was -21. On the 7<sup>th</sup> of July (Fig. 5-1) the KI was 26.

A data set was created in order to test the ability of the KI and OCI to forecast convection over the Al Hajar Mountains. The Meteosat Second Generation (MSG) high resolution visual images at 1200 UTC during June and July of 2005 and 2006 were investigated in order to classify all days according to their convective

development over the Al Hajar Mountains. The days were classified into Non Active, Active and Very Active. Non Active occurred when there were no convective clouds identified over the Hajar Mountains, Active was identified when convective cloud was observed over the mountains but they were single and small cells and Very Active when the convective development was observed as multi cells covering a large extent of the mountains. MSG data for all days were not available and 83 days were used in this analysis. Twenty eight days were classified as Non Active, 17 as Active and 38 as Very Active.

Table 5-2 shows the average values of KI for the different convective days. Considering all days (83) the average KI was 20, it was 14 for the Non Active days, 25 for Active days and only 20 for Very Active days. Considering the Active and Very Active days together, the average KI was marginally higher than the long term average value for all days at 21 (Table 5-1). These results indicate that the KI may be misleading to identify days with good convection over the mountains.

**Table 5-2: Average KI values for Non Active, Active and Very Active days for the June and July of 2005 and 2006.**

	Total	Non Active	Active	Very Active	Total Active
<b>Number of Days</b>	83	28	17	38	55
<b>Average KI</b>	20	14	25	20	21

A threshold between 20 and 25 of the KI is normally used by forecasters in the Department of Meteorology in Oman in order to predict convection over the Al Hajar Mountains.

The UK Met. Office (UKMO) Source book to the Forecasters' Reference Book (1997), which is used by Oman forecasters, indicated a threshold value of KI of 20 for the possibility of thundershowers. As described at section 2.2, the Table 5-3 is the contingency table where a 'yes' forecast uses a KI threshold of 22 or higher. This value is slightly higher than the long term average of the total Active days.

**Table 5-3: The contingency table of 83 days of different KI values with threshold value of 22.**

		Observed		
		yes	No	Total
Forecast	yes	27	8	35
	no	28	20	48
	Total	55	28	83

The five categorical statistics listed above were found as

- Accuracy = 0.57
- BIAS = 0.64
- POD = 0.49
- FAR = 0.23
- POFD = 0.29

In this situation of using the threshold value of 22 the accuracy score indicates that only 57% of all forecasts were correct. The frequency of convection was under forecast as indicated by the BIAS. The POD indicates that about 49% of the observed convection was correctly predicted. The FAR shows that 23% of the time convection was not observed when it was forecast. The POFD indicates that about 29% of the observed “no convection” events the forecast were incorrect. Generally, the statistics showed the limitations of using the KI. The use of applying this index for predicting the convection over the Al Hajar Mountains is not promising.

### 5.3 The Oman Convection Index (OCI)

The following equation was developed as a forecasting tool to predict convection over the Al Hajar Mountains and is known as the Oman Convection Index

$$OCI = (T_{850} - T_{500}) + T_{LCL} - (T_{50} - D_{50}) \text{ } ^{\circ}C,$$

Where  $T_{850}$  and  $T_{500}$  are the 850 and 500 hPa temperatures, respectively.  $T_{LCL}$  is the temperature at the Lifting Condensation Level and  $T_{50}$  and  $D_{50}$  are the average temperature and dew point temperature in the lowest 50 hPa respectively.

#### 5.3.1 Physical analysis of OCI

The first term,  $T_{850} - T_{500}$  is the same lapse rate term of the KI and it was already discussed in section 5.2.1. This term is left unchanged in the OCI because of the importance of the lower tropospheric lapse rate in the development of convective cloud over the Hajar Mountains.

The second term  $T_{LCL}$  is the temperature (in degrees Celsius) of the LCL. The variation of the LCL pressure during the different days of convection was described earlier in section 4.4.2.4. The height of the LCL was lower (*i.e.* pressure was higher) on days when convection occurred. Figure 5-4 illustrates how the height of the LCL on the 5<sup>th</sup> of July was 3085 m (Fig. 5-4A) while it was only 1065 m on the 10<sup>th</sup> of July (Fig. 5-4B). The LCL height was determined by using the average temperature and dew point temperature values in the lowest 50 hPa of the atmosphere. However, the local variation of temperature and moisture near the surface results in local variations of the computed LCL. The LCL is usually used with reference to the convective clouds base at the saturation level if reached by air in a convective thermal (Wilde, *et al.*, 1985). In one of their case studies of the

LCL height and cumulus onset in Oklahoma, Wilde *et al* (1985) found strong evidence that lower LCL heights should be considered when forecasting cumulus clouds. They also stated the necessity of making accurate boundary layer forecasts of temperature and moisture to calculate the LCL height.

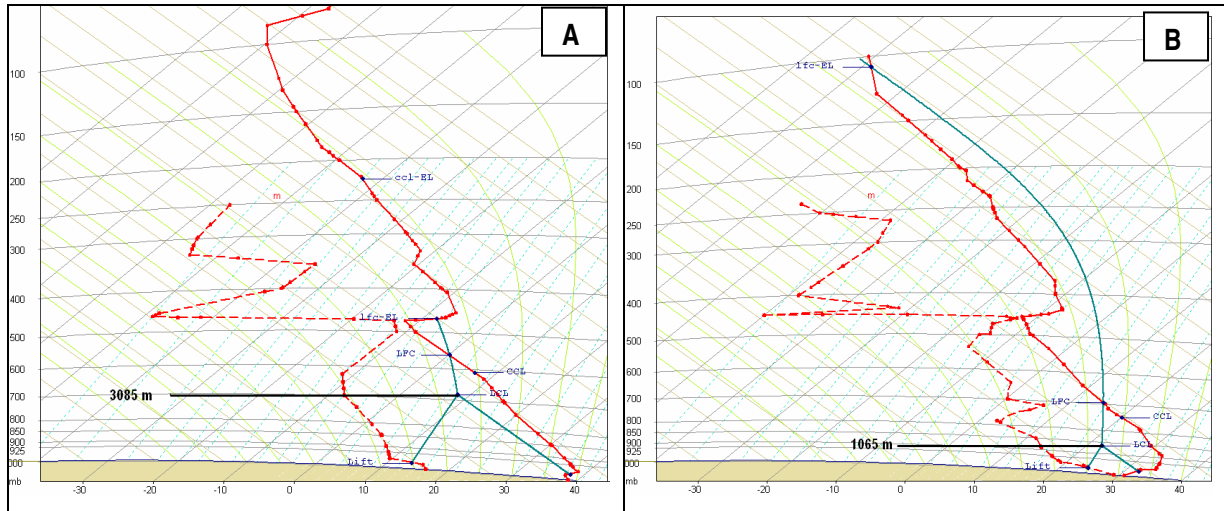


**Figure 5-4: Different LCL height (black line) of Seeb 0000 UTC soundings at 5<sup>th</sup> (A) and 10<sup>th</sup> (B) of July 2004. (Adapted from: RAOB, 2007).**

Many different formulas exist for calculating the pressure and temperature of the LCL, but the Barnes (1968) provided the simplest formula to calculate the temperature at LCL ( $T_{LCL}$ ) which is:

$$T_{LCL} = T_d - (0.0012969T_d + 0.1963)(T - T_d)$$

Where  $T$  and  $T_d$  are the temperature and dew point in degrees Celsius. Here the average values in the lowest 50 hPa are used.

The corresponding pressure  $P_{LCL}$  can be calculated by inverting the Poisson's equation:

$$P_{LCL} = P(T_{LCL} / T)^{C_p / R}$$

Where temperatures in Kelvin,  $C_p / R = 3.5$ .  $T$  and  $P$  are the initial absolute temperature and pressure of the parcel prior to lifting, respectively.

In order to keep the same structure of the KI, the temperature of the LCL is used here to express the different heights of LCL in the OCI. The reason for including the  $T_{LCL}$  as the second term of the OCI is to increase the value of the OCI when the height of the LCL is low.

The third term is  $(T_{50} - D_{50})$  is the average dew point depression of the lowest 50 hPa. In Figure 5-4 the dew point temperature decreases rapidly just above the ground for a day without convection (A) and a convective day (B). Therefore, the average dew point depression of the lowest 50 hPa is used in order to compensate for the rapid decrease in dew point temperature just above the ground. Craven *et al.* (2002) found that using the mixed layer dew point was more representative of the actual parcel associated with convective cloud development. Statistical analysis done here confirmed that better results are obtained by using the average mixed layer values. Figure 5-5 depicts the dew point depression when utilizing only surface values (red) and when the average values of the lowest 50 hPa are used (blue). The values of the dew point depression were larger (*i.e.* dryer) when using the average values except for the 11<sup>th</sup> of July. This is considered to be a better representation of the atmosphere through which the parcel will move and will have a significant influence on the height of the LCL. Figure 5-5 also indicates clearly that the higher values of the dew point depression occurred on the Non Active days of 5<sup>th</sup> and 14<sup>th</sup> of July.

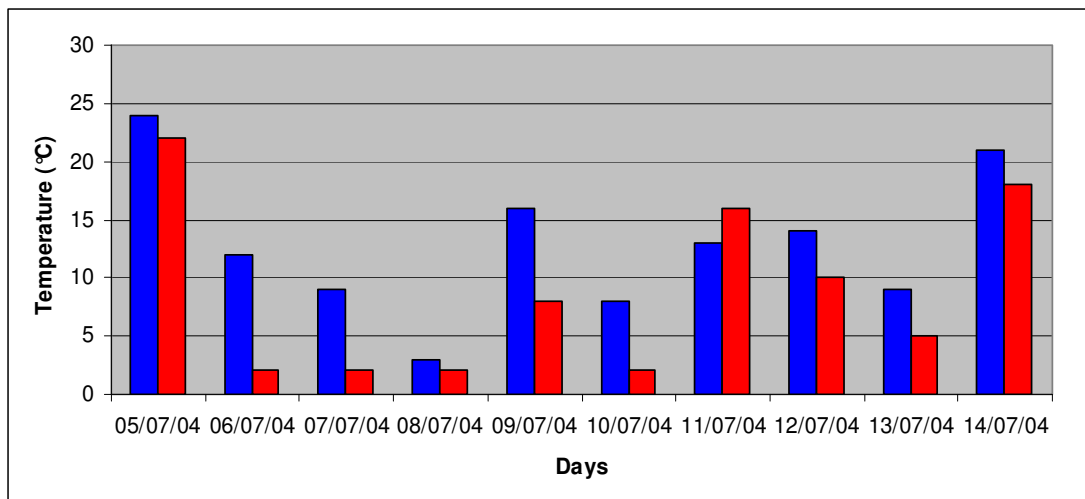


**Figure 5-5: The dew point depression using the average values in the lowest 50 hPa (blue) and surface values (red).**

Figure 5-6 compares the average dew point depression of the lowest 50 hPa (blue) to the dew point depression at 700 hPa (red) during the study period. The KI utilizes the dew point depression at 700 hPa and in Figure 5.6 it is illustrated how using the average dew point depression of the lowest 50 hPa will give better results as the 700 hPa dew point depression remains approximately constant during this period, but at the surface low values occur on convective days. On days when no convection occurred, the 5<sup>th</sup> and 14<sup>th</sup> of July the average dew point depression of the lowest 50 hPa was more than 20 °C, while on days when convection occurred (excluding the 9<sup>th</sup> of July) the air was significantly moister with the dew point depression less than 15 °C. The 700 hPa dew point depression showed much less variability and although there was a slight increase on days when convection occurred, the values were all generally between 15 and 25 °C. In the OCI the average dew point depression of the lowest 50 hPa therefore replaces the dew point depression at 700 hPa in the KI.



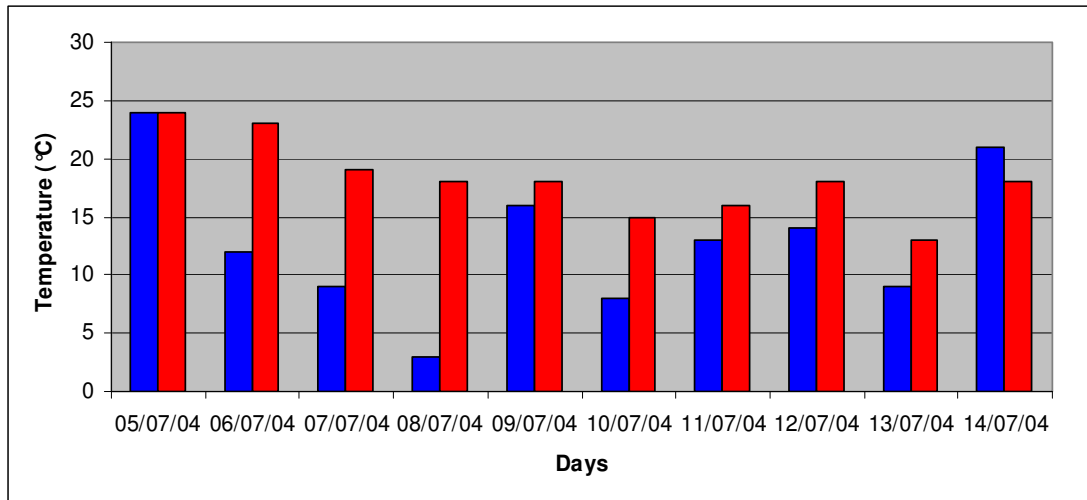


**Figure 5-6:** The dew point depression using the average values in the lowest 50 hPa (blue) and of the 700 hPa (red).

### 5.3.2 Statistical analysis of OCI

The long term average of the first term (850 to 500 hPa lapse rate) was 34 °C, the same as calculated for the KI. The long term average values for the second and the third terms for the months of June and July used to calculate the OCI were also calculated. The long term average values are given in Table 5-4.

**Table 5-4:** The long term average, maximum and minimum values of the OCI and its second and third terms.

	Second term ( $T_{LCL}$ )	Third term ( $T_{50} - D_{50}$ )	OCI
<b>Average</b>	15	14.9	34
<b>Maximum</b>	29	38	67
<b>Minimum</b>	-10	0	-14

The long term average temperature of the LCL was 15 °C but can be as high as 29 °C when the LCL was closer to the surface. On very dry days the temperature of the LCL can be as low as -10 °C. The average surface dew point depression is 15 °C, on very dry days the dew point depression can be as high as 38 °C. The long term average OCI of the Seeb soundings for June and July was found to be 34.

In 5.2.2 the data set was described where all the June and July days of 2005 and 2006 was classified into Non Active, Active and Very Active days. This same data set was used to verify the results of OCI. In Table 5-5 the average values for the different convective thresholds are given. Considering all the days the OCI was 34, the value was 25 for Non Active days, 42 for Active days and 39 for Very Active days. Comparing these results with the KI in Table 5-2 it is interesting to note that in both cases the average values for Active days were higher than for Very Active days.

**Table 5-5: Average OCI values for Non Active, Active and Very Active days for the June and July of 2005 and 2006**

	Total	Non Active	Active	Very Active	Total Active
<b>Number of Days</b>	83	28	17	38	55
<b>Average OCI</b>	34	25	42	39	40

The average of OCI during the total Active days suggests a threshold value of approximately 40 would be appropriate to forecast convection. However, a threshold value of 36 is used for analyzing the OCI by the same statistical method for dichotomous (yes/no) forecasts that was used previously for analyzing the KI. This value is chosen to be consistent with the threshold value of KI (22) by being just two values above the long term average. Also the OCI value of 36 performed well in distinguishing between the Active and Non Active days during this study period (5<sup>th</sup>-14<sup>th</sup> of July 2004) as explained in 5.4.

The five categorical statistics were calculated here from the contingency table (Table 5-6) for the OCI with threshold value of 36.

**Table 5-6: The contingency table of 83 days of different OCI values with threshold value of 36.**

		Observed		
		yes	no	Total
Forecast	yes	37	9	46
	no	18	19	37
	Total	55	28	83

The five categorical statistics are:

- Accuracy = 0.67
- BIAS = 0.84
- POD = 0.67
- FAR = 0.20
- POFD = 0.32

The accuracy is 67%. The frequency of convection was slightly under forecast indicated by the BIAS of 0.84. The POD is 67% and the FAR 20% showing that for a fifth of the forecasts no convection was observed. The POFD indicates that about third of the observed “no convection” events the forecast were incorrect. By comparing the five categorical statistics (Fig. 5-7) of both the KI of 22 and the OCI of 36, the OCI accuracy is about 10 % higher, the BIAS is 20% higher and the POD is 18% higher where the FAR and the POFD are almost similar.

Generally the statistical results show that the OCI fared well in predicting convection over this area. The results are better than the results for the KI. When viewing these statistical results the limitations of the data used should be considered. The 0000 UTC upper air data are utilized to predict convection which starts some 10 hours later and Seeb is more than 150km's away from the study area. Considering all of this, the POD is still close to 70% with the FAR at 20%. For the KI the POD is only 50%.

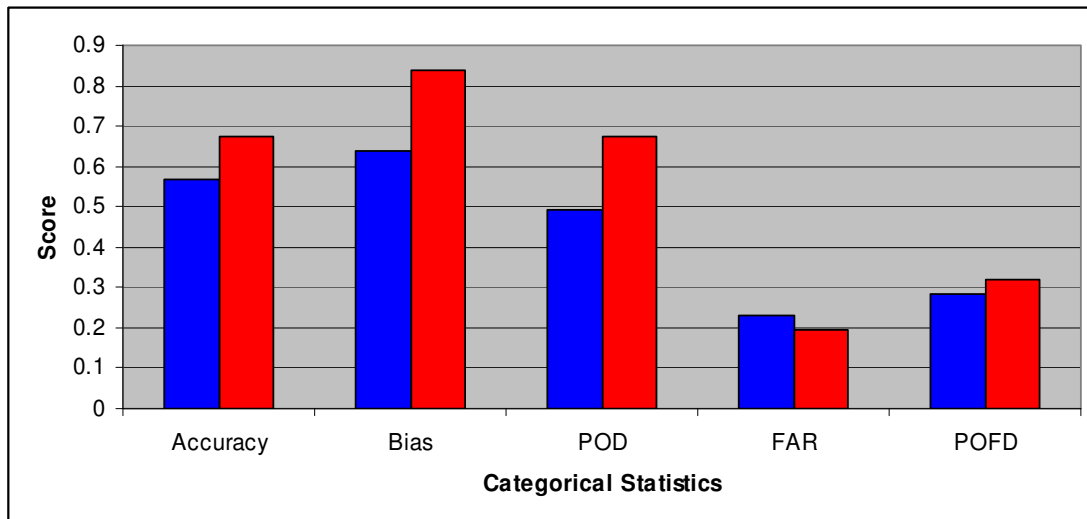


Figure 5-7: The 5 categorical statistics of KI of 22 (blue) and OCI of 36 (red).

#### 5.4 KI and OCI during this study period

The OCI was calculated for the study period and compared with the KI. Figure 5-8 depicts the performance of both the OCI (blue) and the KI (red) from the 5<sup>th</sup> to the 14<sup>th</sup> of July 2004.

If an OCI value of 36 is considered to be indicative of convective development, Figure 5.8 indicates that both the non-convective and convective days were identified accurately. The exception being the 9<sup>th</sup> of July when the value was just below 36.

All the Very Active days occurred with values between 36 and 50. Utilizing a significant value of 22 the KI failed to forecast some Active days like the 6<sup>th</sup> and 9<sup>th</sup> of July. Likewise, on the 14<sup>th</sup> of July the KI was much higher than 22, yet no convection occurred over the SSA. Both indices could not distinguish between Active and Very Active days. However the OCI was capable of identifying the onset of convection on the 6<sup>th</sup> of July as well as the end of the convection on the 14<sup>th</sup> of July, which the KI failed to do. The sounding on the 9<sup>th</sup> of July was not very favorable for convective development as reflected in the low values of the KI and the OCI, however, convection did occur and both indices failed on this day.

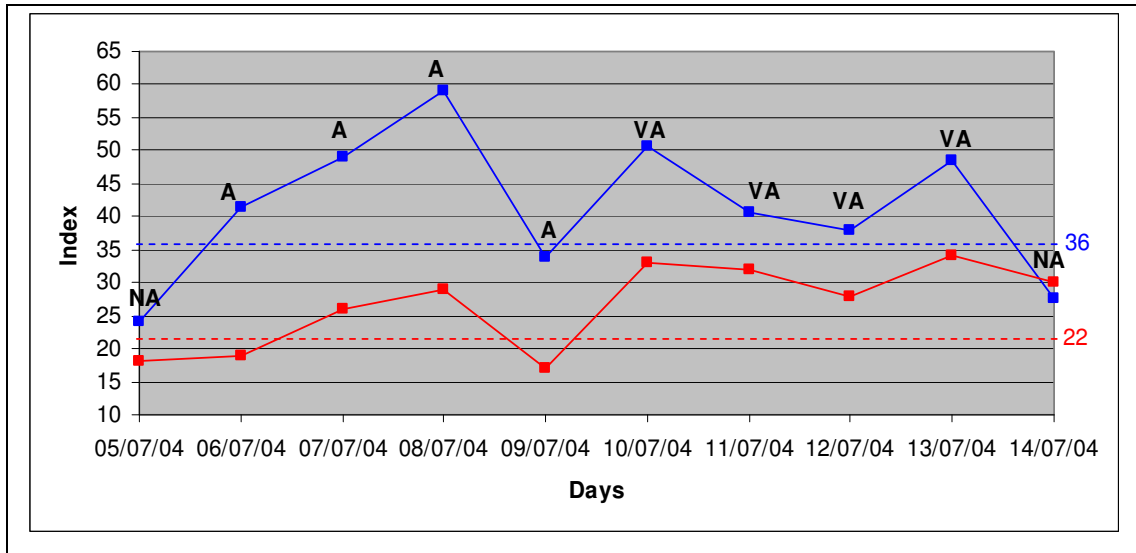


**Figure 5-8:** The OCI (blue) and the KI (red) during the study period (5<sup>th</sup>-14<sup>th</sup> of July 2004). The dashed lines are representing the considered threshold values of OCI (blue) and the KI (red). The marked NA, A and VA means Non Active, Active and Very Active respectively.

These results indicate that using the average dew point temperature in the lowest 50 hPa gives better results than using the 850 hPa dew point temperature. The dew point temperature at 850 hPa was 4.4 °C on the 5<sup>th</sup> of July increased slightly to 5.2 °C on the 6<sup>th</sup> of July. For the rest of the period, excluding the 9<sup>th</sup> of July, the 850 hPa dew point temperature was higher than 10 °C (Fig. 5-2). On the other hand, the average dew point in the lowest 50 hPa was 14 °C on the 5<sup>th</sup> of July and 17 °C on the 14<sup>th</sup> of July with values above 20 °C on the other days, excluding the 9<sup>th</sup> of July.

### 5.5 General discussion

In this chapter a new index called Oman Convection Index (OCI) was developed especially for forecasting convection over the Al Hajar Mountains. The OCI was developed to be similar to the KI but some of the terms were changed to make it more representative of the atmospheric conditions in Oman. The KI and OCI were statistically analyzed and it was shown that the OCI faired better than the KI in predicting convection over the mountains.

The OCI was developed specifically to forecast convective development over the Al Hajar Mountains. The local conditions were investigated and the OCI developed accordingly. Before applying this index at other stations further investigation is required.

It is recommended that the Oman forecasters use and test the OCI during the forthcoming summer months and that verification continues to obtain the optimal threshold value for this index.

## Chapter 6

## Forecasting Techniques

### **6.1 Introduction**

In this chapter methods of forecasting convection over the Al Hajar Mountains is discussed according to the available tools and data used in this research. This includes synoptic scale analysis, surface observations, upper air data and other data used in the research. This chapter addresses new techniques for forecasting the convective clouds over the Western Hajar Mountains.

### **6.2 Techniques formulation and application**

Most of the previous chapters discussed the important factors that influenced convective development over the Al Hajar Mountains. Some of these factors may be investigated prior to the occurrence of the storms over the mountains. Favorable synoptic and upper air conditions are a first approach to predicting convective development over the Al Hajar Mountains.

This chapter provides a summary of the synoptic and upper air conditions conducive to the development of summer thunderstorms over the Al Hajar Mountains. In addition convection forecasting techniques are proposed in the form of a forecasting table, or decision tree.

#### **a. Synoptic situation**

The general synoptic situation over the area should be investigated in advance, using the prognostic fields of NWP models as well as actual observations. The existence and the location of the heat low pressure over the Arabian Peninsula and its deepening provide a good indication of the potential of convection over the mountains. As discussed in chapter 4, the appropriate synoptic condition for convection to occur is a deep heat low over the centre of the Arabian Peninsula which extends a deep trough southward. This low should also be present at 850 hPa. Figure 6-1 is an example of very favorable synoptic scale conditions for the development of thundershowers over the mountains.

#### **b. Upper Air Sounding**

The parameters derived from the upper air data at Seeb at 0000 UTC are essential to predict thunderstorms over the mountains. Some parameters, which were shown in Chapter 3 to be essential to predict convective clouds, are when:

- a. Low LCL height (lower than 1800 m AGL).
- b. The MXR is 12 g/kg or higher

c. The OCI with values higher than 36

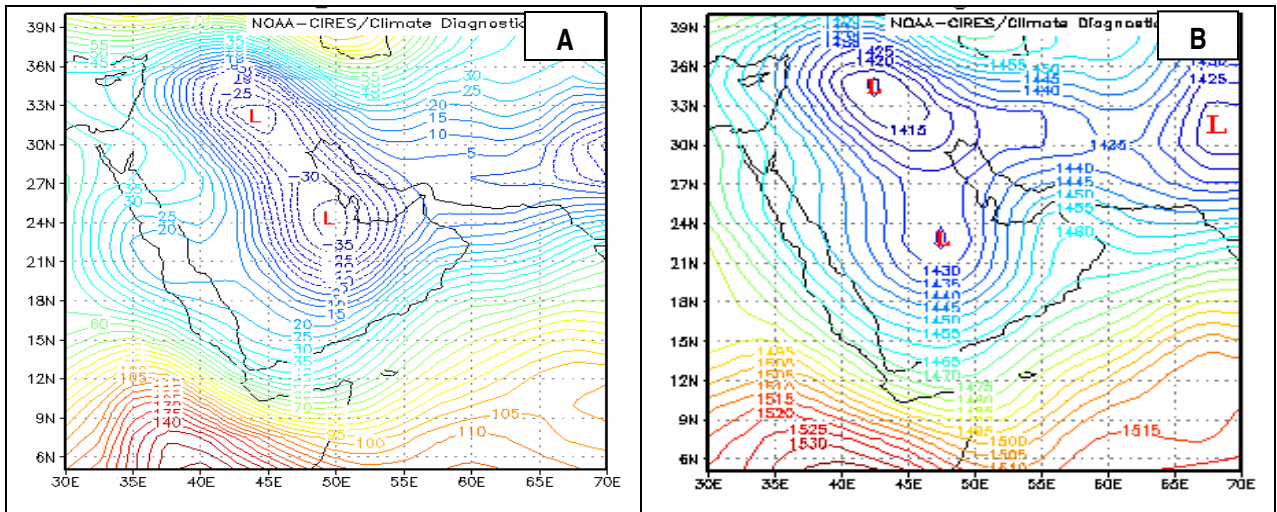


**Figure 6-1:** The 1000 and 850 hPa geopotential heights on the 11<sup>th</sup> of July 2004. The deep low pressure over the Arabian Peninsula is clearly indicated at 1000 hPa (A) and at 850 hPa (B). (Adapted from: NCEP, 2007).

### 6.2.1 Table of convection forecasting techniques (TCFT)

Table 6-1 illustrates the table of convection forecasting techniques (TCFT). These techniques are presented in a simplified manner in this table in order to identify those factors important for convective development over the Al Hajar Mountains.

The TCFT is a (Yes/No) checklist and is based on synoptic and upper air elements that could be used as forecasting guidelines for predicting the convection. If a positive answer (Y) is given for each of the five questions in the table then two points are awarded. A maximum, or perfect, score is ten.

**Table 6-1:** Table of the convection forecasting techniques (TCFT) for predicting the convective storms over the Al Hajar Mountains.

Element	Score (Y=2 Points, N= 0 Points)
Heat low over the centre of Arabian Peninsula (surface/1000 hPa )	
Heat low over the centre of Arabian Peninsula (850 hPa )	
Real latent Instability (CAPE>CIN)	
Mean mixed layer mixing ratio >=12 g/kg	
OCI >=36	
Overall Score	(0-10 points)



The first two elements of the TCFT are synoptically related. They represent the importance of the existence and the deepening of the heat low pressure over the centre of the Arabian Peninsula, which is vital in forecasting the convection. Two points are awarded for each element if low pressure exists over the centre of the Arabian Peninsula.

The other three elements of the TCFT are obtained from the upper air data of the Seeb sounding at 0000 UTC as discussed previously. The conditional instability was discussed in section 4.4.1. Here, two points are awarded if the atmosphere latently unstable. Other two points are given if the mean mixed layer mixing ratio is 12 g/kg or more. The OCI was discussed in chapter 4 and its threshold value of 36 is checked here where two points are given if the OCI is equal to 36 or above.

The perfect score of 10 indicates a good likelihood of convective development (i.e. a Very Active day). The zero score is a good indicator that no convection will occur (i.e. a Non Active day). The values between 0-10 are directly related to the likelihood of convective activity over the Al Hajar Mountains (Table 6-2).

**Table 6-2: The categories of the days' convection forecast according to the overall score of the TCFT.**

<b>Overall Score of TCFT</b>	<b>The days' Convection Forecast</b>
0-2	Non Active day
4-6	Active day
8-10	Very Active day

### **6.2.2 Applications of the TCFT**

The TCFT was applied for the whole study period (from 5<sup>th</sup> to 14<sup>th</sup> July, 2004) and the results are shown in Table 6-3.

The overall score of Table 6-3 clearly indicated the Non Active days of the 5<sup>th</sup> and the 14<sup>th</sup> with scores from 0-2. The Active days are predicted with a score of 6 while the Very Active days' score ranged from 8-10.

The results suggest that the forecasting table could be very useful in predicting thunderstorms over the Al Hajar Mountains. It is recommended that this table is implemented and tested operationally in the Department of Meteorology in Oman.

**Table 6-3: The TCFT application for the whole study period days (5<sup>th</sup>-14<sup>th</sup> of July 2004).**

<b>Condition</b>	<b>5<sup>th</sup></b>	<b>6<sup>th</sup></b>	<b>7<sup>th</sup></b>	<b>8<sup>th</sup></b>	<b>9<sup>th</sup></b>	<b>10<sup>th</sup></b>	<b>11<sup>th</sup></b>	<b>12<sup>th</sup></b>	<b>13<sup>th</sup></b>	<b>14<sup>th</sup></b>
Heat low over the centre of Arabian Peninsula (surface/1000 hPa)	N	N	N	N	Y	Y	Y	Y	Y	N
Heat low over the centre of Arabian Peninsula (850 hPa)	N	N	N	N	Y	Y	Y	Y	Y	N
Real latent Instability (CAPE>CIN)	N	N	Y	Y	N	Y	Y	N	Y	N
Mean mixed layer mixing ratio $\geq 12$ g/kg	N	Y	Y	Y	Y	Y	Y	Y	Y	Y
OCI $\geq 36$	N	Y	Y	Y	N	Y	Y	Y	Y	N
Overall	0	4	6	6	6	10	10	8	10	2

## Chapter 7

## Conclusion and Recommendations

### **7.1 General summary**

In this study, forecasting techniques for seedable storms over the Western Al Hajar Mountains in the Sultanate of Oman were developed. These techniques may be used to predict the occurrence of convective storms suitable for hygroscopic seeding over the area. A total of ten case studies days (5<sup>th</sup>-14<sup>th</sup> of July 2004) were investigated in order to outline the differences between the Non Active, Active and Very Active days. Synoptic and local analysis including the upper air conditions, surface observations, radar and satellite images, NWP and information gathered during the cloud seeding experiment were the data used in this research.

### **7.2 Summary of results**

#### **a. Surface circulation**

The analysis of the synoptic data showed that on days when active convective clouds developed over the mountains heat low pressure existed over the centre of the Arabian Peninsula. The deepening and the position of this low controlled the wind direction and consequently the influx of surface moisture needed for convective cloud to develop. The southeasterly to southerly surface winds along with the sea breeze from the Gulf of Oman were found to be the main source of moisture over the mountains. Occasionally convection occurred during the late afternoon in convergence zones formed by the wind circulation. It was also shown that favorable surface and 850 hPa synoptic conditions are essential for thundershowers to occur but the circulation at 500 hPa is not important.

#### **b. Upper air data**

The upper air sounding data at Abu Dhabi and Seeb were analyzed and compared in order to identify appropriate variables which could be used to forecast convection. The Seeb soundings at 0000 UTC proved to be the most representative to forecast convection over the Al Hajar Mountains. The low level moisture, along with other parameters like the height of the LCL, was crucial in differentiating between Non Active, Active and Very Active days. The Oman Convection Index (OCI) was developed by adapting the KI in order to provide a better prediction of convection. The OCI was physically and statistically analyzed and tested for some cases. The results showed that it could be used with confidence to predict convection and faired significantly better than the KI.

#### **c. Forecasting techniques**

Forecasting techniques were developed for predicting convective storms over the western Hajar Mountains in the Sultanate of Oman. The techniques are presented in a table, consisting of five elements and

where points are given for each element should it present. The techniques considering all the results found in this study to provide a better way of forecasting the convective clouds over the Western Hajar Mountains. The techniques can be used to forecast storms suitable for seeding over the area.

### **7.3 Conclusions**

1. Thunderstorms of the Al Hajar Mountains are notoriously difficult to predict. The forecasting process is made more difficult by the absence of adequate surface and remotely sensed meteorological data. Nevertheless, this research has shown that careful investigation and manipulation of the available data allows for increased accuracy in the forecast of convection.
2. The thunderstorms over the mountains of Oman results from mesoscale circulation. An essential input into convective development is the influx of surface moisture from southeast. This moisture often results from the positioning of the surface low over the central part of the Arabian Peninsula but can occasionally be caused by sea breeze circulation. Localized wind convergence zones near the mountains are good indicators for the onset of convection.
3. The Oman Convection Index (OCI) was developed from the KI and was shown to provide a good indication of convective development over the mountains.
4. A table of the convection forecasting techniques is proposed where circulation patterns are provided as well as critical values for meteorological variables.

### **7.4 Recommendations**

1. This research results showed that the forecasting techniques developed here have some potential to predict convective clouds over the mountains. However, these techniques need to be tested and verified operationally. It is recommended that these techniques are implemented in the Oman forecasting office without delay.
2. Although the forecasting techniques showed good results in predicting the convection over the western Al Hajar Mountains, further studies are needed to support the findings in order to improve the forecast.
3. It must be stressed that predicting convection over this area is complicated and subjected to a lot of challenges and limitations. One of the limitations is the scarcity of essential data especially over Oman. This includes the upper air data, surface observations and radar data. Hence it is strongly recommended to increase these data over the mountain areas in order to facilitate additional research and eventually better

prediction. Obtaining upper air sounding data over the mountains will be especially useful. In order to improve the nowcasting of thunderstorms, including storms suitable for cloud seeding, weather radars need to be erected on the eastern side of the Omani mountains. Data from these radars could be used together with the data from the radars in the UAE to increase the understanding of convective cloud development.

## References

- Al-Maskari, J., Gadian, A. & Smolarkiewicz, P., 2006: A study of orographic convection over the Hajar mountains in northern Oman, European Geosciences Union, 8(01786).
- American Meteorological Society (AMS), 1998: Scientific background for AMS policy statement on planned and inadvertent weather modification, *Bull. Amer. Meteor. Soc.*, 79, 2773-78.
- American Meteorological Society (AMS), 2007: AMS Glossary, <http://amsglossary.allenpress.com/glossary/search?p=1&query=showlater+index&submit=Search>
- Asimakopoulou, D. N., Helmis, C. G., Papadopoulos, K. H., Kalogiros, J. A., Kassomenos, P. & Petrakis, M., 1999: Inland Propagation of Sea Breeze under opposing off-shore Wind. *Meteorology and Atmospheric Physics*, 70, 97-110.
- Barnes, S. L., 1968: An empirical shortcut to the calculation of temperature and pressure and lifted condensation level. *J. Appl. Meteor.*, 7, 511.
- Bechtold, P., Pinty, J. & Mascart, P., 1991: A numerical investigation of the influence of large-scale winds on the sea breeze and inland breeze type circulations. *Journal of applied Meteorology*, 30, 1268-1279.
- Bigg, E. K., 1997: An independent evaluation of a South African hygroscopic cloud seeding experiment, 1991-1995. *Atmos. Res.*, 43, 111-127.
- Bonnardot, V. M. F., Carey, V. A., Planchon, O. & Cautenet, S., 2001: Sea breeze mechanism and observations of its effect in the Stellenbosch wine producing area. *Wynboer*, 10, 107-113.
- Breed, D., Jensen, T., Bruintjes, R., Piketh, S., Al Mangoosh, A. & Al Mandoos, A., 2005: Precipitation development in convective clouds over the eastern Arabian Peninsula, "unpublished report", UCAR, U.S.A.
- Bruintjes, R. T., NCAR, 1999: A review of cloud seeding experiments to enhance precipitation and some new prospects, *Bull. Amer. Meteor. Soc.*, Vol. 80, No. 5, 2773-2778.
- Bruintjes, R.T. & Yates D.N., 2003: Report on review and assessment of the potential for cloud seeding to enhance rainfall in the Sultanate of Oman, Research applications program, NCAR, Boulder, Colorado, USA.
- Clarke, R. H., 1955: Some observations and comments on the sea breeze, *Australian Meteorological magazine*, 11, 47-68.
- Clarke, R. H., 1983: Fair weather nocturnal inland wind surges and atmospheric bores: Part I Nocturnal wind surges, *Australian Meteorological magazine*, 31, 133-145.
- Clarke, R. H., 1984: Colliding sea-breeze and the creation of internal atmospheric bore waves: two dimensional numerical studies, *Australian Meteorological magazine*, 32, 207-226.
- Cooper, W. A., Bruintjes, R. T. & Mather, G. K., 1997: Calculations pertaining to hygroscopic seeding with flares, *Bull. Amer. Meteor. Soc.*, Vol. 36, 1449-1469.
- Craven, J. P., Jewell, R. E. & Brooks, H. E., 2002: Comparison between observed cloud-base heights and lifting condensation level for two different lifted parcels, *Weather Forecasting*, 17, 885-890.
- De Villiers, M.P. & Van Heerden, J., 2007: Dust storms and dust at Abu Dhabi international airport, *Weather*, 62, 339-343.
- Department of Atmospheric Studies (DAS), 2003: Annual climate report, Meteorological section – Ministry of presidential affairs – United Arab Emirates.
- Department of Water Resources Studies (DWRS), 2001-2002: Rainfall enhancement and air chemistry studies, United Arab Emirates.
- Department of Water Resources Studies (DWRS), 2004: Rainfall enhancement assessment program of the United Arab Emirates, phase II operations plan.

- Directorate General of Civil Aviation and Meteorology (DGCAM), 1996: The meteorology of Oman, revised 10/96 – DAM.
- Directorate General of Civil Aviation and Meteorology (DGCAM), 2002: Annual climate summary, Department of Meteorology – Climate Section.
- Directorate General of Civil Aviation and Meteorology (DGCAM), 2005: Annual climate summary, Department of Meteorology – Climate Section.
- Directorate General of Civil Aviation and Meteorology (DGCAM), In press book: The tropical cyclone Gonu, Department of Meteorology, Sultanate of Oman.
- Dixon, M. J. & Wiener, G., 1993: TITAN: Thunderstorms Identification racking UCAR, Analysis and Nowcasting - a radar-based methodology. *J. Atmos. Ocean. Technol.* 10(6), 785-797.
- DU Preez, C. B., 2006: A Mesoscale Investigation of the Sea Breeze in the Stellenbosch Winegrowing District, MSC dissertation, Department of Geography, Geoinformatics and Meteorology - University of Pretoria, South Africa.
- Dupilka, M. L. & Reuter, G. W., 2006: Forecasting tornadic thunderstorm potential in Alberta using environmental sounding data. Part I: wind shear and buoyancy, *Amer. Meteor. Soc.*, 21:325-335.
- Dupilka, M. L. & Reuter, G. W., 2006: Forecasting tornadic thunderstorm potential in Alberta using environmental sounding data. Part II: Helicity, precipitable water, and storm convergence, *Amer. Meteor. Soc.*, 21:336-346.
- Ebert, B., 2007: Forecast Verification - Issues, Methods and FAQ, WWRP/WGNE Joint Group on Verification, Bureau of Meteorology research Centre, Australian Government, [http://www.bom.gov.au/bmrc/wefor/staff/eee/verif/verif\\_web\\_page.html#Contingency%20table](http://www.bom.gov.au/bmrc/wefor/staff/eee/verif/verif_web_page.html#Contingency%20table)
- Estoque, M. A., Gross, J. & Lai, H. W., 1976: A Lake Breeze over Southern Lake Ontario. *Monthly Weather Review* 104, 386-396.
- George, J. J., 1960: Weather Forecasting for Aeronautics, Academic Press, 673 PP.
- Henry, N. L., 2000: A static stability index for low-topped convection, *Amer. Meteor. Soc.*, 15:246-254.
- Jensen & Ziady, 2003: Titan/CIDD installation for UAE, RAP-UCAR, USA, [http://www.rap.ucar.edu/projects/UAE/uae\\_titan\\_cidd.html](http://www.rap.ucar.edu/projects/UAE/uae_titan_cidd.html)
- Jensen, T. L., 2004: Rainfall Enhancement Assessment Program of the United Arab Emirates - Phase II - 2004 Operations Plan, unpublished plan, DWRS, UAE.
- Jensen, T. L., Breed, D. W., Salazar, V., Brintjes, R.T., Piketh, S.J., Ross, K., Al Mangoosh, A. & Al Mandoos, A., 2003: Observed cloud characteristics during hygroscopic cloud seeding research in the United Arab Emirates, WMO, 2003.
- Krauss, T. W., Brintjes, R. T., Verlinde, J. & Kahn, A., 1987: Microphysical and radar studies of seeded and non-seeded continental cloud., *J. Climate Appl. Meteor.* , 26, 585-606.
- Mather, G. K. and Terblanche, D. E., 1993: Rain augmentation in South Africa, *S.A. Jour. Sci.*, 89, 22-23.
- Mather, G. K., 1991: Coalescence enhancement in large multicell storms caused by the emissions from a Kraft paper mill, *J. Appl. Meteor.*, 30, 11134-1146.
- Mather, G. K., Terblanche, D. E., Steffens, F. E. & Fletcher, L., 1997b: Results of the South African cloud-seeding experiments using hygroscopic flares, *J. Appl. Meteor.*, 36, 1433-1447.
- Mather, G. K., Dixon, M. J. & de Jager, J.M., 1996: Assessing the potential for rainfall augmentation – The Nelspruit randomised convective cloud seeding experiment, *J. Appl. Meteor.*, 35, 1465-1482.
- Mather, G. K., Terblanche, D. E., Steffens, F. E. & Fletcher, L. 1997a: Results of the South African cloud seeding experiments using hygroscopic flares, *Journal of Applied Meteorology*, 36, 1433-1447.



- MODIS, National Aeronautics & Space Administration (NASA), USA,  
<http://modis.gsfc.nasa.gov/>
- National Survey Authority, 2007: Atlas of Oman. In press book, Ministry of Education. Sultanate of Oman.
- Network Overseas, London, UK, 2007,  
<http://www.networkoverseas.cc/images/oman/map-oma.gif>.
- Orville, H. D., 1995: Report on the Sixth WMO Scientific Conference on Weather Modification, *Bull Amer. Meteor. Soc.*, 76, 372-373.
- Physick, W. L., 1980: Numerical experiments on the inland penetration of the sea breeze. *Quarterly Journal of the Royal Meteorological Society*, 106, 735-746.
- Physick, W. L., 1982: Sea Breezes in the Latrobe Valley, *Australian Meteorological Magazine*, 30, 255-263.
- Pielke, R. A., 1974: A three dimensional model of the sea breezes over south Florida, *Monthly Weather Review*, 102, 115-139.
- Rawinsonde Observation Program (RAOB), Environmental Research Services, USA, a program registered to Directorate General of Civil Aviation & Meteorology, Sultanate of Oman.
- Rasmussen, E. N., 2003: Refined supercell and tornado forecast parameters, *Weather Forecasting*, 18, 530-535.
- Schultz, D. M., Schumacher, P. N. & Doswell III, C. A., 2000: The Intricacies of instabilities, *Amer. Meteor. Soc.*, 128:4143-4154.
- Silverman, B. A., 2000: An independent statistical reevaluation of the South African hygroscopic flare seeding experiment, *J. Applied Meteorology*, 39, 1373-1378.
- Silverman, B. A., 2000: An independent statistical reevaluation of the South African hygroscopic flare seeding experiment, *J. Appl. Meteor.*, 39, 1373-1378.
- Simpson, J. E., Mansfield, D. A. & Milford, J. R., 1977: Inland penetration of sea-breeze fronts. *Quarterly Journal of the Royal Meteorological Society*, 103, 47-76.
- Simpson, J. E., Westcott, N. E., Clerman, R.J. & Pielke, R.A., 1980: On cumulus mergers. *Arch. Meteor. Geophys. Bioklim., Ser. A.*, 29, 1-40.
- Simpson, J. E., 1994: Sea breeze and local winds, Cambridge University Press, New York, 243 PP.
- Sohoni, V. V. & Paranjpe, M. M., 1937: Latent instability in the atmosphere revealed by some Indian tephigrams, *Mem. India Meteor. Dept.*, 26, 131-149. plus 10 plates.
- Terblanche, D. E., Mittermaier, M. P., Piketh, S. J., Brintjies, R. T. & Burger, R. P., 2000: The Aerosol Recirculation and Rainfall Experiment (ARREX): an initial study on aerosol-cloud interactions over South Africa, *South African Journal of Science* 96, January 2000.
- Terblanche, D. E., Steffens, F. E., Fletcher, L., Mittermaier, M. P. & Parsons, R., 2000: Toward the operational application of hygroscopic flares for rainfall enhancement in South Africa, *J. Appl. Meteor.*, 39, 1811-1821.
- The University Corporation for Atmospheric Research (UCAR), 2006,  
<http://www.ucar.edu/ucar/>
- UK Meteorological Office (UKMO), 1997: Source book to the Forecasters' Reference Book, Meteorological Office College, Met.O.1024, Bracknell, UK, ISBN 0 86180 321 3.
- University of Wyoming, 2006: Upper Air, Department of Atmospheric Science, College of Engineering, USA,  
<http://weather.uwyo.edu/upperair/sounding.html>.

Wallace, J. M. & Hobbs, P. V., 1977: *Atmospheric Science, An introductory survey*, Academic Press, INC., Orlando, Florida 32887.

Wikimedia Commons, Wikimedia Foundation Inc., San Francisco, USA, 2007  
[http://upload.wikimedia.org/wikipedia/commons/archive/7/79/20070708123814!Oman\\_Topography.png](http://upload.wikimedia.org/wikipedia/commons/archive/7/79/20070708123814!Oman_Topography.png).

Wilde, N. P., Stull, R. B. & Eloranta, E. W., 1995: The LCL zone and cumulus onset, *Journal of climate and applied meteorology*, 24:64-657.

World Meteorological Organization (WMO), 2001: Annex III, WMO statement on the status of weather modification, Annex to agenda item 5.6 of the General Summary.

World Meteorological Organization (WMO), 2001: Annex IV, Guidelines for advice and assistance related to the planning of weather modification, Annex to agenda item 5.6 of the General Summary.